

**N 70 36928**  
**CR 112867**

**INTERIM FINAL TECHNICAL REPORT**

**CHARGED PARTICLE RADIATION DAMAGE IN SEMICONDUCTORS, XV:  
STUDY AND DETERMINATION OF AN OPTIMUM DESIGN  
FOR SPACE UTILIZED LITHIUM DOPED SOLAR CELLS,  
PART I**

**19 JUNE 1970**

**13154-6011-R0-00**

**Contract No. 952554**

**JET PROPULSION LABORATORY  
CALIFORNIA INSTITUTE OF TECHNOLOGY  
PASADENA, CALIFORNIA**

**CASE FILE  
COPY**

**TRW**  
**SYSTEMS GROUP**

**ONE SPACE PARK • REDONDO BEACH, CALIFORNIA 90278**

INTERIM FINAL REPORT

STUDY & DETERMINATION OF AN OPTIMUM DESIGN FOR  
SPACE UTILIZED LITHIUM DOPED SOLAR CELLS, PART I

R. G. Downing  
J. R. Carter  
R. E. Scott  
W. K. Van Atta

19 June 1970

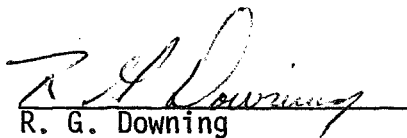
13154-6011-R0-00

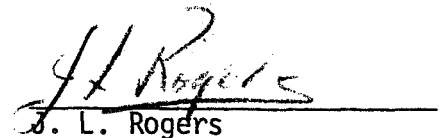
Contract 952554

Jet Propulsion Laboratory  
California Institute of Technology  
Pasadena, California

Prepared by:

Approved by:

  
R. G. Downing

  
J. L. Rogers

TRW Systems Group  
One Space Park  
Redondo Beach, California 90278

This work was performed for the Jet Propulsion Laboratory,  
California Institute of Technology, as sponsored by the National Aero-  
nautics and Space Administration under Contract NAS7-100.

TABLE OF CONTENTS

	<u>Page</u>
ABSTRACT	v
I. INTRODUCTION	1
II. KINETICS OF LITHIUM IN SILICON	3
A. Hall Coefficient Measurements	4
B. Carrier Removal in Cells	9
C. Defect Structures in Cells	16
D. Lithium Counterdoping of p-type Silicon	19
E. Large Substitutional Dopants in Silicon	22
III. LITHIUM SOLAR CELL EVALUATION	24
A. Centralab Cells	25
B. Texas Instruments Cells	26
C. Heliotek Cells	26
D. Solar Simulator Measurements	30
IV. SUMMARY	31
A. Lithium-Doped Quartz Crucible Silicon	31
B. Lithium-Doped Float Zone Silicon	32
C. Solar Cell Evaluation	33
V. PROGRESS IN THE NEXT REPORT PERIOD	34
VI. NEW TECHNOLOGY	34
VII. PAPERS AND PUBLICATIONS GENERATED	34
REFERENCES	35

LIST OF ILLUSTRATIONS

<u>TABLES</u>	<u>Page</u>
I SUMMARY OF P-TYPE LITHIUM COUNTERDOPED SAMPLES	36
II LITHIUM SOLAR CELL MANUFACTURING PARAMETERS	37
III LITHIUM SOLAR CELL RECOVERY CHARACTERISTICS AFTER $3 \times 10^{15}$ , e/cm <sup>2</sup> , 1 MeV	38
IV RECOVERED LEVEL AND HALF RECOVERY TIME (Hours)	39
V COMPARISON OF PEAK RECOVERED LEVELS ( $I_{SC}$ -TUNGSTEN)	40
<u>FIGURES</u>	
1 HALL COEFFICIENT VS. TEMPERATURE, IRRADIATED LI-DOPED Q.C. SILICON	41
2 CORRECTED HALL COEFFICIENT VS. TEMPERATURE, IRRADIATED LI-DOPED Q.C. SILICON	42
3 HALL COEFFICIENT VS. TEMPERATURE, IRRADIATED LI-DOPED Q.C. SILICON	43
4 NORMALIZED HALL COEFFICIENT VS. TEMPERATURE, IRRADIATED LI-DOPED Q.C. SILICON	44
5 HALL COEFFICIENT VS. TEMPERATURE, IRRADIATED LI-DOPED F.Z. SILICON	45
6 HALL COEFFICIENT VS. TEMPERATURE, IRRADIATED LI-DOPED F.Z. SILICON	46
7 NORMALIZED HALL COEFFICIENT VS. TEMPERATURE, IRRADIATED LI-DOPED F.Z. SILICON	47
8 CARRIER REMOVAL RATE DUE TO DEEP LEVEL DEFECT VS. LI DONOR CONCENTRATION	48
9 RECOVERY OF LI-DOPED Q.C. CELL	49
10 DONOR CONCENTRATION VS. BARRIER WIDTH, CELL AF 14-4921	50
11 REMOVAL RATE VS. BARRIER WIDTH, CELL AF 14-4921	51
12 REMOVAL RATE VS. LI CONCENTRATION, CELL AF 14-4921	52
13 DONOR CONCENTRATION VS. BARRIER WIDTH, CELL H3A 7249	53
14 REMOVAL RATE VS. BARRIER WIDTH, CELL H3A 7249	54
15 DONOR CONCENTRATION VS. BARRIER WIDTH, CONVENTIONAL P/N CELL	55
16 SOLAR CELL CHARACTERISTICS, CELL C3-18	56
17 DONOR CONCENTRATION VS. BARRIER, CELL C3-18	57
18 DONOR CONCENTRATION VS. FLUENCE, CELL C3-18	58
19 SOLAR CELL CHARACTERISTICS, CELL AF 14-4903	59
20 DONOR CONCENTRATION VS. BARRIER WIDTH, CELL AF 14-4903	60

LIST OF ILLUSTRATIONS (Cont.)

	<u>Page</u>
21 DONOR CONCENTRATION VS. FLUENCE, CELL AF 14-4903	61
22 SOLAR CELL CHARACTERISTICS, CELL T4-10	62
23 DONOR CONCENTRATION VS. BARRIER WIDTH, CELL T4-10	63
24 REMOVAL RATE VS. LI CONCENTRATION F.Z. CELLS	64
25 REMOVAL RATE VS. BARRIER WIDTH, F.Z. CELLS	65
26 DONOR CONCENTRATION VS. BARRIER WIDTH, VARIOUS F.Z. UNIRRADIATED CELLS	66
27 LI CONCENTRATION GRADIENT VS. CONCENTRATION AT JUNCTION EDGE, LINEAR GRADIENT CELLS	67
28 CAPACITANCE VS. TEMPERATURE, VARIOUS FREQUENCIES	68
29 ACTIVATION ENERGY PLOT, CELL H3A 7284	69
30 CAPACITANCE VS. TEMPERATURE, VARIOUS FREQUENCIES, F.Z. CELL	70
31 ACTIVATION ENERGY PLOT, CELL C5D-100	71
32 LI COMPENSATED P-TYPE SILICON, Q.C.	72
33 LI COMPENSATED P-TYPE SILICON, Q.C.	73
34 LI COMPENSATED P-TYPE SILICON, F.Z.	74
35 SOLAR CELLS WITH LARGE SUBSTITUTIONAL IMPURITY ATOMS	75
36 RECOVERY OF GROUPS C8A AND C8B LI SOLAR CELLS	76
37 RECOVERY OF GROUPS C8C AND C8D LI SOLAR CELLS	77
38 RECOVERY OF GROUPS C8G AND C8H LI SOLAR CELLS	78
39 RECOVERY OF GROUP T9 LI SOLAR CELLS	79
40 RECOVERY OF GROUP T10 LI SOLAR CELLS	80
41 RECOVERY OF GROUP H8 LI SOLAR CELLS	81
42 RECOVERY OF GROUP H10 LI SOLAR CELLS AT 100°C	82
43 RECOVERY OF GROUP H10 LI SOLAR CELLS AT 60°C	83
44 RECOVERY OF GROUP H3A LI SOLAR CELLS AT 100°C	84
45 RECOVERY OF GROUP H3A LI SOLAR CELLS AT 60°C	85
46 RECOVERY OF GROUP H9 LI SOLAR CELLS AFTER $3 \times 10^{14} \text{e/cm}^2$	86
47 RECOVERY OF GROUP H9 LI SOLAR CELLS AFTER $3 \times 10^{15} \text{e/cm}^2$	87
48 ANNEALING TIME VS. STORAGE TEMPERATURE FOR CRUCIBLE LI SOLAR CELLS	88
49 EFFECT OF OXYGEN ON DIFFUSION COEFFICIENT OF LI IN SILICON	89
50 RECOVERY OF MAXIMUM POWER POINT OF BEST CRUCIBLE CELLS AT 100°C USING SOLAR SIMULATOR ILLUMINATION	90

ABSTRACT

Hall coefficient measurements have been made on lithium-doped silicon having dopant concentrations comparable to those found in solar cells. The results of the measurements of these materials indicate that two defect complexes are formed during irradiation. The  $E_C-0.17$  eV acceptor (oxygen-vacancy pair) is one of these defects. The other defect is associated with a deeper lying energy level which may be a lithium-vacancy pair; this level is found only in float-zone silicon. Capacitance measurements on irradiated lithium-doped solar cells have been made as a function of voltage and frequency. This work indicates that the irradiation of quartz crucible silicon solar cells results primarily in the formation of  $E_C-0.17$  eV acceptor defects. These defects are later annihilated by reaction with lithium donors. Similar studies of lithium-doped float silicon solar cells indicate the formation of a deeper lying energy level defect during irradiation.

Lithium was diffused into p-type silicon to form lithium compensated p-type silicon with resistivities in the practical device range. Lithium compensated p-type silicon has been irradiated and the electrical measurements suggest that lithium reacts with radiation defects in a manner which may provide a hardening effect on n/p solar cells. A study was performed to evaluate the effectiveness of bismuth and tin doping to achieve radiation hardness with negative results.

The solar cell evaluation program shows continued improvement in the fabrication of high efficiency radiation resistant lithium-doped cells. Additional evidence has been acquired indicating the superiority of longer time lower temperature diffusion schedules in producing higher pre-irradiation and post-annealing solar efficiencies. Solar simulator measurements on several of the better groups clearly show the superior radiation resistance of lithium-doped p/n cells relative to the contemporary 10 ohm-cm n/p cell following exposure to  $3 \times 10^{15}$  e/cm<sup>2</sup> 1 MeV electrons and annealing.

## I. INTRODUCTION

This interim report covers effort during the first 12-month period under JPL Contract No. 952554 in the study of lithium-doped solar cells. Interest in this field began with Vavilov's report of a radiation resistant diode made with lithium-doped, crucible grown silicon.<sup>1</sup> Wysocki later reported lithium-doped solar cells which degraded under electron irradiation, but rapidly recovered at room temperature.<sup>2</sup> Float zone silicon, with a characteristic lower oxygen concentration, was used to achieve this result. Subsequent work in this laboratory indicated that recovery also occurred in lithium-doped, quartz crucible silicon solar cells.<sup>3</sup> Since this initial work, the general subject has been studied in two ways. Empirical changes in the manufacturing techniques for lithium-doped solar cells were evaluated with the aim of optimizing the recovery effect. Other studies were directed at the development of a physical model of the degradation and recovery processes in lithium-doped silicon.

Some of the more pertinent facts gained during the previous studies are as follows. The lithium concentration in a solar cell is not uniform, but increases in a linear or near linear manner with distance from the solar cell junction.<sup>4,5</sup> Solar cells with low or insufficient lithium concentration do not recover in a satisfactory manner. Float zone silicon solar cells with exceptionally high lithium concentrations lose efficiency during storage in the unirradiated condition. These same cells, when irradiated and recovered, also exhibit a time-dependent loss of efficiency.<sup>5</sup> This loss has been related to the room temperature diffusion of lithium into the active area of the cell.<sup>6</sup> It has also been observed that higher lithium concentrations cause faster recovery rates.<sup>5,6</sup> This observation agrees with simple considerations of kinetic theory. It has also been observed that increased

fluence, i.e., greater populations of radiation defects, decrease the recovery rates of lithium cells. This single fact appears to conflict with the consideration of reaction kinetics theory.<sup>7</sup> However, the reaction of significant quantities of lithium donors to form defect complexes during irradiation reduces the concentration of lithium donors present during recovery. Such behavior will reduce the recovery rate of irradiated cells with increased electron fluences.

Despite the above mentioned problems, the manufacturing techniques for production of lithium solar cells have been optimized to produce cells which recover from electron irradiation to output levels significantly greater than those of similarly degraded conventional n on p solar cells. When such lithium-doped cells are irradiated with energetic protons or neutrons, the advantage of the lithium-doped cells over conventional n on p cells becomes much more pronounced.<sup>2,5</sup>

The current work at TRW Systems has involved basic studies of the underlying physical and chemical phenomenon of lithium behavior in irradiated silicon and the evaluation of systematic attempts to improve the fabrication technology of lithium-doped solar cells developed for JPL by other contractors. Hall coefficient measurements have been employed to study the changes which occur in lithium-doped silicon during irradiation and after recovery. By this technique it has been possible to identify the major defects produced during the irradiation of this material, and monitor the changes which occur after irradiation. All irradiations discussed in this report were done with 1 MeV electrons. Extensive capacitance measurements on lithium-diffused solar cells have allowed similar studies of the changes in donor concentration which confirm and support the Hall measurements.

The evaluation program consisted of time dependent measurements of lithium-doped float zone silicon solar cells irradiated at  $3 \times 10^{14}$  e/cm<sup>2</sup> and



$3 \times 10^{15}$  e/cm<sup>2</sup> with 1 MeV electrons during storage at room temperature. The evaluation of lithium-doped quartz crucible solar cells was performed at storage temperatures of 60°, 80°, and 100°C after irradiation to  $3 \times 10^{15}$  e/cm<sup>2</sup> with 1 MeV electrons. Lithium concentrations near the junction were determined by capacitance and related to observed behavior.

## II. KINETICS OF LITHIUM IN SILICON

The principal theoretical problem remaining, in connection with the study of radiation damage in lithium-doped silicon, is the confirmation of a physical model for the production and annealing of damage in this material. There have been five approaches to this problem prior to this contract. Since two types of silicon (float zone and quartz crucible) have been used in these studies, all of the results can not be compared. The results can be summarized as follows:

1. Vavilov, et. al. has suggested that in quartz crucible silicon, damage results from "A" center formation and annealing results from pairing of "A" centers with lithium donors.<sup>9</sup>

2. The RCA group has proposed the damage recombination centers of Li-V<sup>-</sup> in float zone and Li-O-V<sup>-</sup> in quartz crucible silicon. The annealing occurs by pairing of lithium donors with the respective damage center.<sup>6</sup>

3. The TRW group experiments, on float zone silicon cells, support the concept of Li-V<sup>-</sup> formation during irradiation with annealing by reaction of one or more lithium donors with the recombination centers.<sup>8</sup>

4. Stannard of NRL has irradiated lithium-doped float zone silicon at lower temperatures and allowed it to recover at room temperature.<sup>10</sup> The results indicated that the irradiation resulted in the production of an unidentified deep acceptor. A similar loss of lithium donors occurred at the same time. During the room temperature anneal the deep acceptors were removed. A loss

of lithium also occurred during the annealing. The lithium loss during annealing was roughly twice the deep acceptor loss.

5. Pignoret at the University of Lyon has presented evidence to show that silicon "A" centers are formed during the irradiation of both float zone and quartz crucible silicon doped with lithium.<sup>11</sup> In addition, lithium vacancy pairs also form in the float zone silicon. These defects subsequently react with lithium donors to form inactive complexes.

In general, most investigations support a view of annealing or recovery as caused by the reaction of one or more lithium donors with the dominant recombination centers. Such a model explains most of the observations which have been reported for lithium solar cells. The major point in need of clarification is the nature of the recombination centers formed during irradiation of lithium-doped silicon.

#### A. Hall Coefficient Measurements

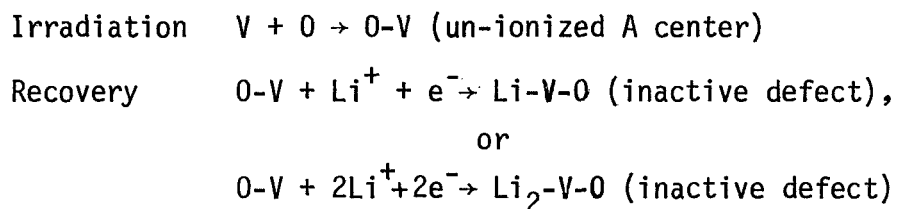
Lithium was diffused into wafers of 50 ohm-cm n-type quartz crucible silicon to make several Hall specimens. The lithium concentrations were about  $7 \times 10^{14}$  atoms/cm<sup>3</sup>. This doping level is comparable with that found in lithium-doped solar cells. In this way it was hoped that the results would be typical of behavior in lithium-doped solar cells.

Our initial results in the irradiation of this material are shown in Figure 1. The sample was irradiated with a fluence of  $1 \times 10^{16}$  e/cm<sup>2</sup> of 1 MeV electrons. Figure 1 shows a plot of reciprocal Hall coefficient versus reciprocal temperature for sample Q-2A. The reciprocal Hall coefficient can be interpreted as conduction carrier concentration. The before irradiation data indicated a constant electron concentration throughout the temperature range investigated. Irradiation produced a small change in the room temperature electron concentration. The low temperature electron concentration

was greatly lowered in a manner that indicates that the irradiation produced a large concentration of acceptor defects with a deep lying level. The manner in which the Hall coefficient of the irradiated specimen changes with temperature indicates that the Fermi level has become pinned to the energy level of the radiation produced defect. The defect energy level calculated from the slope shown in Figure 1 is 0.19 eV below the bottom of the conduction band. This value is not properly corrected for the temperature variation of the density of states in the conduction band. To properly account for the density of states, the quantity  $\log 1/T^{3/2} R_H$  must be plotted against  $1/T$ . This has the effect of lowering the apparent energy level a small amount. This analysis is shown in Figure 2. It is apparent that the true energy level will lie very close to the known position of the Si-A center (0.17 eV). This data strongly suggests that one of the main defects produced during room temperature irradiation of lithium-doped quartz crucible silicon is the Si-A center. A second sample (Q-2C) was irradiated with an electron fluence of  $1 \times 10^{15}$  e/cm<sup>2</sup>. The data for this sample is shown in Figure 3. It can be seen that there is evidence of a deep level after irradiation, and annealing reduces the concentration of deep level defects and conduction electrons. To assist in analysis of the data, it was normalized to the before irradiation results. In this way the temperature variation of the Hall factor is removed from the data. These results are shown in Figure 4. Several observations can be made from this data. The concentration of the deep level defects produced by irradiation is about  $2 \times 10^{14}$  cm<sup>-3</sup>. The indicated defect production rate would be 0.2 cm<sup>-1</sup>. The Si-A center has an energy level at 0.17 eV below conduction band, assuming a degeneracy factor of 1/2, the two-thirds ionization point will be reached at a temperature of 195°K (1000/TK = 5.15). Additional calculations show the Fermi level of sample (Q-2C) at 195°K after irradiation to be at 0.17 eV below the bottom

of the conduction band. There also appears to be some evidence of other extremely shallow energy level defects, because the carrier concentration is again declining at 120°K. After an anneal of 150 hours at 100°C, the concentration of A centers was reduced to  $7 \times 10^{13} \text{ cm}^{-3}$ . During the same period the concentration of carrier electrons or lithium donors was reduced by  $3.3 \times 10^{14} \text{ cm}^{-3}$ . The loss in A centers was  $1.4 \times 10^{14} \text{ cm}^{-3}$ . These results indicate that roughly two lithium donors are consumed in the anneal of one Si-A center. This behavior is very similar to that reported by Vavilov (Radiation Damage in Semiconductors, p. 115, Academic Press, N.Y., 1964). The defect production in this case is much greater than that reported by Vavilov for A centers.

Since the Si-A center is known to be an effective recombination center, the previous results form the basis for the model of irradiation damage and recovery in lithium-doped quartz crucible silicon solar cells. The behavior in cells may follow the following model:



The apparent consumption of two lithium donors per annealing A center may be misleading. The data admits to the possibility of other defects with more shallow lying energy levels. It is entirely possible that some lithium donors are consumed in the annealing of such defects.

Our previous Hall coefficient measurements on lithium-doped float zone silicon have been concentrated on heavily doped specimens. These heavy doping levels are not typical of those found in solar cells. To extend the previous work, float-zone specimens were prepared with lithium concentrations

in the range of  $10^{14}/\text{cm}^3$  to  $10^{15}/\text{cm}^3$ . The float-zone silicon used for this work was originally 1000 ohm-cm n-type silicon. This purity level restricts the possible defect interactions with impurities to those with lithium and possibly oxygen. Sample E-4 is an example of such a specimen. The Hall coefficient data relating to the irradiation and recovery of this sample is shown in Figure 5. Since the reciprocal Hall coefficient is closely related to the conduction band carrier concentration, the results in Figure 5 can be interpreted as changes in carrier concentration. The results of the irradiation of similar samples of quartz crucible silicon show a very small carrier concentration change at room temperature after irradiation. Those results support the production of Si-A centers (oxygen-vacancy pairs) during irradiation of the lithium-doped quartz crucible silicon. Two significant points can be observed regarding the after-irradiation results of sample E-4. First, the carrier removal at room temperature is approximately  $0.1 \text{ cm}^{-1}$ . The second point is the large inflection in the Hall coefficient at temperatures at which the Fermi level is near 0.17 eV below the bottom of the conduction band. Although alternate explanations can be proposed, the simplest model would be the formation of two types of defects during the irradiation; one defect being the Si-A with ionization energy of 0.17 eV and a second defect being defect of undetermined structure with an ionization greater than 0.3 eV from the conduction band. The second defect is probably a lithium-vacancy pair. The introduction rate of the Si-A center in this sample appears to be approximately  $0.2 \text{ cm}^{-1}$ . The value is in excellent agreement with that found in similar quartz crucible silicon. It is important to note that this sample contains only  $3.7 \times 10^{14}$  lithium donors/ $\text{cm}^3$ . Since the residual oxygen concentration in float-zone silicon is believed to be in the range of  $10^{15}/\text{cm}^3$ , oxygen is probably the dominant impurity in a float-zone specimen such as E-4.

In this regard it is not unusual that the Si-A center should be produced during irradiation. After irradiation the sample was stored at room temperature to study recovery changes. After 310 hours at 26°C, the carrier concentration was greatly reduced during storage. At this time the decline of the reciprocal Hall coefficient at temperatures below room temperature indicates that many shallower level defects (i.e., Si-A centers) remain in the sample. After 1500 hours the conduction electron concentration has been reduced to only a few percent of that present immediately after the irradiation. It appears that the time dependent decrease of carrier concentration is directly related to the reaction of lithium donor ion cores and their attendant electrons with radiation defects.

A similar specimen, F-2, with a somewhat higher lithium concentration, was studied in the same manner. The results of this study are shown in Figures 6 and 7. In this sample, the concentration of lithium donors was  $1.5 \times 10^{15} / \text{cm}^3$ . This is roughly four times the amount present in sample E-4. The float-zone silicon used in samples E-4 and F-2 was purchased from the Wacker Chemical Corp., Los Angeles. Figure 5 shows the reciprocal Hall coefficient versus reciprocal temperature plot for sample E-2 before irradiation. To facilitate easy interpretation of this data, it was normalized to the before irradiation results and replotted on a linear scale in Figure 7. The features of the change produced by irradiation of this sample are very similar to those shown in Figure 5 for sample E-4. The presence of both the Si-A center and the defect with a deeper level are implied after the irradiation. The introduction rate for Si-A centers in sample F-2 is approximately  $0.2 \text{ cm}^{-1}$ . This is the same as that found in sample E-4. It is also the same as that found in a quartz crucible sample (sample Q-2C, Figure 3) with similar lithium concentrations. After 800 hours at room

temperature, the results in Figure 5 indicate greatly reduced carrier concentration. The data also indicates a very much reduced concentration of defects with energy levels less than 0.32 eV (i.e., Si-A centers). The one significant difference between the results in sample F-2 and those in sample E-4 is the introduction rate of defect with deeper energy (about  $0.2 \text{ cm}^{-1}$  in former and  $0.08 \text{ cm}^{-1}$  in the latter case). It would appear that increased lithium concentrations cause higher concentrations of the subject defect to be formed during irradiation. The room temperature removal rates for several lithium-doped float zone specimens of varying lithium concentrations have been determined in an effort to clarify the nature of the deep lying level produced by irradiation. This data is shown in Figure 8. It is apparent that removal rate or introduction rate of the defect increases in a near linear manner of lithium donor concentration. Because of mass action principles, such a monotonic relationship indicates that lithium is involved in the structure of the defect under consideration. In addition to the previously discussed data, a dashed line is shown on Figure 8. The line represents the experimental relationship proposed by Pigneret for a very similar group of experiments.<sup>11</sup> The removal rates reported by Pigneret are higher by a factor of two than those reported herein. Despite this difference, the general trend of removal rate versus lithium donor concentration is very similar. Pigneret has proposed that the defect responsible for this carrier removal is a lithium-vacancy pair ( $\text{Li}_s$ ) with an energy level about 0.4 eV below the conduction band.

#### B. Carrier Removal Studies in Cells

Parallel studies of capacitance and electrical output were made on a quartz crucible cell, AF14-4921. The concentration of lithium donors at the junction ( $V_a=0$ ) and the short circuit current were studied during

irradiation and recovery at 100°C. This data is again shown in Figure 9. In general, the results are very similar to those of float zone cells, in that a large decrease of lithium concentration occurs simultaneously with a recovery of the degraded short circuit current. The point of interest is that during the irradiation of  $3 \times 10^{15} \text{ e/cm}^2$ , only  $2 \times 10^{13}$  carrier electrons/cm<sup>3</sup> are removed. This is an order of magnitude lower than that observed in float zone cells. Since the lithium lost during recovery is comparable to both float zone and quartz crucible silicon, one can assume that similar numbers of radiation induced recombination centers were present in both types of cells. Even if the damage centers are un-ionized, the small quantity of carriers removed during irradiation would not indicate a lithium loss adequate to allow a lithium atom in the structure of each damage center. This result tends to support the need for an entirely different model of the damage in the case of quartz crucible cells.

A more extensive analysis of the above sample was completed. By use of capacitance measurements, the donor concentration was determined at depths up to 5 microns into the n-type region. This data is shown in Figure 10. It can be seen that the small "loss of donors" during irradiation is a general condition which extends deep into the n-type region. The change which occurs during the 500 hour recovery period appears to vary greatly with distance into the cell. To permit a closer analysis of the data, it was converted into removal rates ( $dn/d\phi$ ) and plotted as a function of distance into the n-type region. The removal rates during irradiation and recovery are both shown in Figure 11 as a function of distance. It is readily apparent from this data that the low apparent removal rate ( $0.006 \text{ cm}^{-1}$ ) during irradiation extends deep into the n-type region. The removal rate during recovery rises very rapidly with distance. A different view of this data is



shown in Figure 12 where the two removal rates are plotted as functions of the lithium donor concentration at a point in the cell where the particular removal rate was determined. Two facts are apparent; the removal rate during irradiation is not a function of lithium concentration, and the removal rate during recovery is a very strong function of the lithium concentration.

The results of lithium-doped quartz-crucible cell irradiation can be explained with a model consistent with previously discussed Hall coefficient measurements. To explain the results in these cells, one needs to examine various parameters relating to various charge states in the cell. The Fermi level in the n-type region near the junction is 0.28 eV below the bottom of the conduction band. A further calculation indicates that the Fermi factor or fraction of ionization for Si-A centers is only 0.03. This means that if such defects were generated during irradiation, only 3% of the Si-A centers would be ionized. This ionized fraction would be the only portion detected by carrier removal measurements at room temperature. Assuming the above situation, the introduction rate of Si-A centers would actually be  $0.006/0.03$  or  $0.2 \text{ cm}^{-1}$ . This is the same value determined by Hall coefficient measurements, as discussed in the previous section. An identical analysis was made on a different lithium-doped quartz crucible cell (H3A 7249) which exhibited superior initial and recovered electrical output characteristics. Cells of this group will be discussed further in later sections of this report. The donor concentration as a function of barrier width for this cell is shown in Figure 13 and the removal rate data is shown in Figure 14. These results are very similar to those of cell AF 14-4921, except that

the lithium concentration is somewhat higher relative to the phosphorus concentration. It is also clear from Figure 14 that the removal rate during recovery increases value much higher than  $0.2 \text{ cm}^{-1}$  deep in the cell. Since the introduction rate of Si-A centers is believed to be  $0.2 \text{ cm}^{-1}$  in these cells, the data supports a model in which more than one lithium donor atom reacts to neutralize the defect complex.

Since the result of the capacitance measurements of removal rates during irradiation of lithium-doped quartz crucible cells strongly indicates that Si-A centers are formed, it would be interesting to examine similar measurements made on conventional p on n solar cells. The silicon "A" center is believed to be the major recombination center in the conventional p/n solar cell (quartz crucible silicon). In Figure 15 the donor concentrations, determined by capacitance measurements, are shown for a non-lithium solar cell (CEG 112) as a function of distance into the n-type base region. The measured carrier removal rate is constant throughout the distance investigated with a value of  $0.013 \text{ cm}^{-1}$ . Under the conditions in this cell, Si-A centers would be about 9% ionized. The actual introduction rate of "A" centers would be  $0.15 \text{ cm}^{-1}$ . This value is quite close to the value of  $0.2 \text{ cm}^{-1}$  which is calculated from similar measurements on lithium-doped quartz crucible solar cells. This result tends to support the previous conclusions that oxygen-vacancy pair (Si-A centers) play a prominent role in the degradation process of all p/n silicon solar cells.

In this section the changes in carrier concentration during and

after irradiation are analyzed for three lithium-doped, float zone solar cells of widely varying lithium concentrations. The current-voltage plot for Cell C3-18 is shown for several stages of irradiation and recovery in Figure 16. In Figure 17 the donor concentration as a function of distance into the n-type region is shown for the same cell in the same stages of irradiation and recovery illustrated in Figure 16. It appears the donor removal during irradiation is a strong function of distance into the n-type region. In addition the amount of donors removed during recovery for 200 hours is much larger than that removed during irradiation. After 400 hours the lithium donor concentration deep in the cell has risen somewhat, apparently from diffusion of lithium into this region. The increase in lithium concentration is probably the cause of the slight regradation in short circuit current which occurs between 200 and 400 hours after irradiation. The data relating to donor concentration changes is replotted in Figure 18 for various depths in the n-type region as a function of electron fluence. The data in Figure 18 indicates that the removal rate appears linear with electron fluence. The removal rate, however, increases rapidly with distance into the n-type region. The removal rate at the original edge of the space charge region ( $1.4\mu$ ) is only  $0.04 \text{ cm}^{-1}$ . Measurements made with barrier width at  $3.7\mu$  indicate a removal rate of  $0.206 \text{ cm}^{-1}$ . A five-fold increase in removal rate has occurred in a distance of only  $2.3\mu$  from the original unbiased space charge region.

Cell C3-18 is typical of a low lithium cell. The initial lithium concentration at the junction was  $3.8 \times 10^{14}$  atoms/cm<sup>3</sup>. A similar study will now be discussed for a cell with a somewhat higher lithium concentration. The solar cell current-voltage characteristic of Cell AF 14-4903 is shown in Figure 19 for several stages of irradiation and recovery. Figure 20 presents the results of the capacitance analysis during stages shown in Figure 19. In general, the donor concentration changes in Cell AF 14-4903 are very similar to those discussed for Cell C3-18. After 312 hours of recovery the donor concentration is approaching that of the original phosphorus concentration ( $2 \times 10^{14}$  atoms/cm<sup>3</sup>) of the silicon. To further analyze the data in Figure 20, the donor concentrations for specific widths of the space charge region (distance into the n-type region) is replotted in Figure 21 as a function of electron fluence. In Cell AF 14-4903 the removal rates found during irradiation are somewhat higher than those found in Cell C3-18. A rapid increase in removal rate is also noted with increases in barrier width.

An additional cell (T4-10) with a much higher lithium concentration was studied in the same manner. The current-voltage relationships are shown for before and after irradiation and after recovery in Figure 22. The lithium concentrations as a function of barrier width for Cell T4-10 are shown in Figure 23. In this cell the lithium concentrations are large enough at all depths to allow recovery without making major changes in the lithium concentration. It can be noted that the lithium loss during irradiation is exceeded by that during recovery by 50 to 100%. This data is of importance in formulating a physical model for the process. The removal rates during the irradiation of Cell T4-10 at various distances into the n-type region are shown in Figure 24. Similar data is also shown for Cells AF 14-4903, C3-18,

and C5D-100. Figure 24 provides graphic example of the extreme variation of removal rate (during irradiation) with depth that is possible within this type of solar cell. These variations may, in part, be responsible for the wide differences in removal rate reported by different investigators. The exact reason for this pattern of removal rate is not clear. The trend can be roughly described as a tendency for the removal rate to go to zero at the position of zero barrier width and rise rapidly from this value in some manner directly related to the lithium donor concentration. To further clarify this relationship the removal rate data was replotted versus the lithium concentration at the point in the cell at which the rate was determined. It is very obvious from the data in Figure 25 that certain lithium concentrations will not result in a specific removal rate. A particular point of interest regarding Figure 25 is that removal rate data for Cell AF 14-4903 and T4-10 do show near linear behavior in respect to lithium concentration. The fact that the individual curves are considerably displaced indicates the presence of some other strong factor in the determination of the removal rate. It is possible that distance from the space charge region edge and lithium concentration both act to determine the removal rate during irradiation of lithium-doped float zone silicon cells. It is reasonable to expect the lithium concentration to affect the removal rate during irradiation. Simple mass action principles suggest that areas with higher concentrations of lithium donors should capture more displacement produced vacancies before annihilation than similar areas of lower lithium concentration. It is more difficult to postulate an independent effect which would cause the apparent defect production rate to be so low adjacent to the space charge region and increase so rapidly with distance from the barrier.

To more graphically show the differences in lithium concentration and gradient, the pre-irradiation donor concentrations and gradients for all float zone silicon cells studied are shown in Figure 26. It can be seen from the data that the gradient of lithium concentration ( $\Delta N/\Delta W$ ) appears to vary directly with the lithium donor concentration at the edge of the space charge region. To further explore this variation, the analytical relationship was derived for linear graded junction (i.e., one with a voltage-capacitance relation of  $VC^3 = k$ ). Since the precise  $VC^3 = k$  relationship is not always found in lithium-doped cells, the derivation is not general for all cells. If the space charge region is assumed to expand to both sides when a reverse bias is applied, the relationship is:

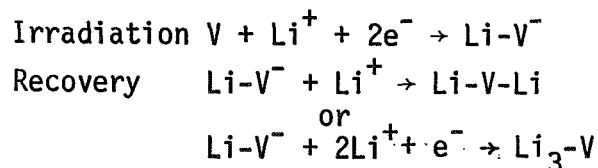
$$\frac{dN}{dW} = \sqrt{\frac{2q}{3\epsilon V}} N^{3/2}$$

If the space charge region is assumed to be constrained as one edge, but expands into a graded region at the other edge, the relationship is:

$$\frac{dN}{dW} = \sqrt{\frac{16q}{3\epsilon V}} N^{3/2}$$

In Figure 27 these relationships are shown along with experimental data determined by RCA and TRW Systems. The two TRW points were from cells with close to  $VC^3 = k$  behavior. This information was not available for the RCA cells. Although there is considerable scatter in the data, there is some experimental basis for treating the gradient as being proportional to three halves power of the lithium donor concentration at the edge of the junction.

The results tend to support the following model of the damage and recovery processes. The model is as follows:



The data which supports this model is as follows:

1. Lithium donors apparently react with displacement products.
2. Lithium apparently reacts with defect complexes during the recovery.
3. The lithium consumed during recovery is roughly equal to or greater than that consumed in irradiation.

C. Defect Structures in Cells

In our previous final report, the possibility of using the frequency dependence of solar cell capacitance in the study of radiation defects was explored. This technique has recently been used to study lithium solar cells. The results of this experimentation appear to be very significant, and should provide an excellent means of study in the future. In this measurement the region of the solar cell space charge region is caused to widen and contract under a high frequency voltage. When deep lying energy levels are present, under certain conditions of frequency and temperature, these defects are not able to change their charge state rapidly enough by thermal emission and capture as the space charge region passes through their position. This difficulty provides a relaxation effect which can be studied to determine the energy levels of defects present. This behavior is illustrated by the data in Figure 28. In this work lithium-doped quartz crucible silicon solar cells were studied in the unirradiated and irradiated conditions by capacitance measurements at temperatures from 27°C to -190°C and frequencies of 5 KHz to 400 KHz. In the case of a typical lithium-doped solar cell the donor concentration at the edge of the space charge is related to the capacitance in the following expression:

$$N_D = \frac{S V C^2}{q \cdot \epsilon}$$

All of the factors in this expression are constant before and after irradiation except S, which is related to exponent of the  $k = VC^n$  relationship of

the cell. In this case the "S" factor was observed to be unchanged by irradiation. For this reason changes in donor concentration caused by irradiation can be studied by examining the changes in the square of the ratio of capacitance after irradiation to that observed before irradiation. This parameter is plotted on the ordinate of Figure 28. Examination of the data indicates that at higher temperatures no frequency dependence is observed. As the sample temperature is reduced a divergence in the data for various frequencies is observed. The lower frequency (5 KHz) capacitance values diverge first as the sample temperature is decreased, followed by those of higher frequency at still lower temperatures. At  $-190^{\circ}\text{C}$  ( $1000/T=12$ ) the capacitance variation with frequency again converges. The behavior in general is indicative of deep lying traps produced by the electron irradiation. The point at which the transition from maximum to minimum donor population is half complete is marked for each frequency used. This point is defined as the cutoff frequency at that particular temperature. It can be assumed that the reciprocal of the cutoff frequency is proportional to the relaxation time of the electronic capture process dominating the process.

$$\tau = k \frac{1}{f_c}$$

The relaxation time of such processes can be determined from statistical considerations. In a case which can be described as a net loss of donors, the expression would be

$$\tau = 1/C_n N_c \exp [-\Delta E/kT]$$

To facilitate the analysis we have assumed the reciprocal of the cutoff frequency is equal to the relaxation time. To determine the energy level of the centers involved in the relaxation ( $\Delta E$ ), an activation energy plot is presented in Figure 29. In order to construct a plot in which the slope



will directly reflect the value of  $\Delta E$ , the relaxation time corrected by the density of states is plotted versus the reciprocal temperature. The data indicates the value of  $\Delta E$  to be 0.17 eV. Since this value is also identified with the ionization energy of the Si-A center, these measurements add more support to previously discussed evidence indicating that the primary defect produced during irradiation of lithium-doped quartz crucible silicon solar cells is the oxygen-vacancy pair or Si-A center. Certain factors such as spin degeneracy, temperature dependence of capture cross-section, and width of the space charge region have been neglected in this analysis. It is believed that consideration of such factors would not significantly alter the conclusions. The same analysis was repeated after the cell was allowed to recover for 250 hours at 100°C. This data is also shown in Figure 28. The data reflects a drop in the population of the 0.17 eV level defect and also a decrease in the lithium donor concentration.

A variable frequency capacitance study was also done on a lithium-doped float zone solar cell. The cell used was C5D-100. The cells of this group will be more fully discussed in other sections of this report. This cell was irradiated with a fluence of  $1.5 \times 10^{15}$  1 MeV e/cm<sup>2</sup>. The capacitance data is shown in Figure 30. This cell exhibits a much wider variation of capacitance with frequency after irradiation than that shown in Figure 28. At temperatures slightly lower than room temperature the capacitances for various frequencies begin a wide divergence, which again converges at lower temperatures at a capacitance value less than 90% of the original values. The pattern is indicative of the presence of a radiation produced deep lying energy level. The temperatures at which critical frequencies are reached are plotted in Figure 31 in a manner to indicate the position of the energy level of the defect under study. The slope in Figure 31 suggests an energy

level 0.54 eV below the bottom of the conduction band. Since measurements made by other means have indicated the presence of a deep lying level in irradiated lithium-doped float zone silicon, it may be that data concerns the same defect. It is also of interest to note that the presence of the 0.17 eV level is not indicated by the data in Figure 30. Presence of the 0.17 eV level in sample C5D-100 would be difficult to detect because of the large change in capacitance caused by the deep level defect. It is also of interest to note that the capacitance values for various frequencies also appear to diverge with temperatures above 300°K. There is not sufficient data to determine if this indicates the presence of a second defect level.

#### D. Lithium Counterdoping of P-Type Silicon

The benefits of radiation hardening by lithium doping have been so far confined to n-type silicon. This is an unfortunate circumstance, as n-type silicon is inherently more prone to displacement type radiation damage than is p-type silicon. Lithium doping has made n-type silicon competitive and in some cases superior to p-type silicon in regard to radiation hardness. A much more desirable situation would be to further increase the radiation hardness of p-type by lithium or any other type of doping. In an effort to determine if any such advantage does in fact exist, we have fabricated p-type silicon which is counterdoped by the diffusion of lithium. The results of electrical measurements made on a few p-type lithium counterdoped samples are summarized in Table 1. Two of these samples were made with quartz-crucible silicon and the other from float zone silicon. In all cases the resistivity after lithium diffusion is much higher than the original resistivity of the crystal. This is evidence that many of the boron donors originally present in the crystals have been compensated by

the presence of the lithium donors. This compensation was also confirmed by Hall coefficient measurements. The boron and lithium concentrations shown in Table 1 were determined in this manner. The Hall mobility of each specimen after the lithium diffusion is also shown. It can be noted that the mobilities shown are relatively low for samples of the resistivities exhibited after lithium diffusion. This is because mobility reflects the total concentration of scattering centers (i.e., both boron and lithium ion cores). The mobilities shown are more typical of the original crystal, since the possible scattering center population has been increased although the net carrier concentration in the valence band has been decreased. For this reason a lithium compensation diffusion of a p-type crystal will raise the Hall coefficient and decrease the Hall mobility. A large decrease in mobility may not be detected because of pairing of the lithium and boron atoms. The significant point is that p-type silicon can be lithium counter-doped to achieve resistivities of interest to the device designer and lithium concentrations which could be of importance in radiation hardening.

In an effort to obtain some indication as to possible hardening mechanisms, the p-type lithium doped silicon samples discussed in Table 1 were irradiated with 1 MeV electrons. In this work only the Hall coefficients and resistivity were monitored. In this way any radiation induced reactions which affect majority carrier behavior can be detected. Although this does not measure the minority carrier lifetime, similar measurements in n-type reflect the reaction of lithium with the radiation generated defect complexes. In Figure 32 the hole concentration of sample Li-P-Q.C.-1-1 is plotted versus electron fluence. After an irradiation of  $3 \times 10^{16}$  e/cm<sup>3</sup> the sample was stored at 100°C. The slightly elevated temperature was used because of the known reduction of effective diffusion constant of lithium in quartz crucible silicon.

As shown in Figure 32 the hole concentration was significantly increased during the storage at 100°C. Since defects in p-type silicon do not normally anneal at this temperature, it appears that lithium may have reacted with some of the defects generated during the irradiation to annihilate them. In this p-type of sample, a decrease in lithium donors causes the hole concentration to increase because of the lowered compensation. These results are by no means conclusive, but do indicate that further work is warranted.

The data shown in Figure 33 relates to a similar sample which was lithium counterdoped to a much higher resistivity (Li-P-Q.C.-10-4). In the sample the removal rate during irradiation was  $0.03 \text{ cm}^{-1}$  which is similar to that of ordinary boron-doped silicon. In this sample the hole concentration also increased during storage at 100°C. The initial increase was larger than that of the previous sample; however, after 40 hours at 100°C the hole concentration decreased to less than that observed after the irradiation. The nature of this change is not clear at this time.

The data in Figure 34 represents our only study to date on p-type lithium counterdoped float zone silicon (Table 1). This material is of interest, in this case, because of the lower oxygen concentration. This lower oxygen concentration may allow any lithium reactions occurring to be observed in a shorter period of time at room temperature. In Figure 34 the hole concentrations before and after irradiation are plotted on the ordinate of the graph. The hole concentrations at various times after completion of the irradiation are shown in the figure. It is apparent that after the decrease of hole concentration caused by irradiation, a large time-dependent increase in hole concentration occurs. The hole concentration reaches a maximum of 40 hours after irradiation and then declines somewhat from the

maximum. The magnitude of the hole increase observed with time is much greater than that of the decrease which occurred during irradiation. It is difficult to give a full explanation of these effects on the basis of this limited work. It does appear that in some way, irradiation of this material initiates a time dependent reaction, probably involving lithium donors, which results in a very significant increase in the hole concentration. Because of equilibrium considerations involving boron, this loss of donors can not be explained as a simple precipitation of lithium. In view of the known behavior of annihilation of recombination centers in n-type, the behavior of annihilation of recombination centers in n-type, the behavior observed in p-type lithium compensated silicon strongly suggests that similar reactions between lithium and recombination centers may also occur in p-type silicon. If this is in fact the case, the development of lithium-doped n on p solar cells with a highly superior radiation resistance may be within practical achievement. Further work in this area appears to be warranted, although Pignoret's results are not encouraging.<sup>11</sup>

#### E. Large Substitutional Dopants in Silicon

We have previously evaluated silicon doped with larger substitutional atoms in regard to a possible radiation hardening mechanism. In previous work, a single crystal silicon - 13% germanium alloy was grown by the quartz crucible technique.<sup>5</sup> This alloy crystal was doped with boron in the usual manner to produce an 8 ohm-cm p-type crystal. This material was fabricated into solar cells and evaluated for radiation resistance. The cells produced from this alloy were satisfactory in regard to photo output, but proved to be more prone to radiation damage than conventional n on p cells. The basis for this work was as follows. The vacancies produced by the energetic particles are surrounded by a tensile strain field. Substitutional atoms larger than silicon atoms are surrounded by a compressive

strain field. If radiation produced vacancies could be trapped by large substitutional atoms, due to the lowering of their collective strain energy, the vacancies would be prevented from forming complexes which are recombination centers. This logic is in error in the case bismuth since a vacancy trapped next to a bismuth atom is simply a Si-E center (i.e., a possible recombination center). In the case of germanium the strain field is limited because that atom is only 3% larger than silicon.

Our current effort involved two silicon crystals doped with larger substitutional atoms. Both crystals were grown from quartz crucibles. One crystal was n-type silicon doped with bismuth to a resistivity of 0.5 ohm-cm, The other crystal was a p-type silicon - 0.5% tin alloy doped with boron to 20 ohm-cm.

We are indebted to Peter Iles of Centralab Semiconductor Division who fabricated several wafers of these two crystals into solar cells for evaluation. The two groups of cells were evaluated by monitoring the short circuit current with a one sun equivalent of tungsten illumination during a 1 MeV electron irradiation. The data from this work is presented in Figure 35. The behavior of typical p/n and n/p solar cells are also shown as dashed lines in Figure 35. The short circuit currents of the bismuth cells (2,5) are slightly higher during irradiation than that of a comparable p/n cell. This difference does not appear to be of any practical significance. In the case of the silicon-tin alloy cells (A4, B2), they appear to degrade under electron fluence well before the comparable n/p cells which are in common use today. In view of these results it must be concluded that little or no practical hardening advantage can be achieved by addition of large substitutional atoms to the silicon lattice. In fact the addition of the large neutral substitutional atoms to p-type silicon appears to promote the

formation of more or more effective recombination centers. No further work is planned in this area.

### III. LITHIUM SOLAR CELL EVALUATION

In this phase of the program lithium-doped solar cells from the three manufacturers, Centralab, Heliotek, and Texas Instruments, have been irradiated with electrons and their recovery characteristics have been studied. Several different processing experiments were represented in these cells, including an oxygen layer adjacent to the junction, lithium diffused through both front and back surfaces, phosphorus  $n^+$  layer near the junction, and cells processed from whole slices. The groups evaluated are listed, along with their material and processing variables, in Table I.

Most of the cells received a radiation exposure of  $3 \times 10^{15}$  e/cm<sup>2</sup> at 1 MeV. Tungsten I-V characteristics and capacitance versus voltage measurements were then obtained as a function of time at either room temperature or 100°C. The general radiation damage and recovery characteristics of each group of cells are summarized in Table II. The recovered levels given in the table are the peak of the recovery curve and do not take into account any redegradation that may have occurred. The one-half recovery time is the time necessary for the short circuit current to reach a point midway between the damaged level and the peak recovery level. In general it can be observed that the higher lithium concentrations result in lower initial characteristics, higher recovered levels, and more rapid annealing rates while with lower lithium concentrations, higher initial levels and slower recovery rates exist.

In Table III, the peak recovery levels are compared graphically with each other and with the equivalent damage level for contemporary 10  $\Omega$ -cm n/p solar cells. The spread of the data and the half recovery time are also

shown. It should be noted that most cell groups tested here are not only inferior in recovered level to the best groups tested previously but are also no improvement over contemporary n/p cells.

A. Centralab Cells

In Centralab groups C8A through C8D, the important feature is an oxygen-rich layer approximately 1 mil thick formed by diffusion in an oxidizing atmosphere prior to formation of the  $p^+$  layer. The hope was that this oxygen layer would prevent redegradation of the recovered level without affecting the bulk-dependent rapid recovery in float zone and Lopex material. However, in both the float zone cells (C8A and C8B) and the Lopex cells (C8C and C8D) the oxygen layer slowed the recovery rates by more than two orders of magnitude (see Figures 36 and 37) at room temperature. This is reasonable since the capacitance data in Table 1 indicate lithium concentrations of an order of magnitude less in the oxygen layer cells than in the non-oxygen layer cells for both materials.

To find out if recovered levels were stabilized it was necessary to accelerate the recovery process for half of the cells by annealing them at 100°C. No noticeable stability improvement was seen for the float zone cells, but in the Lopex case much less (2% versus 25%) redegradation was observed in the oxygen layer cells as compared to the non-oxygen layer cells after 1000 hours.

Centralab groups C8E through C8H had lithium diffused through the  $p^+$  layer on the front of the cells as well as through the back. The reasons for this experiment are to prevent excess lithium concentrations and severe lithium gradients. The initial outputs of the float zone cells (C8E and C8F) were so poor, about 30 ma. for C8E, that they were not included in the testing program. The crucible grown cells (C8G and C8H) had fairly good



initial outputs, were irradiated, and were annealed at 100°C (Figure 38). Lithium concentrations in the front-back diffused cells were 3 to 10 times higher than in the back-only cells, and as expected, they annealed faster. However, the front-back diffused cells did not recover as far as expected with peak short circuit currents of only 30 ma. compared to 33 and 38 for the back-only cells.

#### B. Texas Instruments Cells

The Texas Instruments solar cell groups (T9 and T10) were processed from whole slices to eliminate potential edge effects due to non-uniform lithium concentrations. In addition, the lithium diffusion was designed to produce half the lithium concentration of Texas Instruments standard lithium cells in the T9 group and twice the standard concentration in the T10 group. The capacitance measurements confirm this plan, indicating a factor of four in lithium concentration between the two groups. Recovered levels for both groups (Figures 39 and 40) are disappointing, however, as neither cell group reached 35 ma. while last year's T6 group reached 40 ma. As expected, the annealing rate of the T10 group is far faster than that of the T9 cells, but this rapid recovery is associated with a significant redegradation, about 35% after 700 hours. It is concluded, as in last year's final report, that the reducing of edge effects does not improve recovery performance.

#### C. Heliotek Cells

Heliotek solar cell group (H8) has a phosphorus  $n^+$  layer diffused near the junction prior to the boron  $p^+$  diffusion. Except for this additional phosphorus layer, these cells were identical to the H4 group tested last year. The H8 cells have recovered a few milliamps farther (37 versus 33) than the H4 cells, but at a factor of four more slowly (Figure 41). The H7 cells tested last year and several other Heliotek groups are superior in

recovered level with the best between 40 and 45 ma. and recovery rates similar to those for the H8 cells (Table IV).

The recovery characteristics of the most recent groups of cells, H3A (325/480, H9 (425/90/60), and H10 (425/90/60), have been determined as a function of time and temperature after irradiation with 1 MeV electrons and compared with the best of previous cell groups. A brief summary of the comparison is presented here separately for the crucible and float zone base material. The best prior groups of crucible cells annealed at 100°C are shown in Table V. Although the H14 group was not constructed specifically for this program, it represents one of Heliotek's better crucible groups and is included here for comparison purposes. The two new groups, H10 and H3A, exhibited recovery levels of 38-40 ma. and 40-41 ma., respectively, with half-annealing times of 1 hour at 100°C. In addition, the H3A group exhibited higher initial outputs than any prior group of lithium doped cells tested to date which possessed annealable characteristics. As indicated, the recovered short circuit current levels are slightly lower for the latter groups compared to the best prior data which were represented by the T2 and T7 groups; however, the H3A group exhibited less curve factor degradation and to date less redegradation effects than the prior groups, which would indicate overall superiority in terms of preservation of maximum power output. It is of interest to note that the longer time, lower diffusion temperature groups are continuing to exhibit characteristics competitive with or better than the best of the shorter time, higher diffusion temperature groups. (See Tables II-V, Figures 42-45).

A similar comparison can be made for the recovery characteristics at room temperature of float zone lithium doped cells. As in the previous comparison, all of the groups of cells were not directly associated with

this particular contract, but are included as being representative of the state-of-the-art. The best yet groups are shown in Table V. The new groups now under study are H9 (425/90/60) with maximum recovered level of 38 ma. in half-annealing time of 5 hours. Although we have not yet tested any recent long time, low temperature diffused float zone lithium cells, there appears to be a measurable difference, though slight, in the superiority of the 120 minute redistribution over the 60 minute redistribution. The new groups of cells have not to date exhibited any detrimental curve factor decay or redegradation. (See Tables II-V, Figures 46-47).

A study was also made of annealing rates at various temperatures for irradiated lithium-doped quartz crucible solar cells. The cells studied this year (H3A and H10) appear to be consistent with data developed under previous contract.<sup>8</sup> The combined data is shown in Figure 48. In this figure the reciprocal of the half time for recovery, based on short circuit current changes, is plotted versus the reciprocal of the annealing temperature. Also shown on this figure are dashed lines representing slopes of exponential relationship with activation energies of 0.63 eV and 1.10 eV. The relative positions of the dashed lines in Figure 48 are arbitrary and of no significance. The most recently proposed value for the activation energy of lithium diffusion in silicon is 0.63 eV. Pell has shown that the presence of oxygen in silicon reduces the effective diffusion coefficient of lithium in the following manner:<sup>13</sup>

$$D_{\text{eff}} = \frac{D}{1 + \frac{[O]}{C}}$$

where:  $D = 2.65 \times 10^{-3} \exp(-0.62\text{eV}/kT)$

$C \approx 4 \times 10^{23} \exp(-0.52\text{eV}/kT)$

[O] = the concentration of oxygen in solution

Using the above relationship, the effective diffusion coefficient for lithium was calculated for silicon with various concentrations of oxygen present. This information is shown in Figure 49. It is clear that the apparent activation energy of lithium diffusion can vary between 0.63 and 1.10 eV depending on the oxygen concentration of the silicon. Since the oxygen concentration of quartz crucible silicon is typically  $5 \times 10^{17}$  atoms/cm<sup>3</sup>, it is reasonable to expect the apparent activation energy of recovery in cells made from quartz crucible silicon to be 1.10 eV. Most of the cell data in Figure 48 closely approaches an apparent activation energy of 1.10. The data of cells of the T7 group is not considered significant because the higher temperature half recovery times are approaching limits of accuracy involved in this experiment. The wide variation in behavior of various groups is due to the wide differences in lithium concentrations found between the different groups.

An additional observation can be made regarding the behavior shown in Figure 49. In some early work Wysocki determined the apparent activation energy for the recovery process in irradiated lithium-doped float zone silicon. A compilation of several samples indicated an activation energy of 0.61 eV for recovery near room temperature. This value is nearly identical to that of lithium diffusion. Considering the relationships in Figure 49, Wysocki's data indicates that float zone silicon typically has much less than  $5 \times 10^{15}$  oxygen atoms/cm<sup>3</sup> in solution. Pell proposed a more specific method of using lithium diffusion to determine the oxygen concentration of silicon.<sup>13</sup> Pell's method utilized the kinetics of lithium precipitation rather than kinetics of radiation recovery.

Several trends seem to be evident in the summary presented above of cells fabricated over the last two years. First it appears that the 325°C,

480 minute diffusion consistently produces cells which are equal to the best produced with the higher temperature, longer time diffusion, whereas the average response over all the cells produced with the latter diffusion schedule is considerably poorer and widely variant. Other variables, such as initial resistivity, paint-on versus evaporated source, inclusion of an  $N^+$  layer, and variation of parent dopant do not seem to have measurable or significant effects on overall cell performance.

#### D. Solar Simulator Measurements

The majority of the I-V curves obtained in the evaluation program have been obtained using tungsten illumination because of its convenience, reliability, and amplification of radiation induced degradation. In addition, the majority of the annealing data has been taken at the short circuit current point. Although most cell groups exhibit stable I-V characteristics allowing qualitative linear comparisons for anticipated responses, under solar simulation, the quantitative magnitude of the annealing performances under solar simulation is difficult to extrapolate for the lithium cell. For these reasons, solar simulator measurements have been performed on a selected number of cell groups which are representative of the most superior lithium doped p/n cells evaluated to date. The pre-irradiation, post-irradiation, and after-annealing maximum power points have been plotted in Figure 50. The annealing rate curves shown are the same as those observed under tungsten illumination and are assumed to have been the same under solar simulation. As is indicated in the curves, the pre-irradiation initial efficiencies are competitive with contemporary n/p solar cells and the annealed outputs are in every case superior to the contemporary n/p cell after  $3 \times 10^{15}$  e/cm<sup>2</sup>. There is, however, a wide divergence in annealing rates which is probably due to differences in oxygen concentration among the

various groups. It is of interest to note that of the three groups presented, two of them were fabricated utilizing the slower 325°C/480 minute diffusion schedule. This data confirms that significant progress has been made in the last several years in the generation of a technology to manufacture high efficiency stable lithium doped p/n cells which exhibit superior radiation resistance after annealing relative to the contemporary 10 ohm-cm n/p cell.

#### IV. SUMMARY

Experimental data regarding the behavior of lithium in irradiated silicon has been accumulated by several methods. The results obtained by different methods tend to confirm the same model for the damage. The model for the damage appears to be significantly different in float zone and quartz crucible silicon. For this reason it is logical to discuss the model for each material separately.

##### A. Lithium-Doped Quartz Crucible Silicon

1. The Hall coefficient studies of the irradiation of this material with energetic electrons indicate that acceptor type defects with an energy level 0.17 eV below the conduction band are formed.

2. The introduction rate of this defect is  $0.2 \text{ cm}^{-1}$ .

3. Subsequent annealing or recovery at 100°C, reduces the concentration of the subject defects and a simultaneous decrease in lithium donor concentration.

4. The decrease in lithium donor concentration during recovery exceeds the decrease of 0.17 eV level defects by a factor which is approximately two.

5. The 0.17 eV level defect appears to be the Si-A center (i.e., oxygen-vacancy pair).

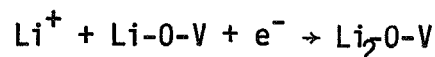
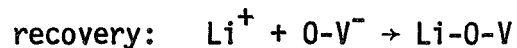
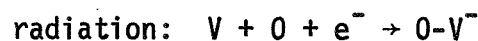
6. Capacitance-voltage measurements on solar cells indicate that little or no lithium reacts in the formation of defect complexes during irradiation.

7. The carrier removal during irradiation of cells is  $0.005 \text{ cm}^{-1}$ . Considering the position of the Fermi level, the value is consistent with the production of 0.17 eV level defects with an introduction rate of  $0.2 \text{ cm}^{-1}$ .

8. Capacitance-voltage measurements on cells indicate that the concentration of lithium donor reacting during the recovery stage is roughly equal to twice the projected concentration of 0.17 eV level defects.

9. Capacitance-frequency measurements on cells indicate that a defect with an energy level 0.17 eV below the bottom of the conduction band is formed during irradiation.

10. All measurements support following defect reaction model:



#### B. Lithium-Doped Float Zone Silicon

1. The Hall coefficient studies of the irradiation of this material also indicate the formation of a defect with an energy level 0.17 eV below the conduction band and an introduction rate of  $0.2 \text{ cm}^{-1}$ .

2. The 0.17 eV level defect appears to be the Si-A center (i.e., oxygen-vacancy).

3. In addition to this defect, a different defect with deeper lying level is formed during the irradiation of this material.

4. The introduction rate of this deep lying level is roughly proportional to the concentration of lithium donors present.

5. This behavior strongly suggests that the structure of the deep lying level involves a lithium-vacancy pair.

6. The amount of lithium donors which react during the recovery is significantly greater than the concentration of defects which form during irradiation.

7. Capacitance-voltage measurements on solar cells indicate carrier removal characteristic of the formation of deep lying levels during irradiation.

8. Removal rates measured by capacitance tend to approach zero at a zero barrier width, and increase with distance into the active region of the cell base.

9. These removal rates are also roughly proportional to the concentration of lithium donors.

10. The quantity of lithium donors reacting during the recovery period greatly exceeds that which reacts during irradiation.

11. Capacitance-frequency measurements on solar cells indicate that a deep lying level, 0.54 eV below the bottom of the conduction band.

### C. Solar Cell Evaluation

It is possible to fabricate excellent lithium-diffused solar cells from either float zone or quartz crucible silicon. When lithium diffused solar cells are fabricated with an optimum diffusion schedule, they are superior in radiation resistance to contemporary n/p cells after electron irradiation of  $3 \times 10^{15}$  e/cm<sup>2</sup>. Such irradiated and recovered lithium cells will produce 10 to 20% more power than a similarly irradiated contemporary n/p solar cell. The lithium diffusion schedules which have produced the best cell studied in this period are:



<u>Temperature</u>	<u>Time</u>	<u>Redistribution</u>
425°C	90 min	60 min
325°C	480 min	0 min

Other fabrication techniques evaluated during the year such as oxygen layer, phosphorus layer, whole slice, front and back lithium diffusion, did not produce any superior results or advantages.

V. PROGRESS IN THE NEXT REPORT PERIOD

During the next report period the irradiation evaluation of JPL-furnished solar cells will be continued. Hall coefficient measurements will be made to further support the damage model. Capacitance measurements will be refined to allow more complete analysis of changes in lithium concentration in the cells. Studies of p-type lithium counterdoped silicon will be expanded to include minority carrier behavior.

VI. NEW TECHNOLOGY

There is no new technology reported for this period.

VII. PAPERS AND PUBLICATIONS GENERATED

Accepted for Publication

Title: "Effect of Electron Irradiation on Lithium-Doped Silicon"

Journal: International Journal of the Physics and Chemistry of Solids

Accepted for Presentation

Title: "Role of Lithium in Irradiated Solar Cells"

Meeting: International Colloquium on Solar Cells, Toulouse, France,  
6 July 1970

Title: "Role of Lithium in Irradiated Solar Cell Behavior"

Meeting: Eighth Photovoltaic Specialists Conference, Seattle, Wn.,  
11 August 1970.

REFERENCES

1. V. S. Vavilov, "Radiation Damage in Semiconductors", p. 115, Academic Press, N.Y. (1964)
2. J. J. Wysocki, IEEE Trans. on Nuclear Science NS-13, 6, 168 (1966)
3. J. R. Carter, Jr., and R. G. Downing, Proc. of the Sixth Photovoltaic Specialists Conference, Vol. III, p. 145 (1967)
4. G. Brucker, et al., RCA Progress Report, Contract No. NAS5-10239 (1968)
5. R. G. Downing, et al., Final Report, Contract No. NAS5-10322 (1968)
6. G. Brucker, et. al., RCA Final Report, Contract No. 952249 (1969)
7. P. H. Fang, et. al., Appl. Phys. Lett. 12, 3, 57 (1968)
8. R. G. Downing, et. al., TRW Final Report, Contract No. 952251 (1969)
9. V. S. Vavilov, et. al., J. Phys. Soc. Japan 18, III, p. 236 (1963)
10. J. E. Stannard, Appl. Phys. Letts, 15, 3, 93 (1969)
11. J. Pigneret, Thesis, University of Lyon (1968) (Available from: Institute de Physique Nucleaire, 43, Boulevard du 11 November 1918, 69 Villeurbanne, France).
12. B. Pratt and F. Friedman, J. Appl. Phys. 37, 4, 1893 (1966)
13. E. M. Pell, Solid State Phys. in Electronics and Telecommunications, Vol. I, p. 261, Academic Press, N.Y. (1960)
14. J. J. Wysocki, IEEE Trans on Nuclear Science, NS-14, 6, p. 103 (1967)

TABLE I. SUMMARY OF P-TYPE LITHIUM COUNTERDOPED SAMPLES

<u>Sample</u>	<u>Orig. Crystal</u>	<u>Boron Conc.</u>	<u>Lithium Diff. Crystal</u>	<u>Lithium Conc.</u>	<u>Hall Mobility</u>
Designation	Type, resistivity	atoms/cm <sup>3</sup>	Type, resistivity	atoms/cm <sup>3</sup>	cm <sup>2</sup> /volts sec.
Li-P-Q.C.-1-1	p, 0.1 ohm-cm, Q.C.	8x10 <sup>17</sup>	p, 1.3 ohm-cm	4x10 <sup>17</sup>	175
Li-P-Q.C.-10-4	p, 1.8 ohm-cm, Q.C.	8x10 <sup>15</sup>	p, 26 ohm-cm	7.5x10 <sup>15</sup>	290
Li-P-F.Z.-10-3	p, 1.5 ohm-cm, F.Z.	1x10 <sup>16</sup>	p, 8 ohm-cm	0.8x10 <sup>16</sup>	300

Cell Group	<u>Base Material</u>		Resistivity $\Omega$ -cm	<u>Lithium Introduction</u>		
	Material Type	Dopant		Diffusion Schedule $^{\circ}$ C/Min/Min	Li Concentration at Junction $\text{cm}^{-3}$	
C8A	F.Z.	P	100	400/120	$3 \times 10^{14}$	Oxygen Layer
C8B	F.Z.	P	100	400/120	$4 \times 10^{15}$	Without Oxygen Layer
C8C	Lopex		90	400/120	$6 \times 10^{14}$	Oxygen Layer
C8D	Lopex		90	400/120	$4 \times 10^{15}$	Without Oxygen Layer
C8E	F.Z.	P	100	400/10	$> 1 \times 10^{16}$	Li Diffused Front and Back
C8F	F.Z.	P	100	400/120	$4 \times 10^{15}$	Li Diffused Back Only
C8G	Cruc.	As	30	400/10	$1 \times 10^{15}$	Li Diffused Front and Back
C8H	Cruc.	As	30	400/120	$< 10^{14}$ & $3 \times 10^{14}$	Li Diffused Back Only
H8	F.Z.	P	100	425/90/60	$6 \times 10^{14}$	Phosphorus Layer
H9	F.Z.	P	20	425/90/60	1.2 to $10.5 \times 10^{14}$	
H10	Cruc.	P	20	425/90/60	2.2 to $6.3 \times 10^{14}$	
H3A	Cruc.	P	20	325/480	0 to $4.1 \times 10^{14}$	
T9	Lopex	P	$> 50$	325/480	$9 \times 10^{14}$	Processed from Whole Slices
T10	Lopex	P	$> 50$	400/135	$4 \times 10^{15}$	Processed from Whole Slices

Table II: Lithium Solar Cell Manufacturing Parameters

CELL GROUP	$N_{Li}$ $cm^{-3}$	Annealing Temp. °C	Initial Level $I_{SC}$ , ma.	Damaged Level $I_{SC}$ , ma.	Recovered Level $I_{SC}$ , ma.	Time (hrs.) to 1/2 Recovery Point
C8A	$2 \times 10^{14}$	25	50	21	Not Yet Peaked	
	$4 \times 10^{14}$	100	47	18	36	< 1
C8B	$4 \times 10^{15}$	25	42	16	33	4
C8C	$5 \times 10^{14}$	25	51	20	Not Yet Peaked	
	$7 \times 10^{14}$	100	50	18	35	< 3
C8D	$4 \times 10^{15}$	25	50	18	33	1.2
C8G	$1 \times 10^{15}$	100	52	16	30	< 3
C8H	$10^{14}$ & $3 \times 10^{14}$	100	60 & 48	25 & 17	38 & 33	7 & .5
H8	$6 \times 10^{14}$	25	37	22	36	12
H9	$9 \times 10^{14}$	25	45	22	38	5
H10	$4 \times 10^{14}$	100	54-58	22-24	38-40	1
	$4 \times 10^{14}$	60	49-55	22	38-40	30
H3A	$3 \times 10^{14}$	100	52-64	21-27	40-41	2
	$3 \times 10^{14}$	60	53-61	22-27	38-42	70
	$2 \times 10^{14}$	25	59	23-25	---	--
T9	$9 \times 10^{14}$	25	53	15	33	20
T10	$4 \times 10^{15}$	25	47	18	30	< 1

TABLE III. Lithium Solar Cell Recovery Characteristics After  $3 \times 10^{15}$  e/cm<sup>2</sup>, 1 MeV

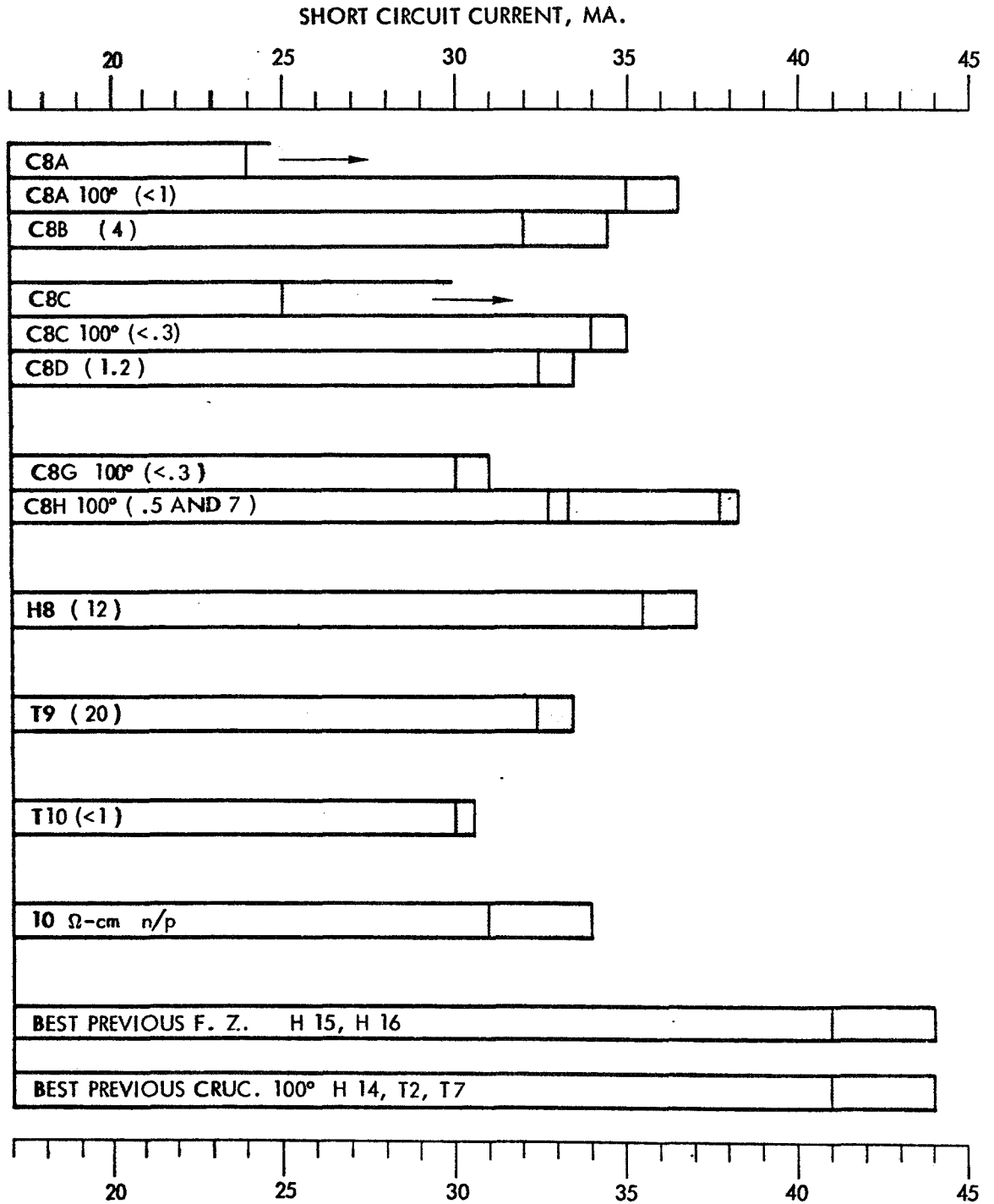


TABLE IV. RECOVERED LEVEL AND HALF RECOVERY TIME (Hours)

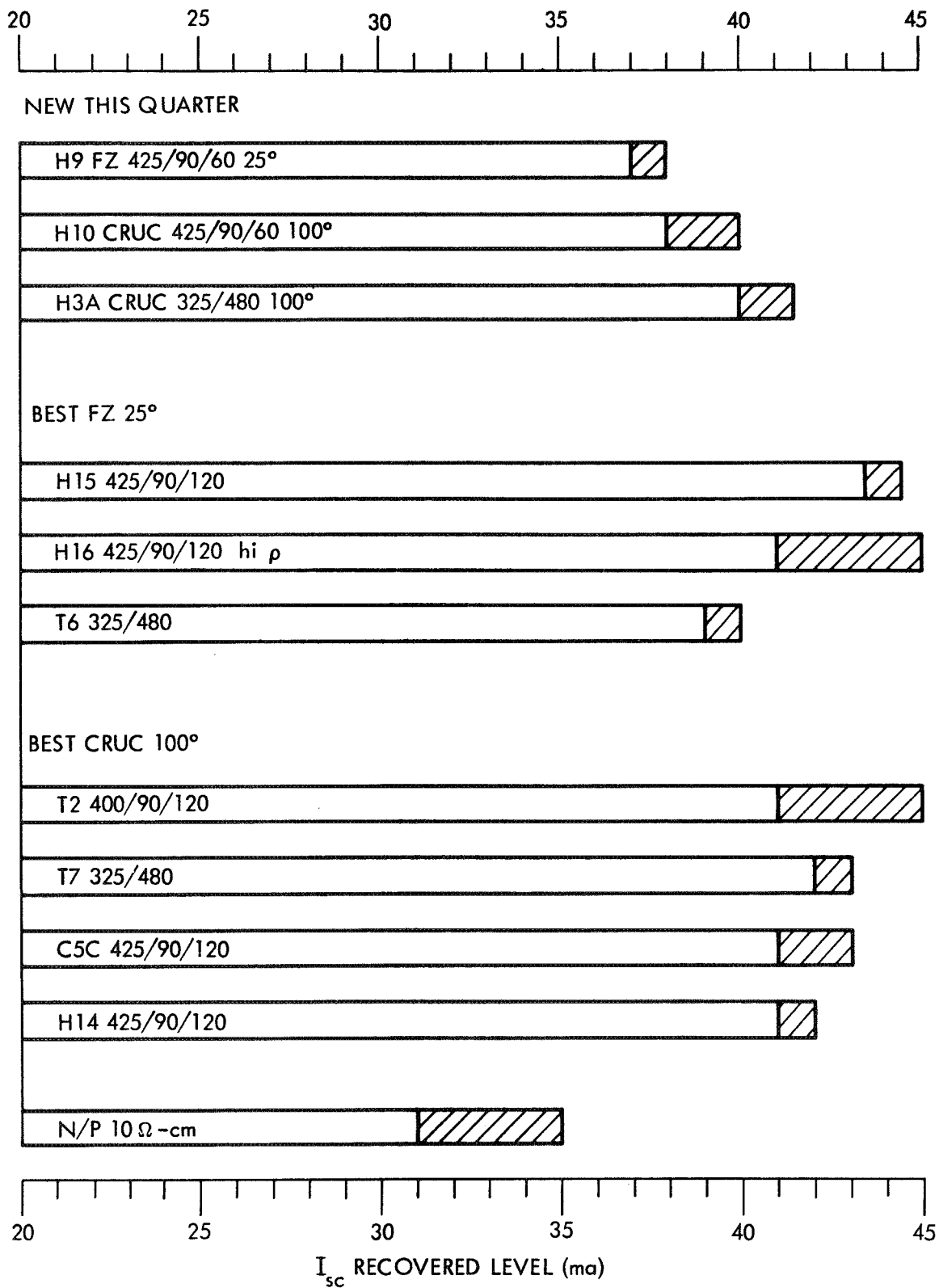


TABLE V. COMPARISON OF PEAK RECOVERED LEVELS ( $I_{sc}$ -TUNGSTEN)

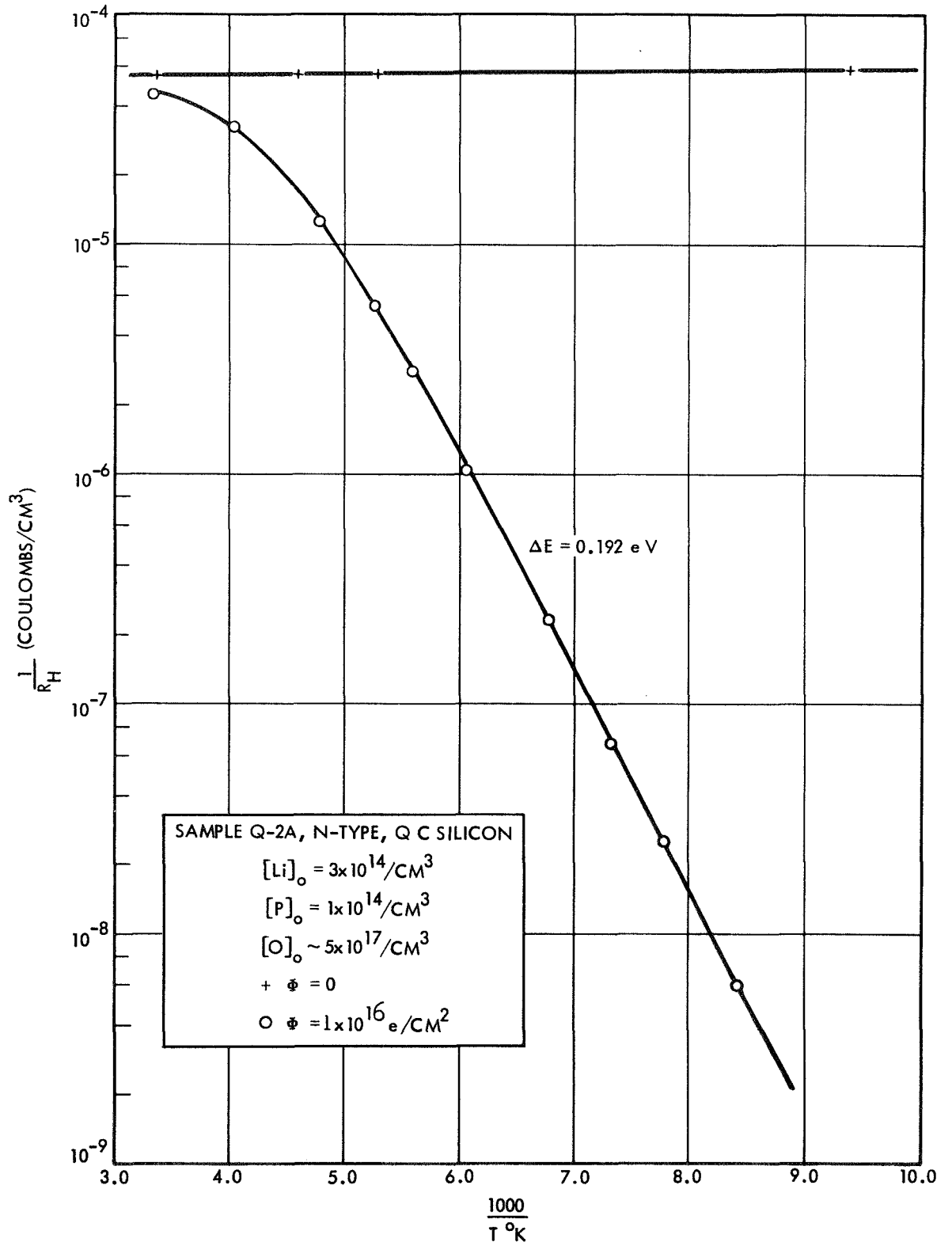


FIG. 1 HALL COEFFICIENT VS. TEMPERATURE, IRRADIATED LITHIUM-DOPED QUARTZ CRUCIBLE SILICON



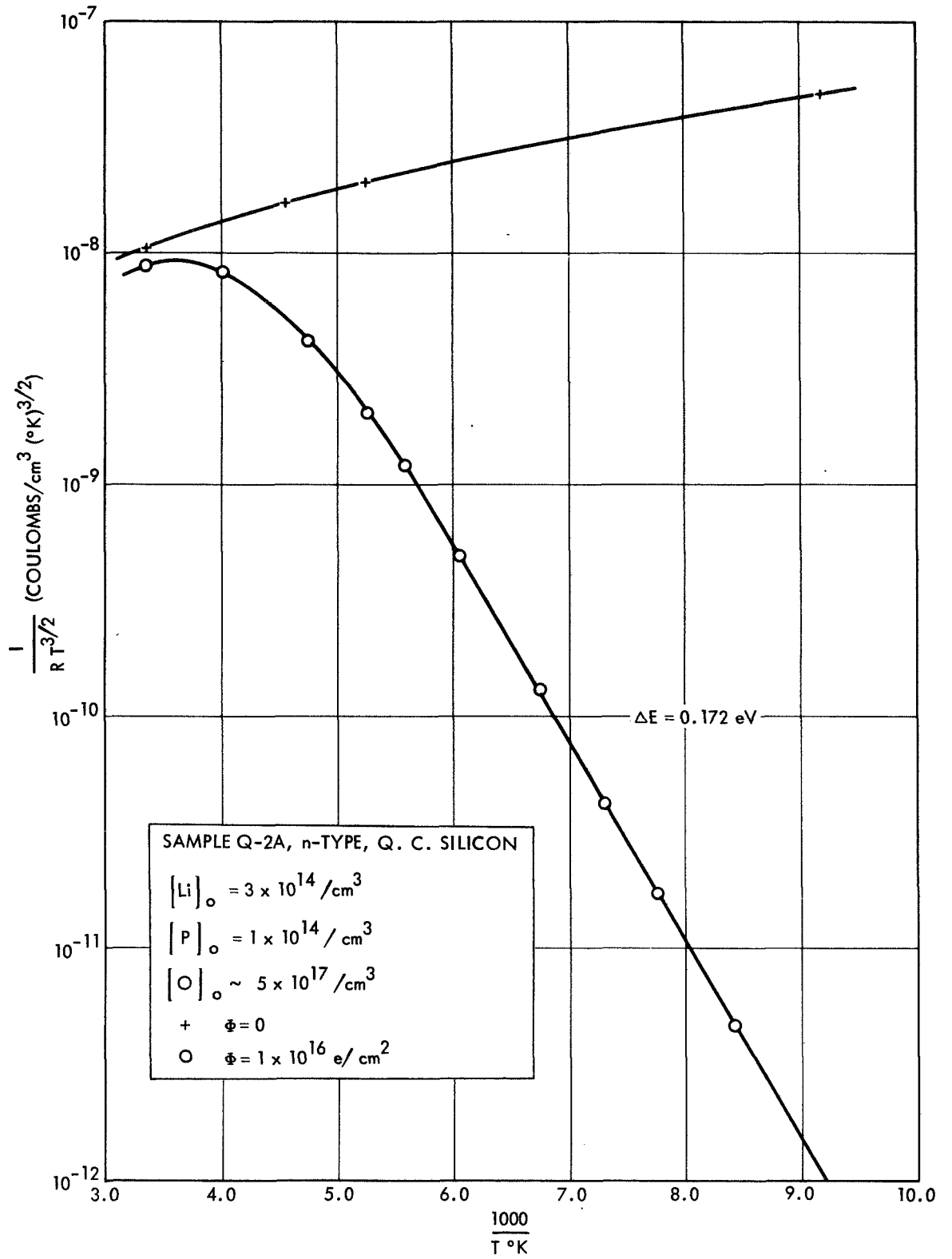


FIG. 2 CORRECTED HALL COEFFICIENT VS. TEMPERATURE,  
IRRADIATED LITHIUM-DOPED QUARTZ CRUCIBLE SILICON

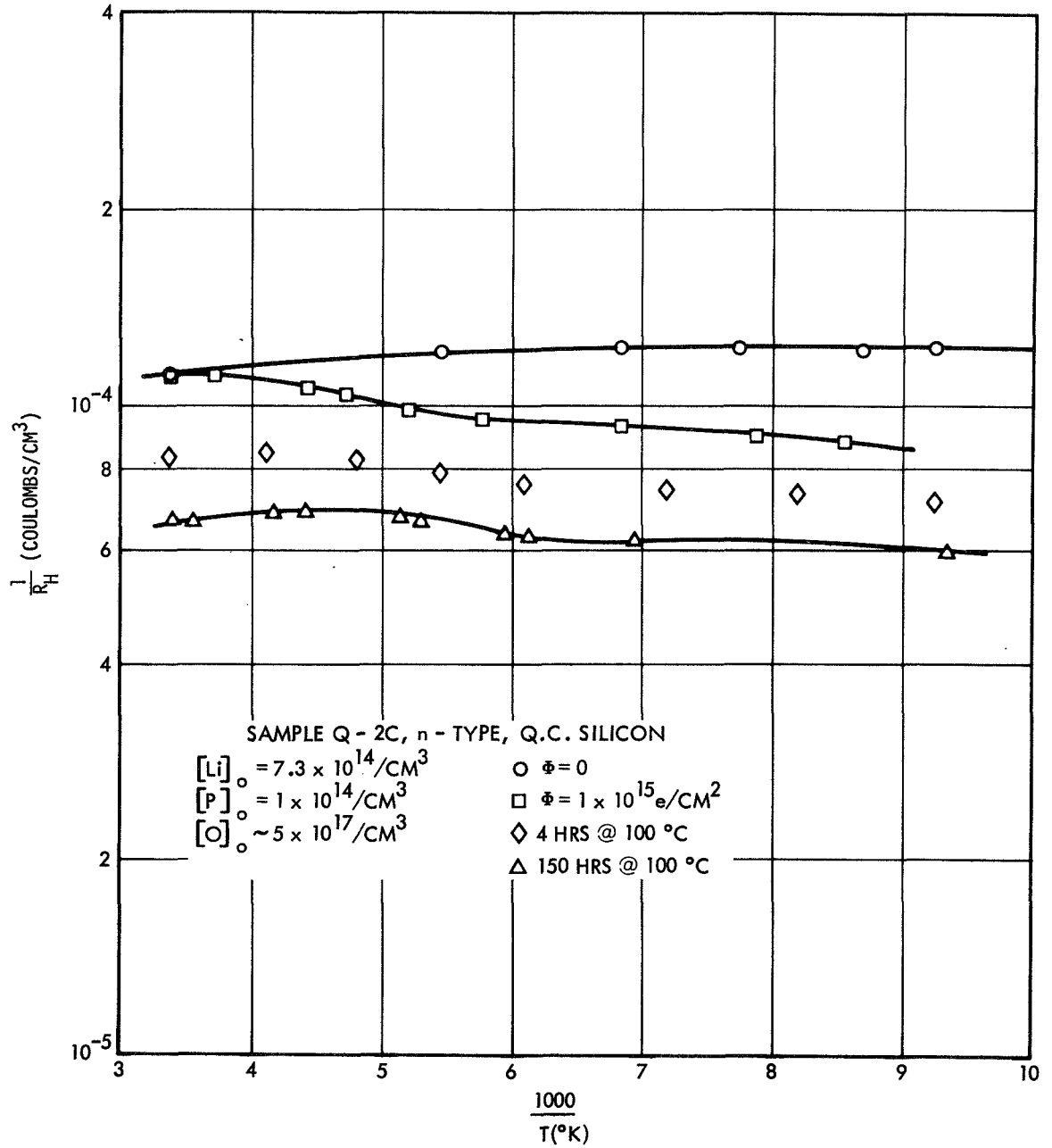


FIG. 3 HALL COEFFICIENT VS. TEMPERATURE, IRRADIATED LITHIUM-DOPED QUARTZ CRUCIBLE SILICON

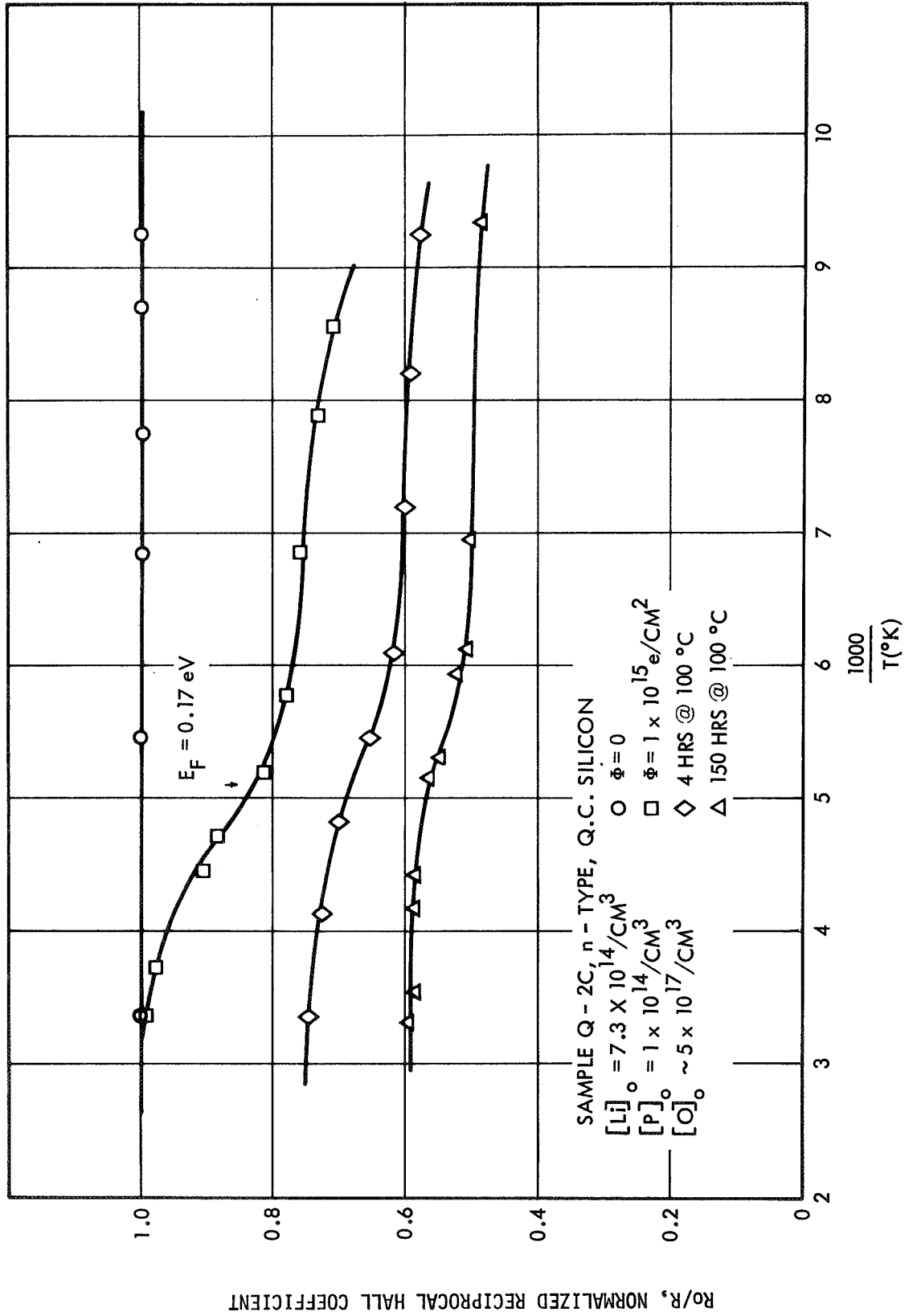


FIG. 4 NORMALIZED HALL COEFFICIENT VS. TEMPERATURE, IRRADIATED LITHIUM-DOPED QUARTZ CRUCIBLE SILICON

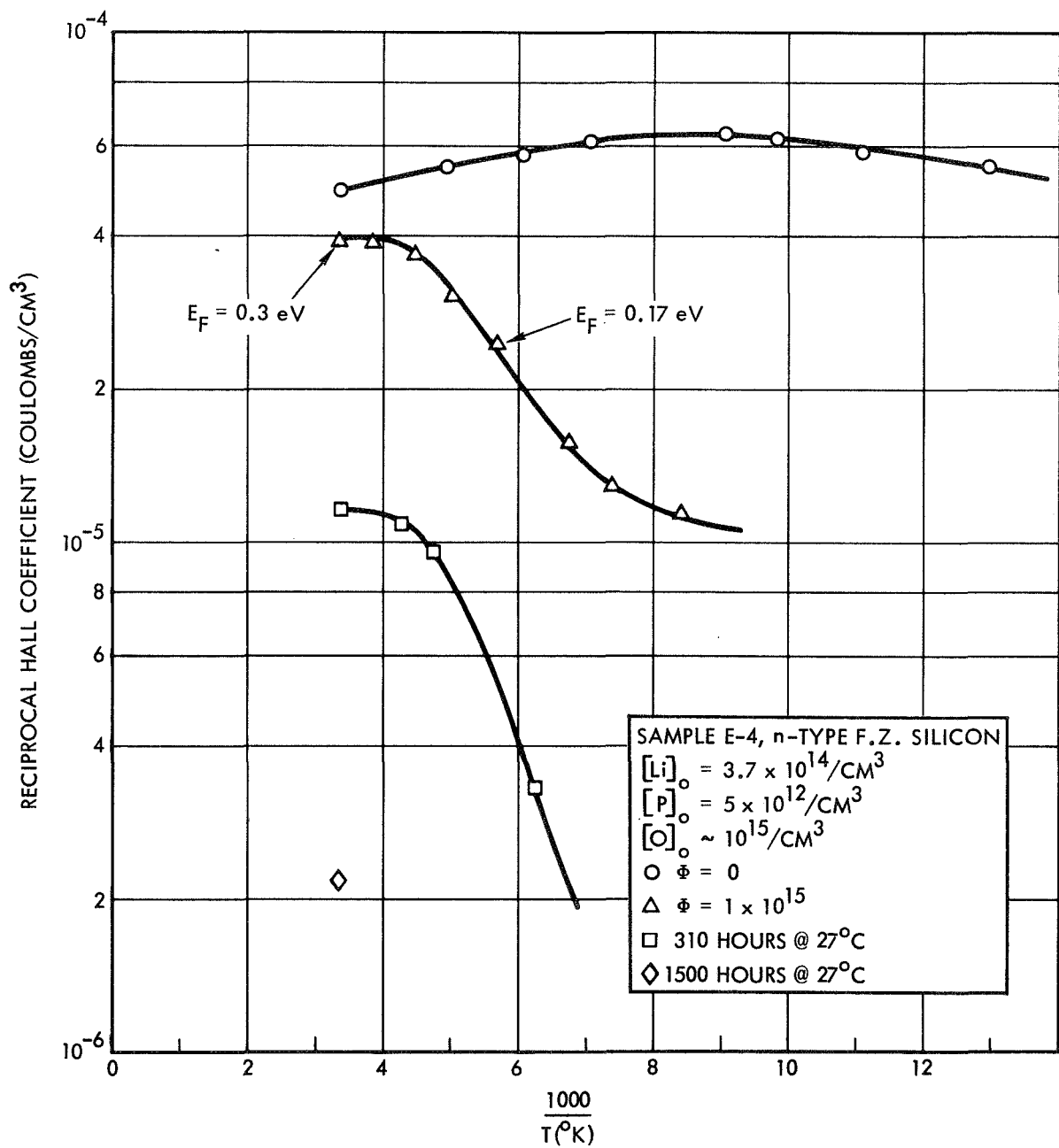


FIG. 5 HALL COEFFICIENT VS. TEMPERATURE, IRRADIATED LITHIUM-DOPED FLOAT ZONE SILICON

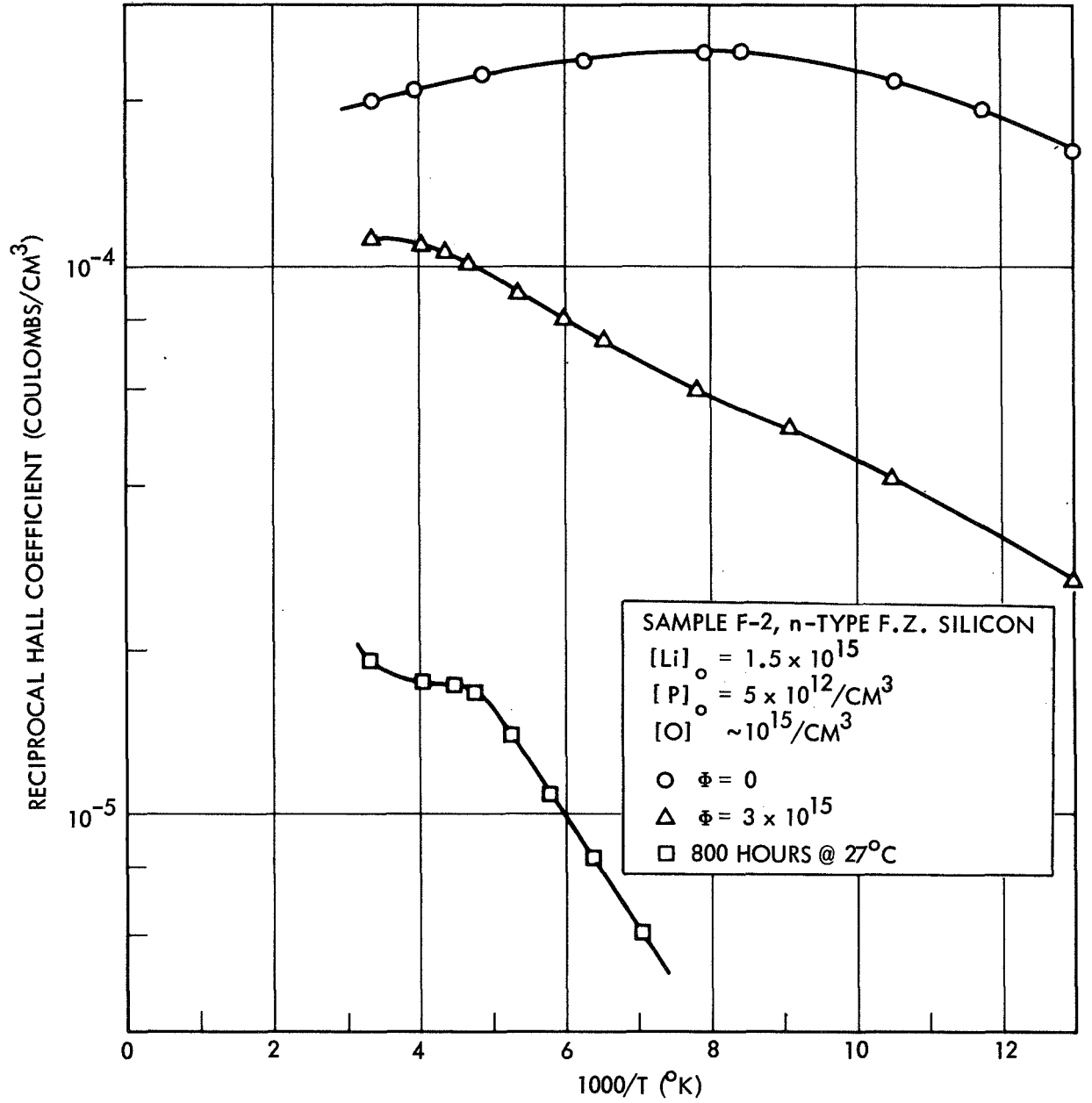


FIG. 6 HALL COEFFICIENT VS. TEMPERATURE, IRRADIATED LITHIUM-DOPED FLOAT ZONE SILICON

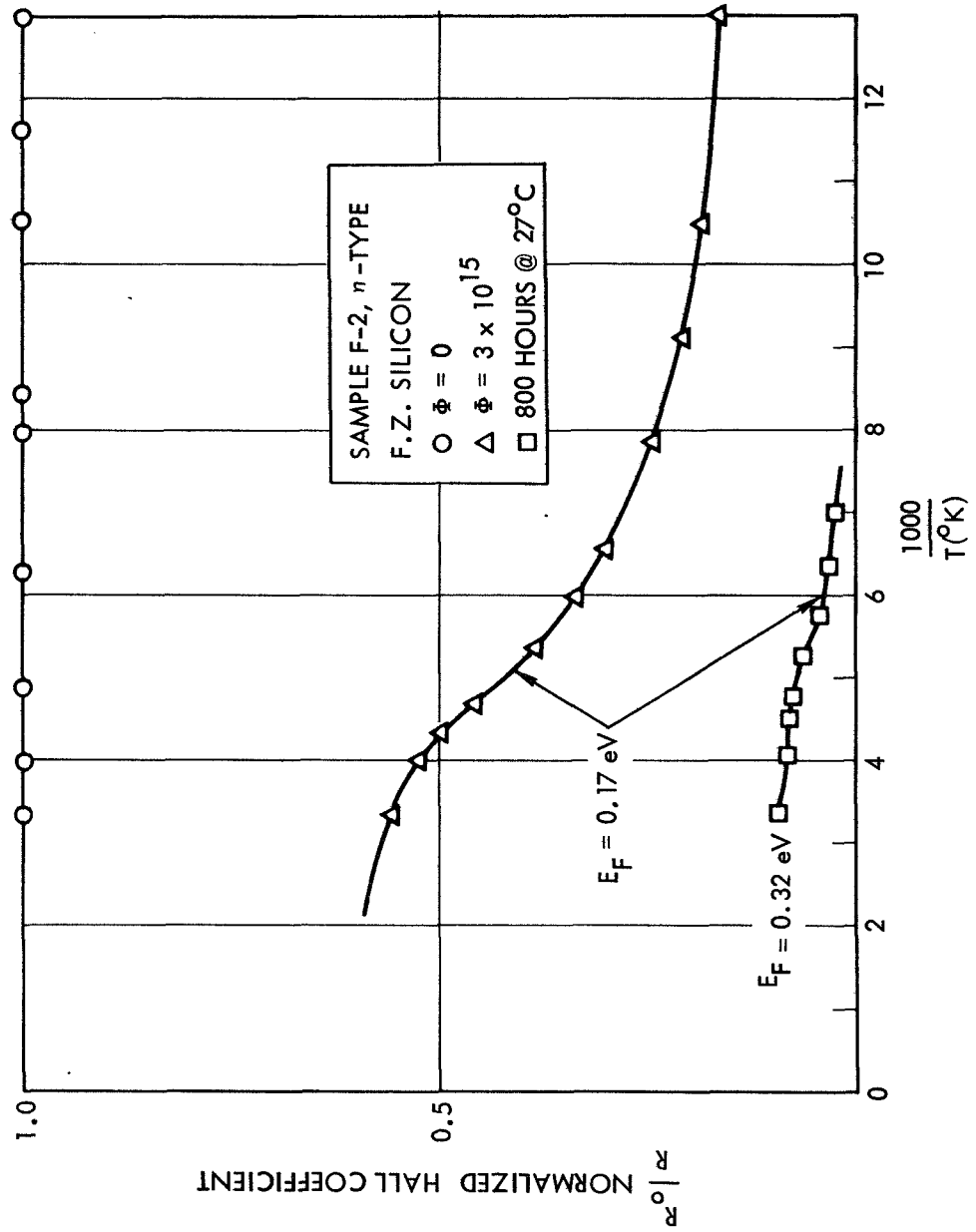


FIG. 7 NORMALIZED HALL COEFFICIENT VS. TEMPERATURE, IRRADIATED LITHIUM-DOPED FLOAT ZONE SILICON

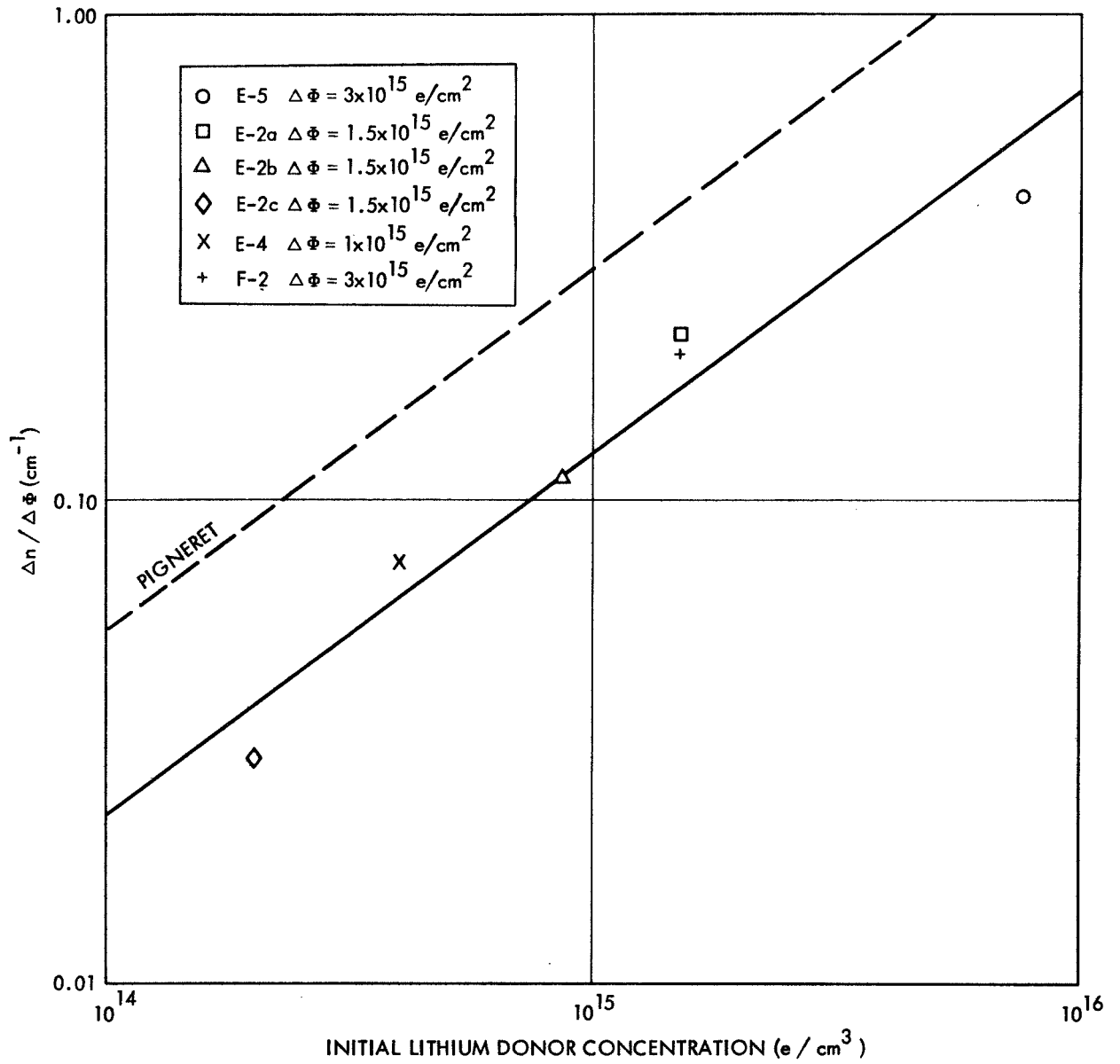


FIG. 8 CARRIER REMOVAL RATE DUE TO DEEP LEVEL DEFECT VS. LITHIUM DONOR CONCENTRATION

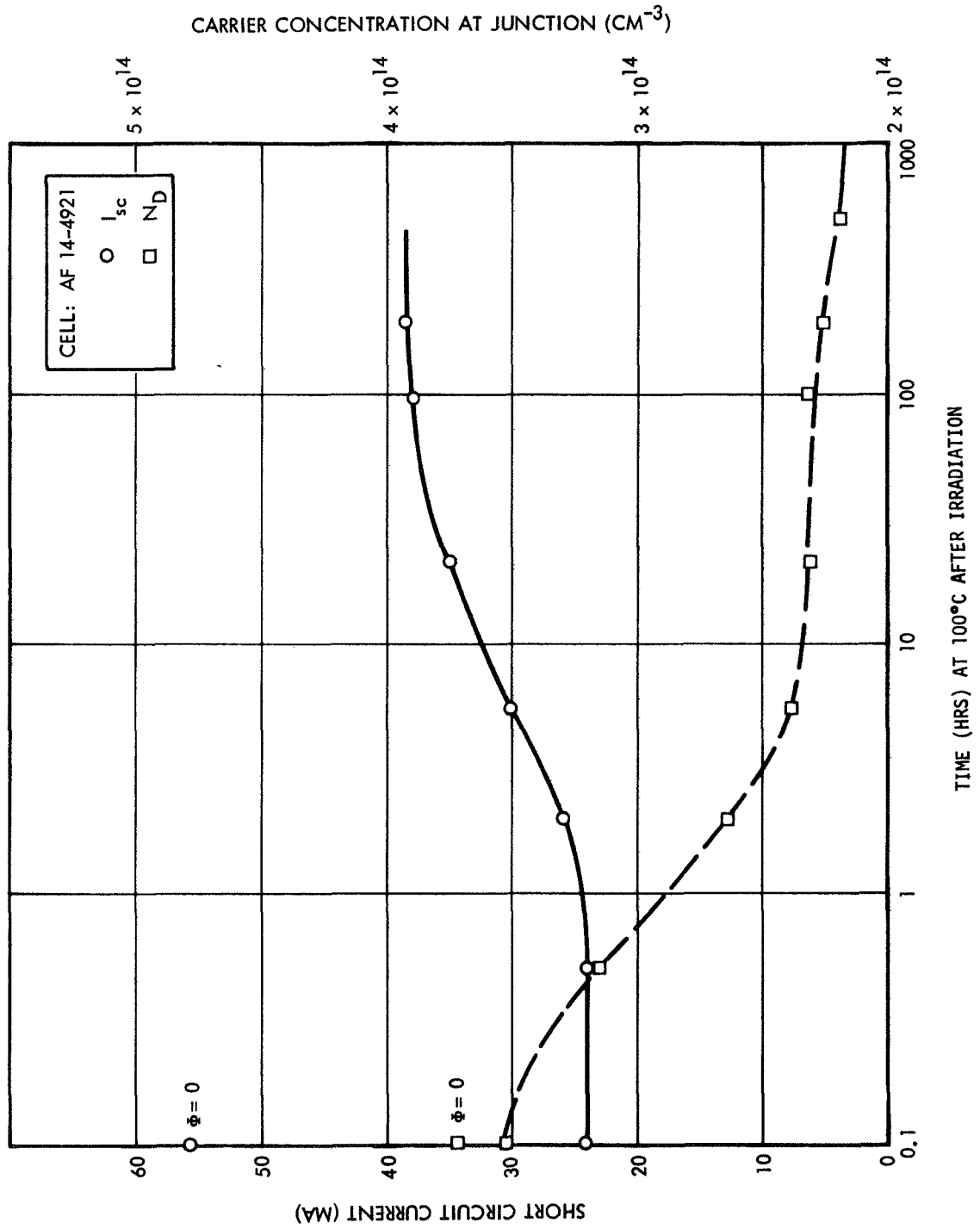


FIG. 9 RECOVERY OF LITHIUM-DOPED QUARTZ CRUCIBLE CELL



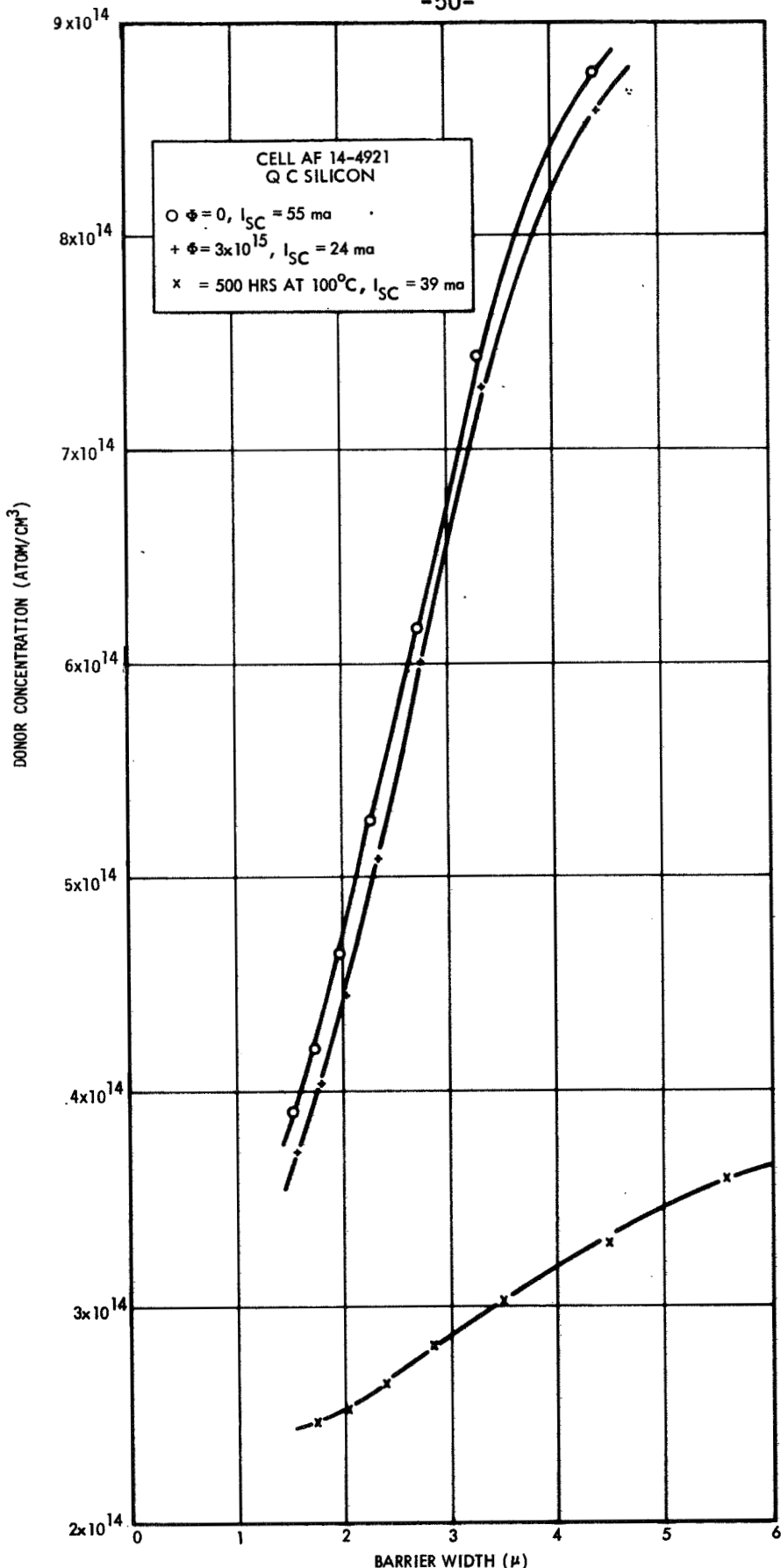


FIG. 10 DONOR CONCENTRATION VS. BARRIER WIDTH, CELL AF 14-4921

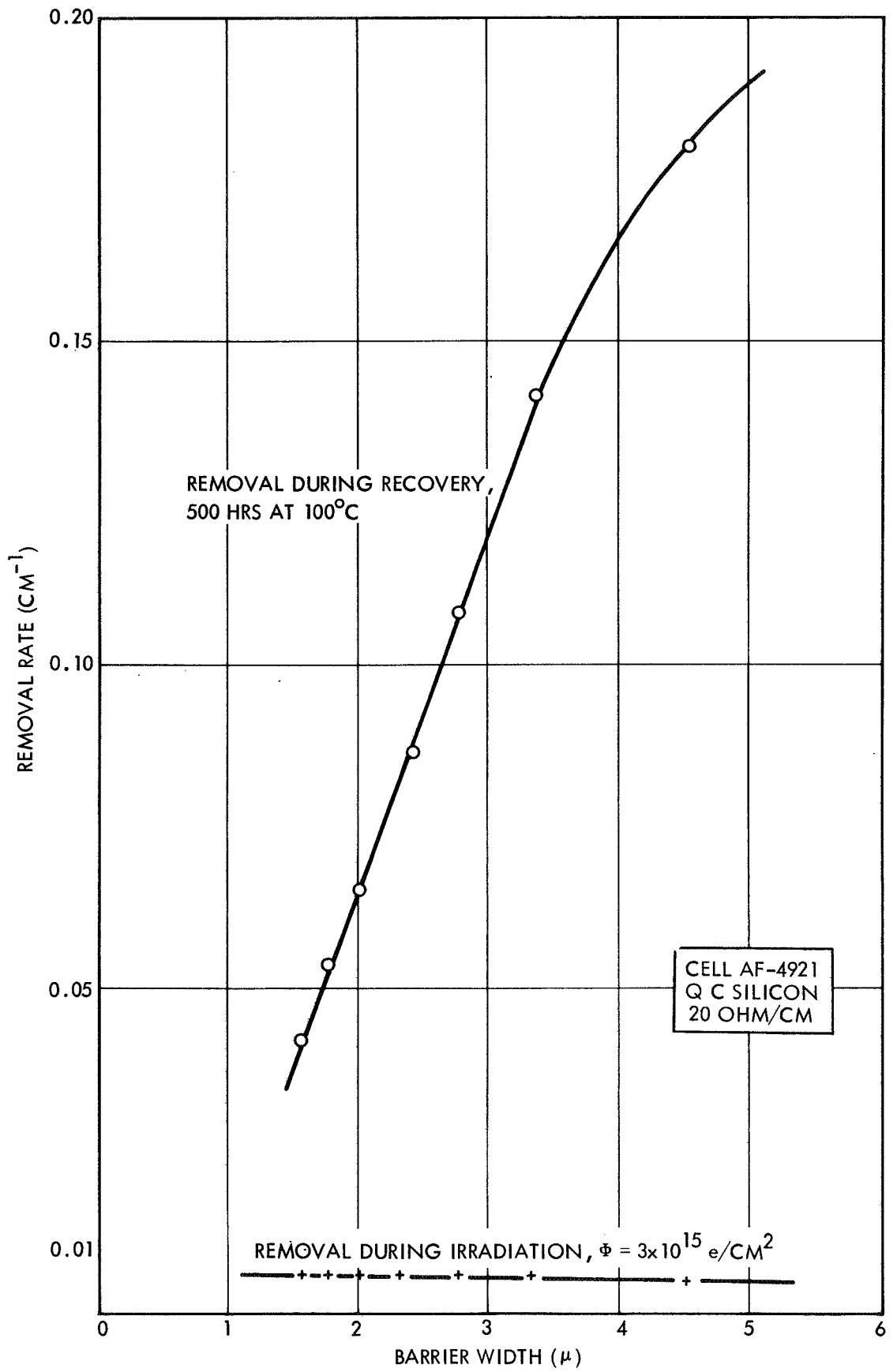


FIG. 11 REMOVAL RATE VS. BARRIER WIDTH, CELL AF 14-4921

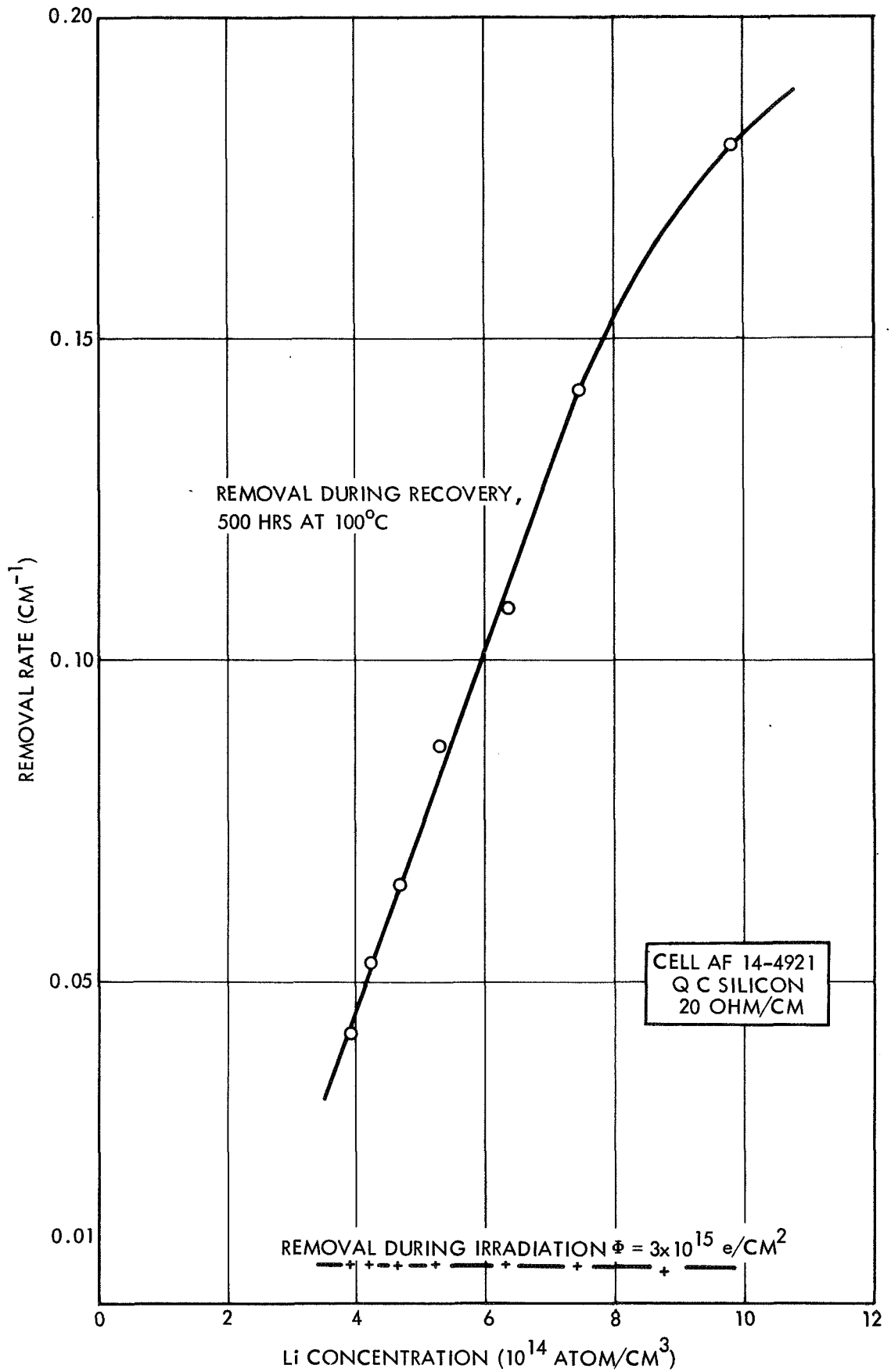


FIG. 12 REMOVAL RATE VS. LITHIUM CONCENTRATION, CELL AF 14-4921

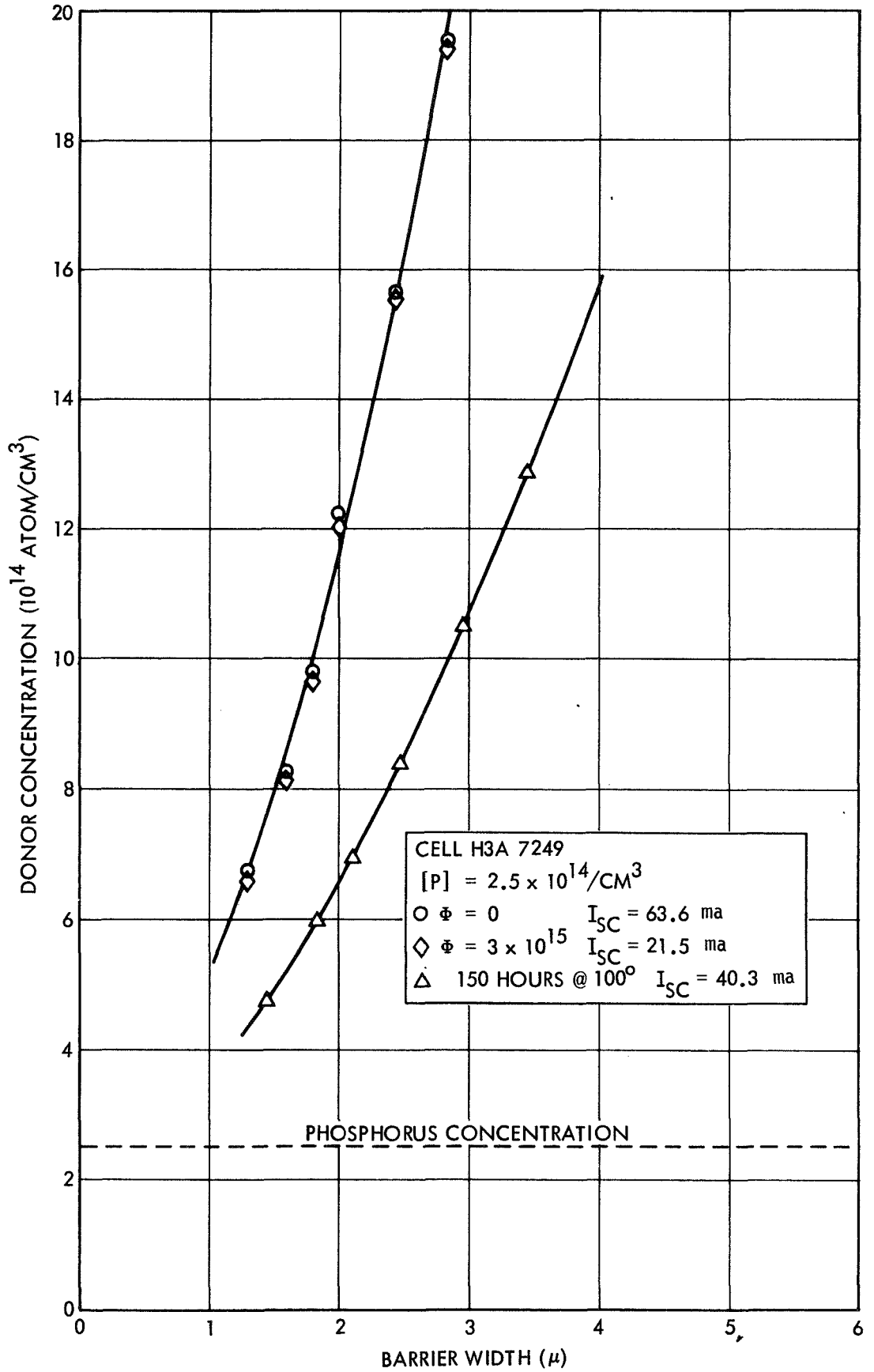


FIG. 13 DONOR CONCENTRATION VS. BARRIER WIDTH, CELL H3A 7249

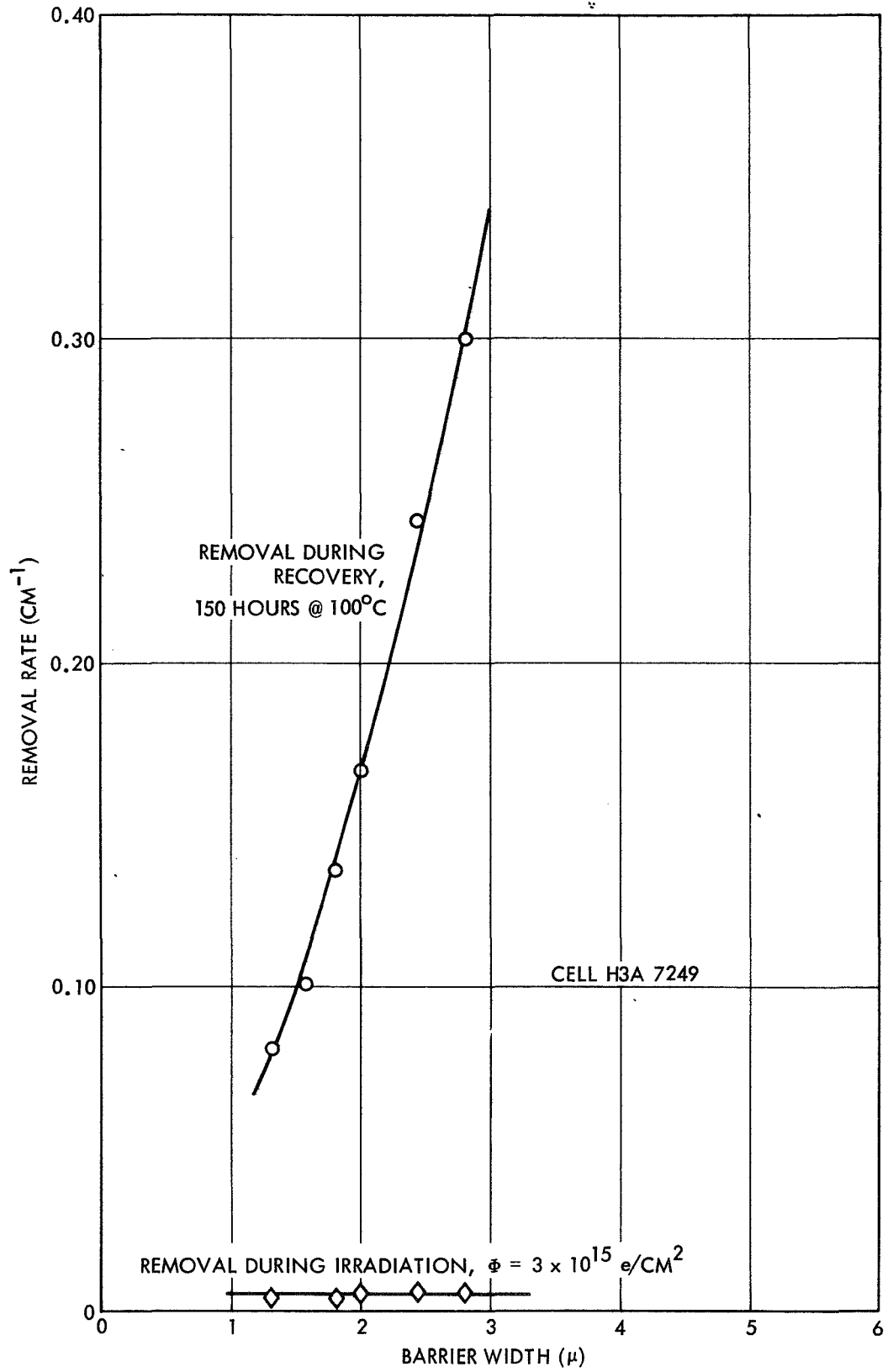


FIG. 14 REMOVAL RATE VS. BARRIER WIDTH, CELL H3A 7249

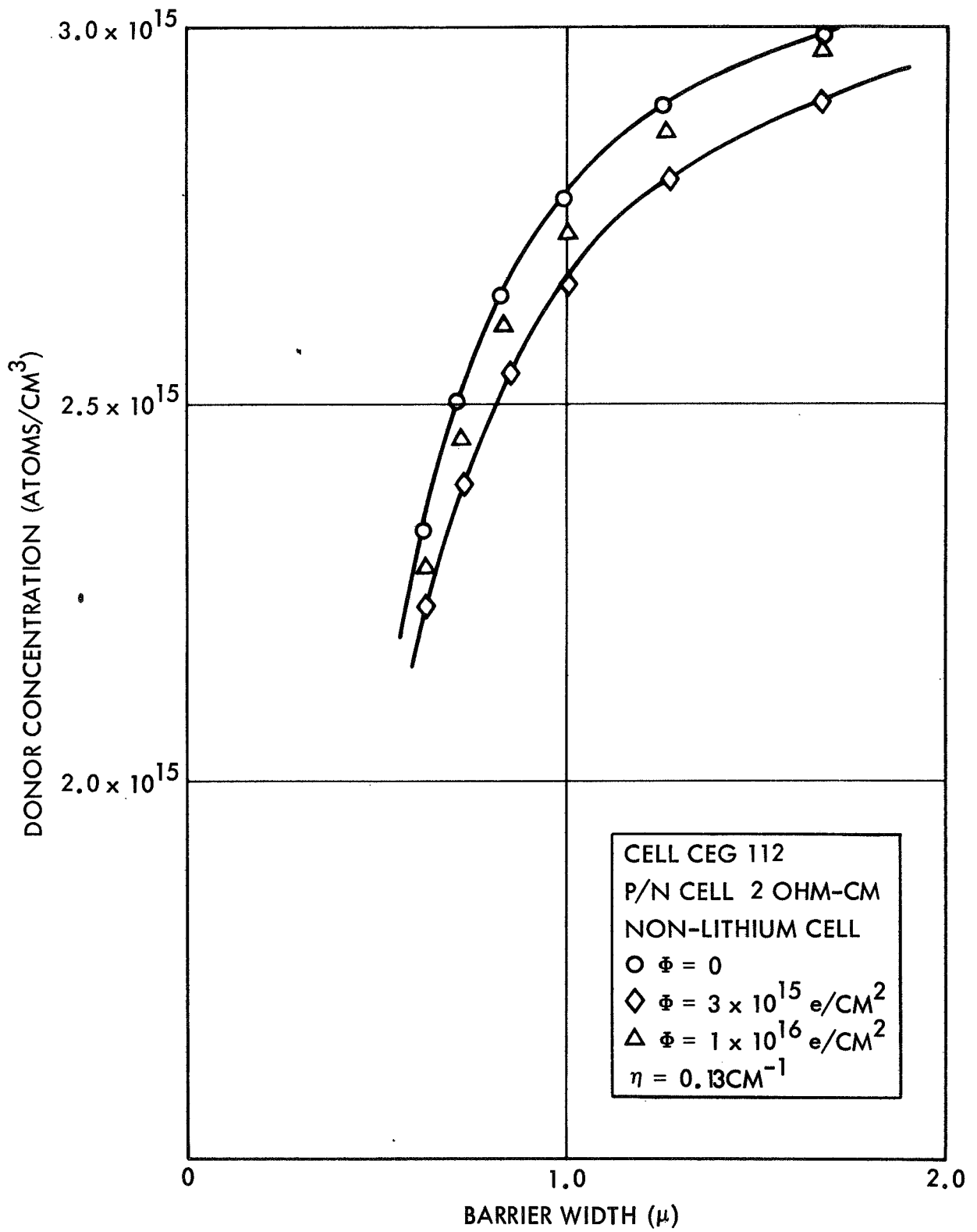


FIG. 15 DONOR CONCENTRATION VS. BARRIER WIDTH, CONVENTIONAL P/N CELL

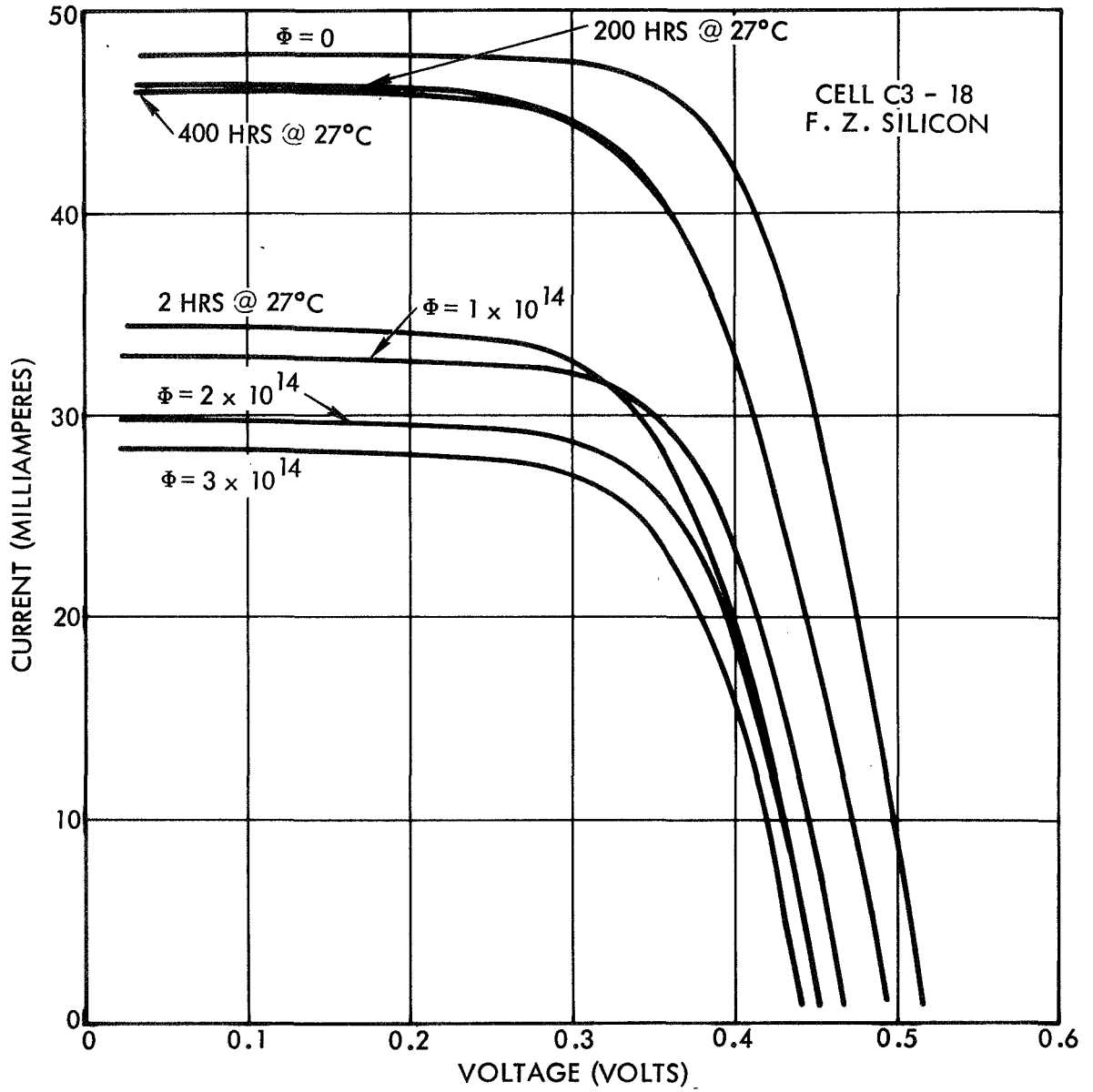


FIG. 16 SOLAR CELL CHARACTERISTICS, CELL C3-18

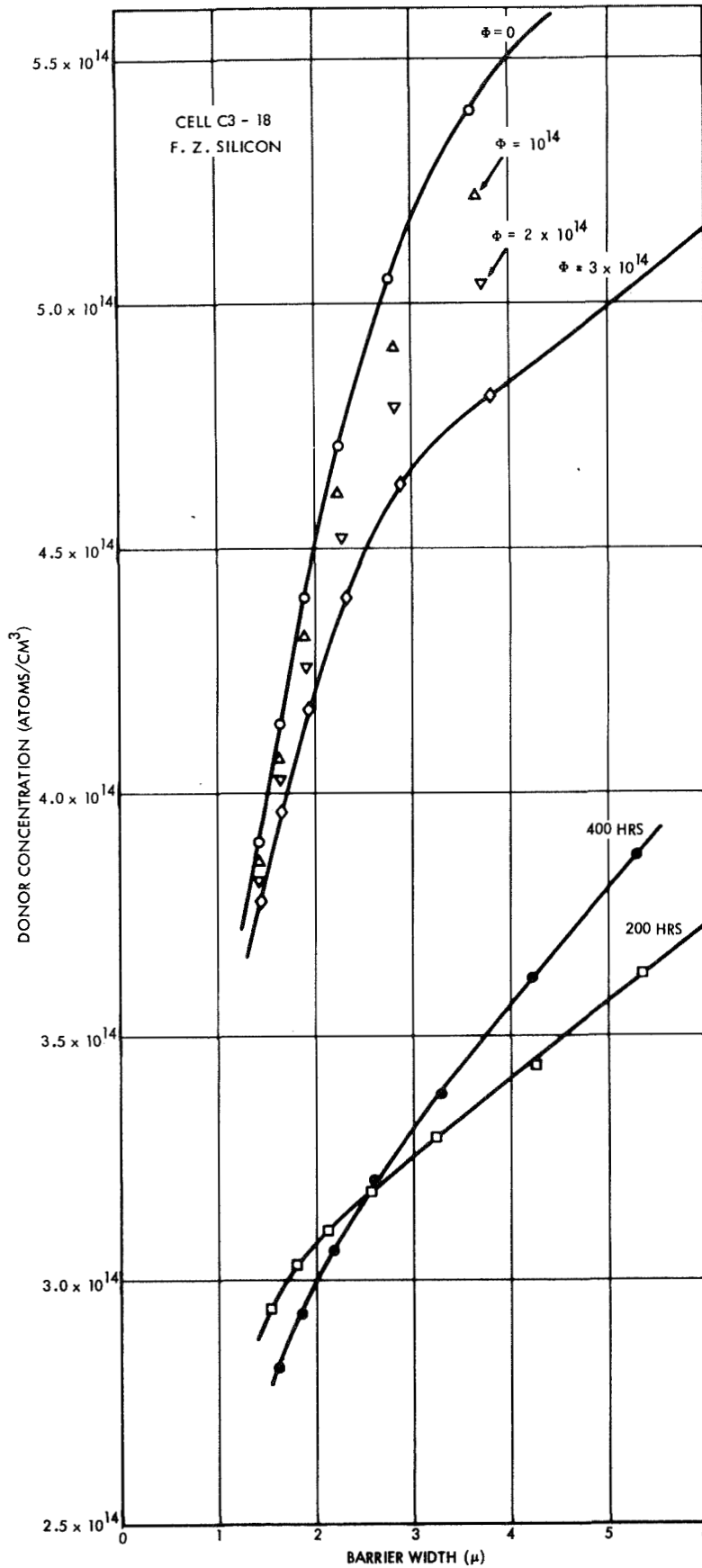


FIG. 17 DONOR CONCENTRATION VS. BARRIER, CELL C3-18



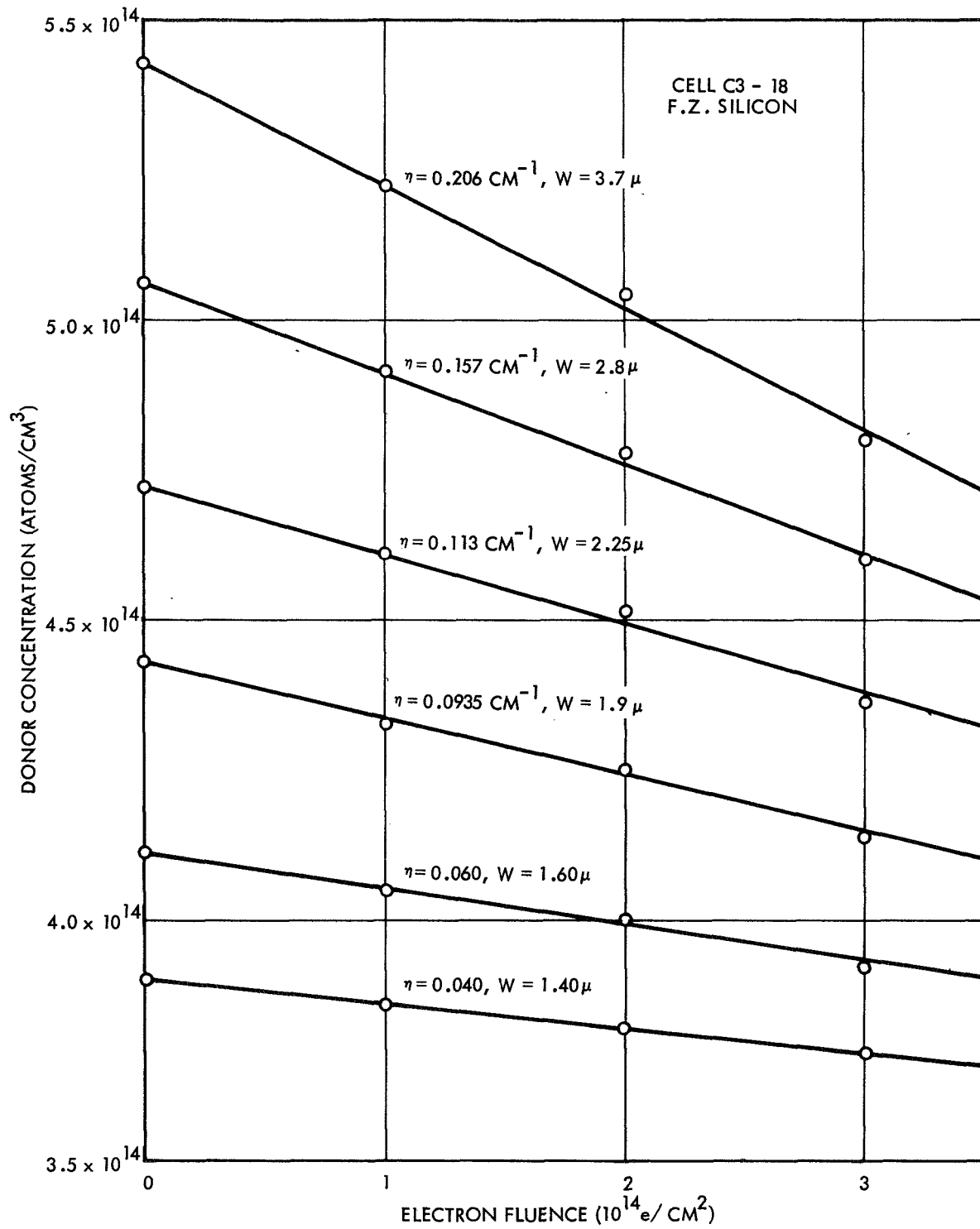


FIG. 18 DONOR CONCENTRATION VS. FLUENCE, CELL C3-18

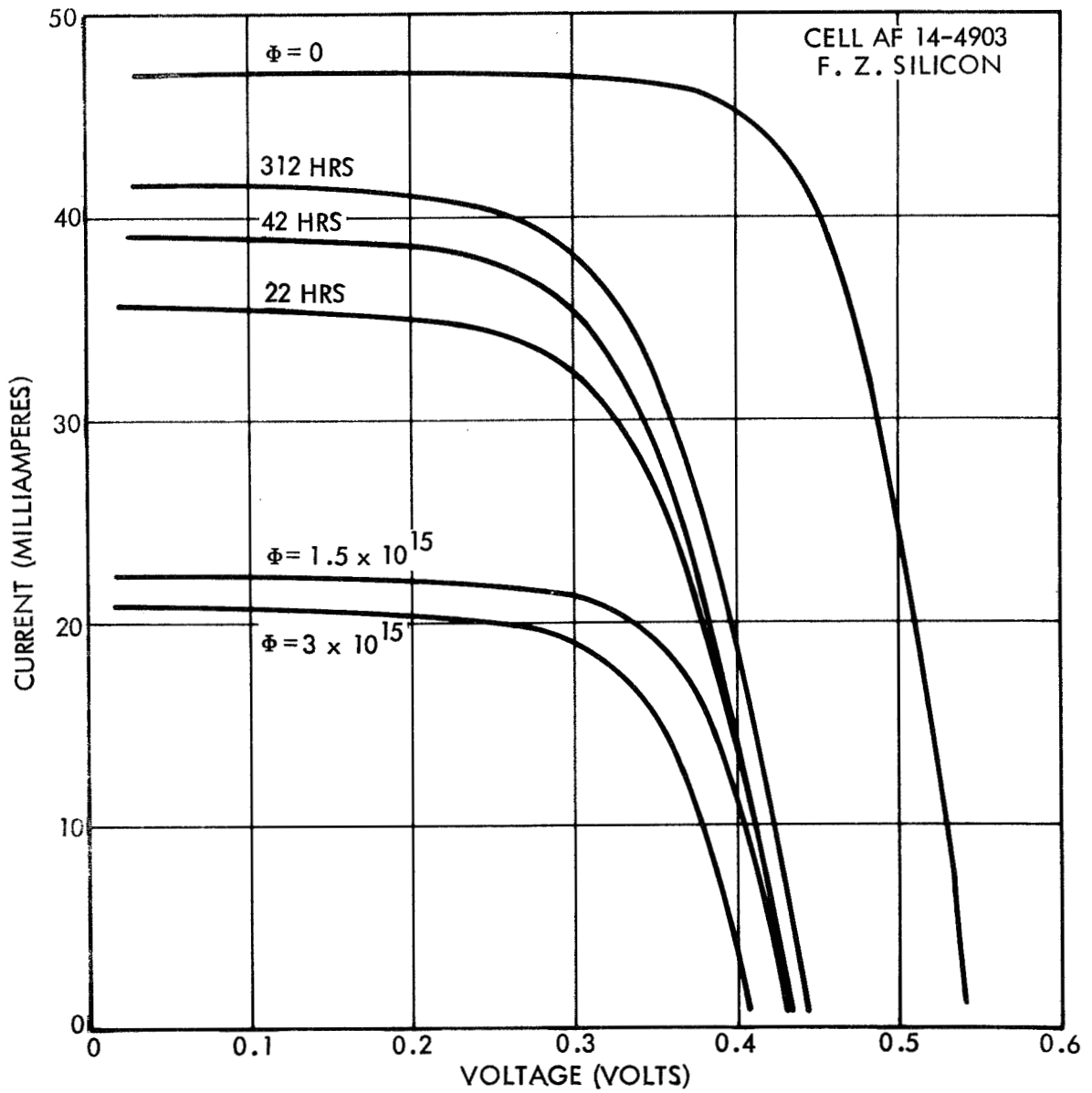


FIG. 19 SOLAR CELL CHARACTERISTICS, CELL AF 14-4903

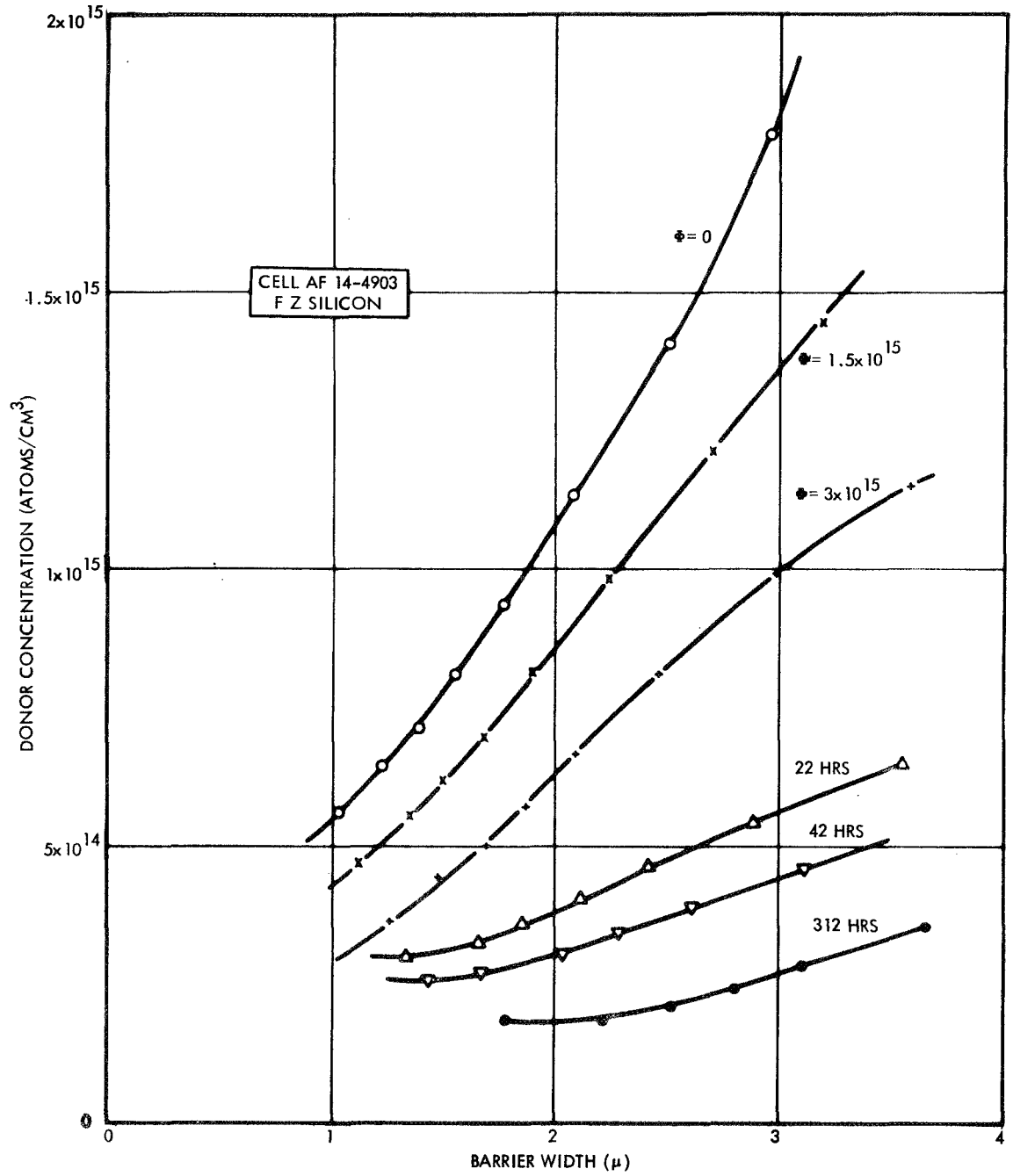


FIG. 20 DONOR CONCENTRATION VS. BARRIER WIDTH, CELL AF 14-4903

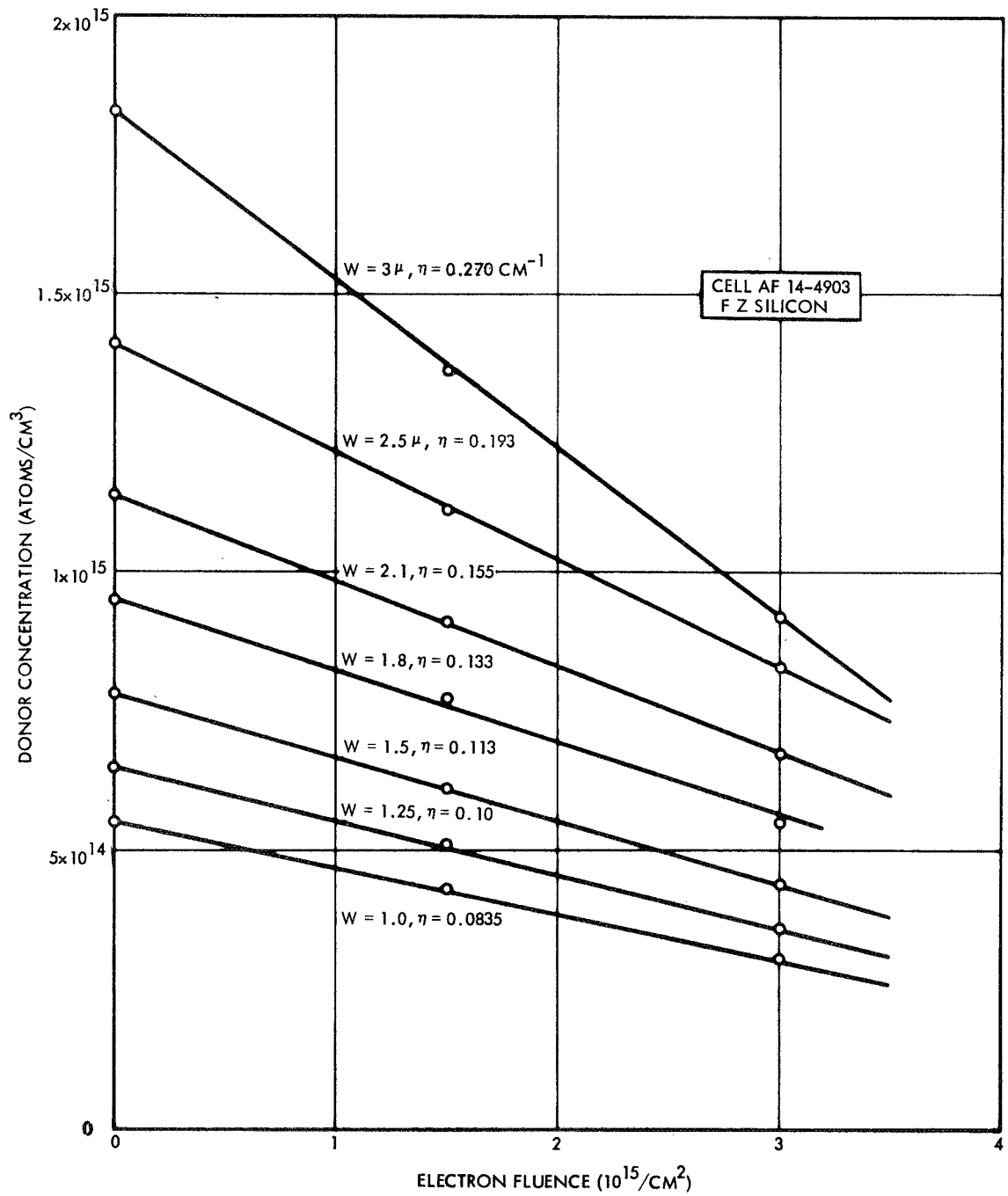


FIG. 21 DONOR CONCENTRATION VS. FLUENCE, CELL AF 14-4903

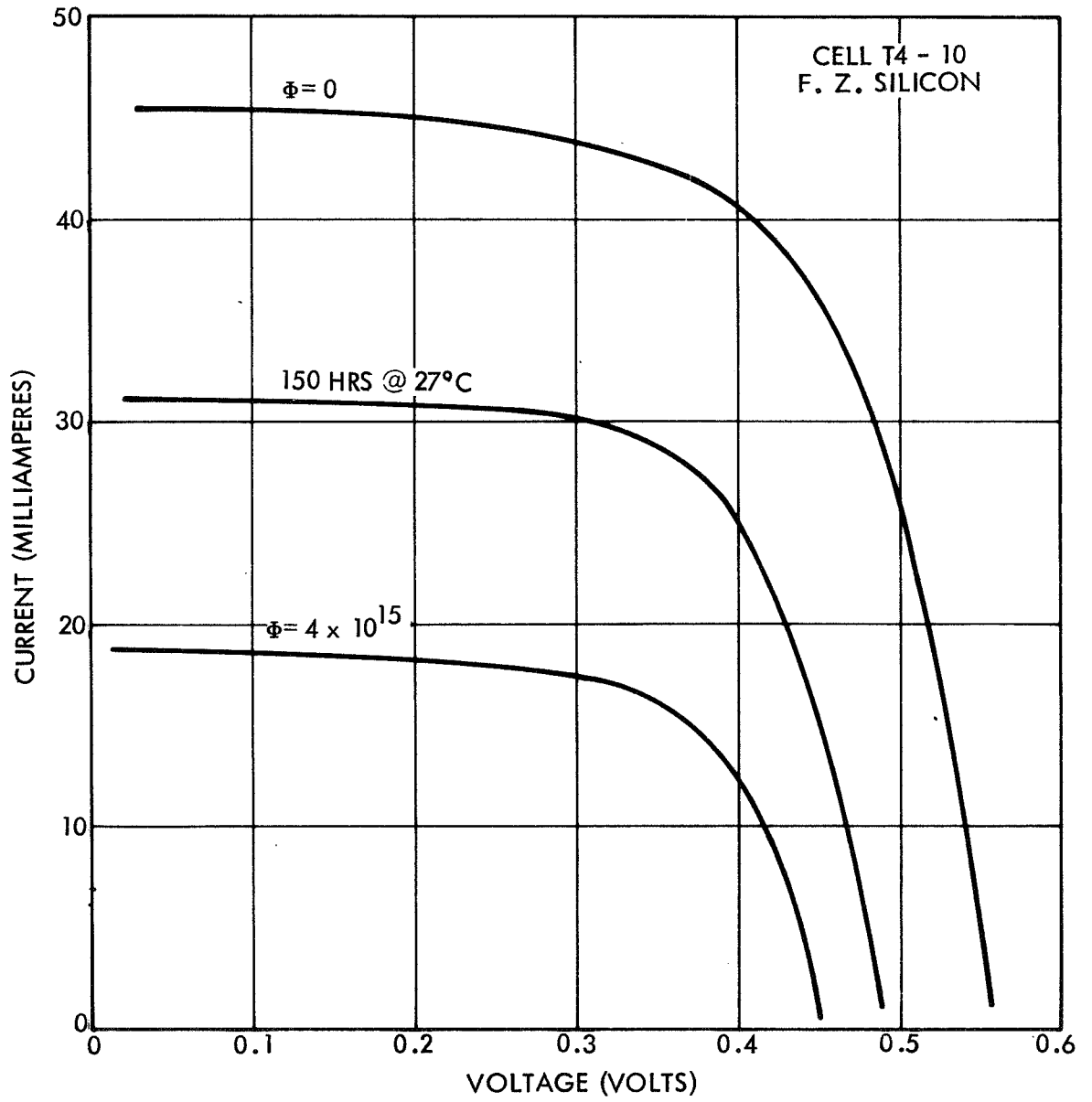


FIG. 22 SOLAR CELL CHARACTERISTICS, CELL T4-10

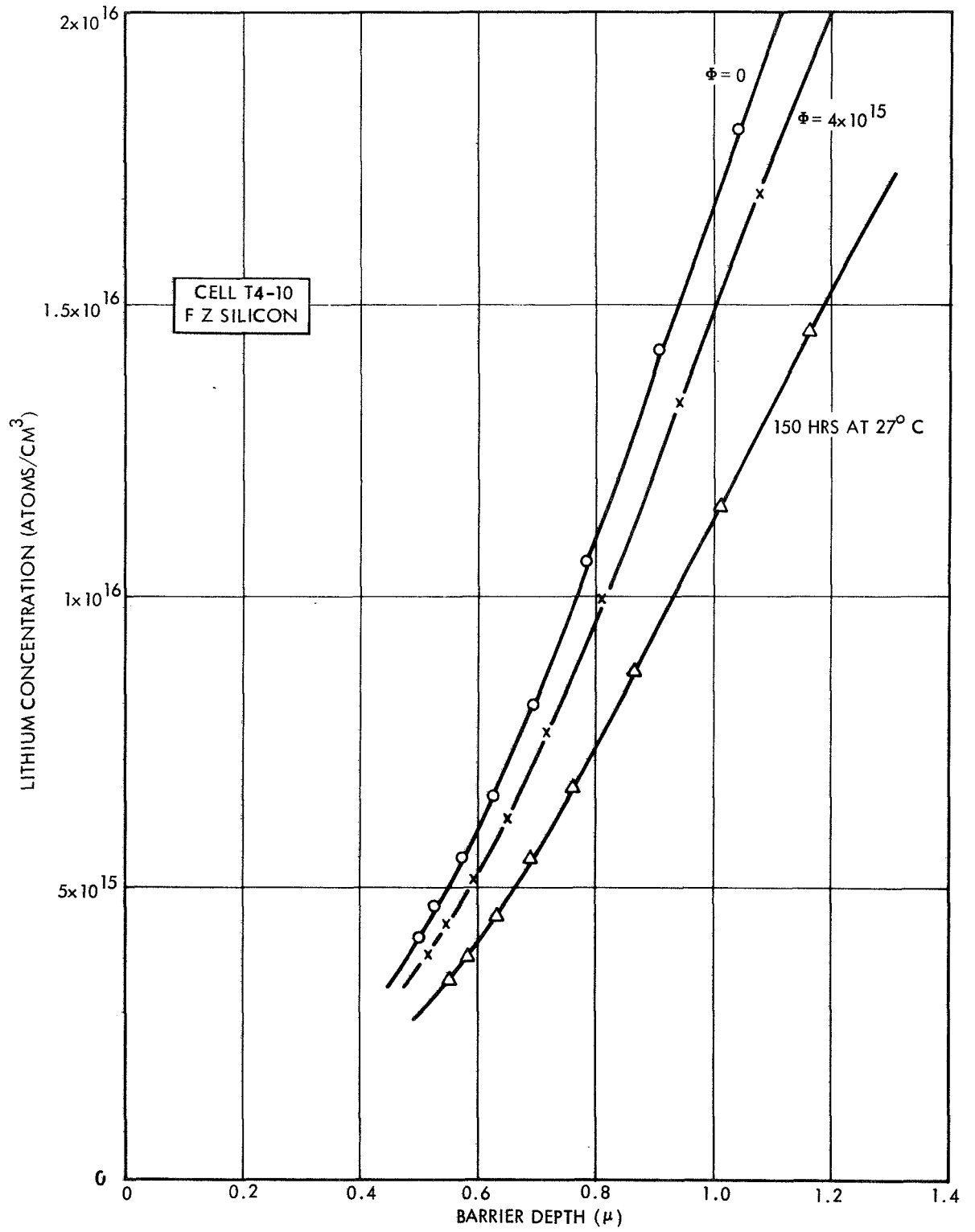


FIG. 23 DONOR CONCENTRATION VS. BARRIER WIDTH, CELL T4-10

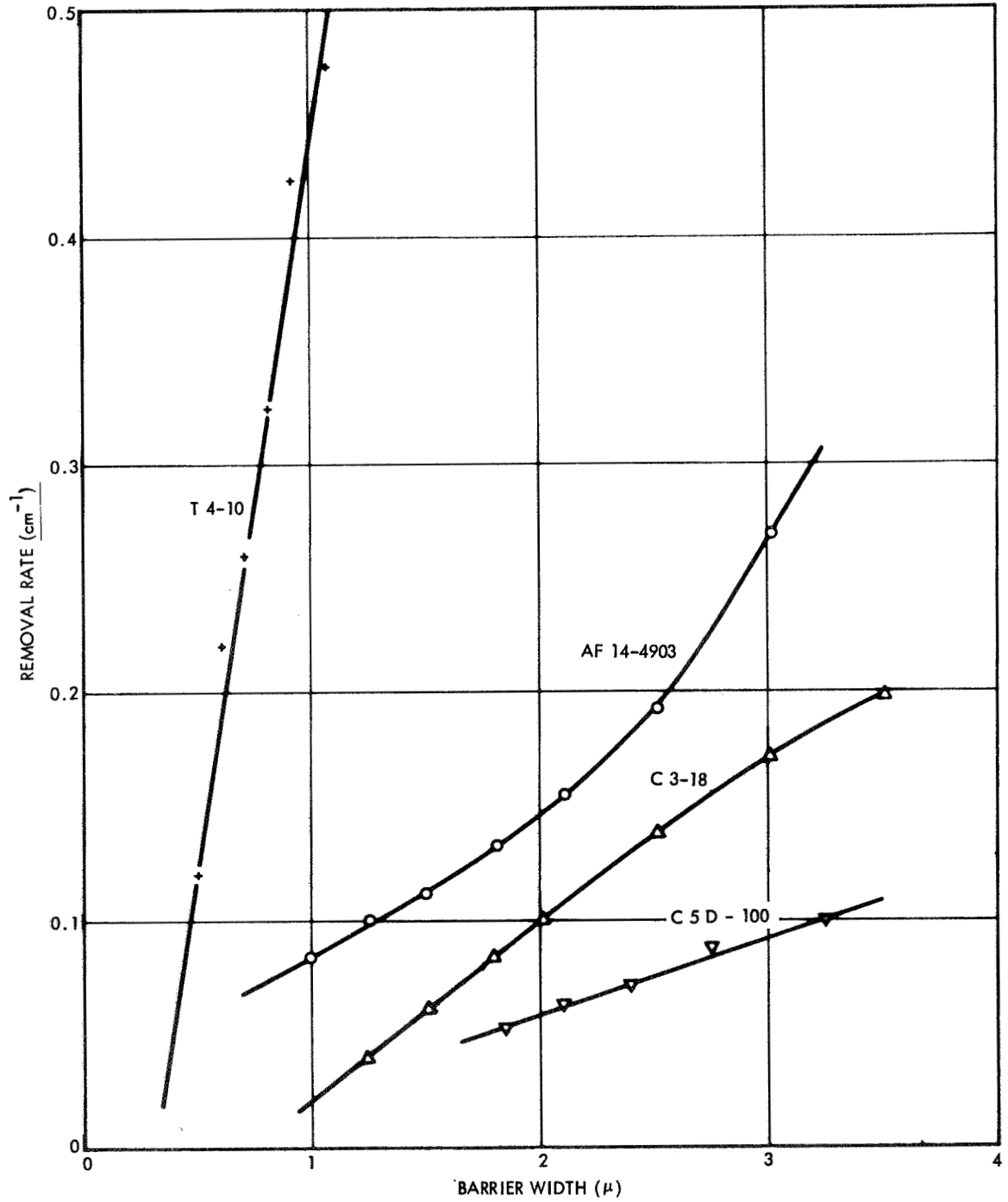
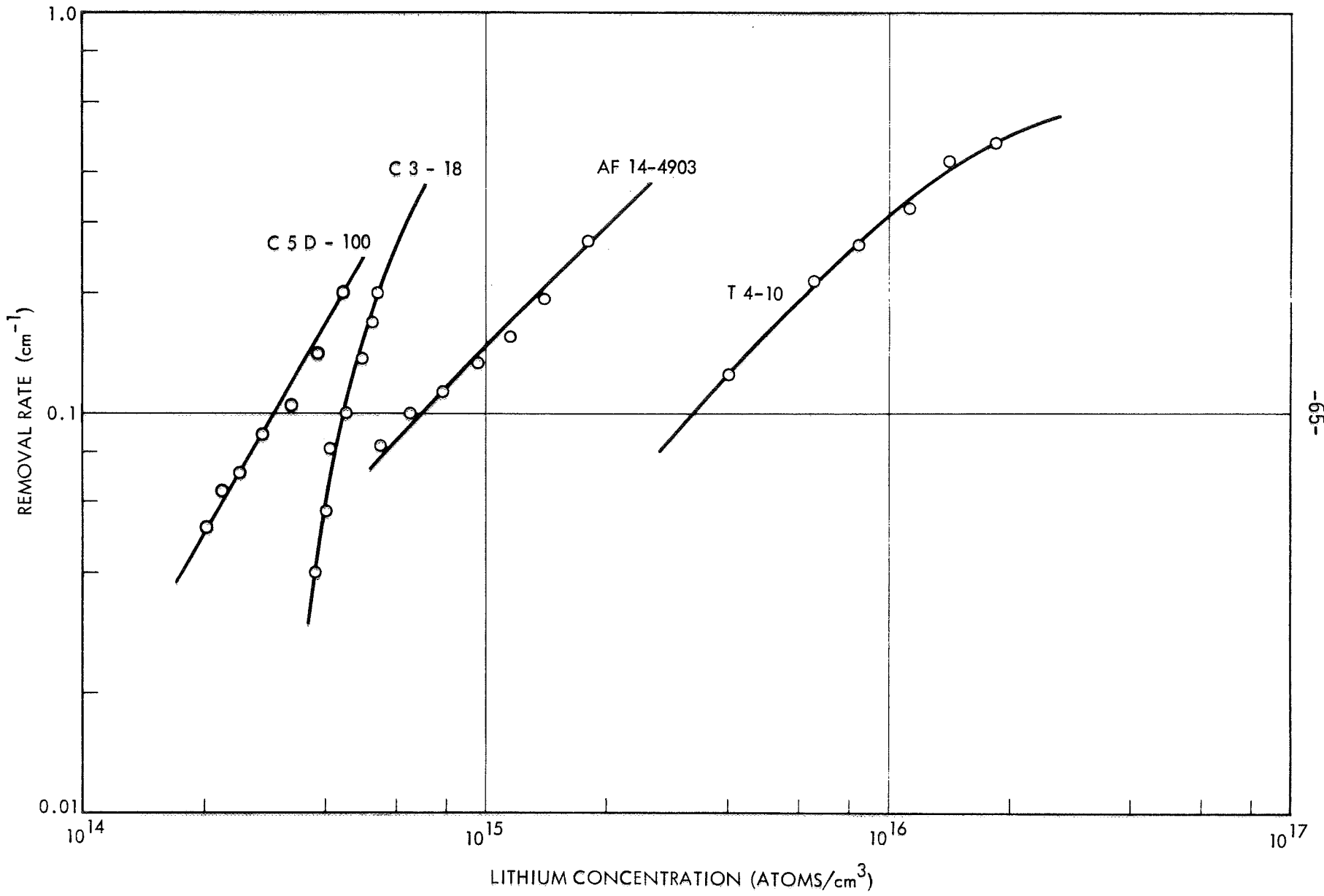


FIG. 24 REMOVAL RATE VS. BARRIER WIDTH, FLOAT ZONE CELLS

FIG. 25 REMOVAL RATE VS. LI CONCENTRATION, FLOAT ZONE CELLS





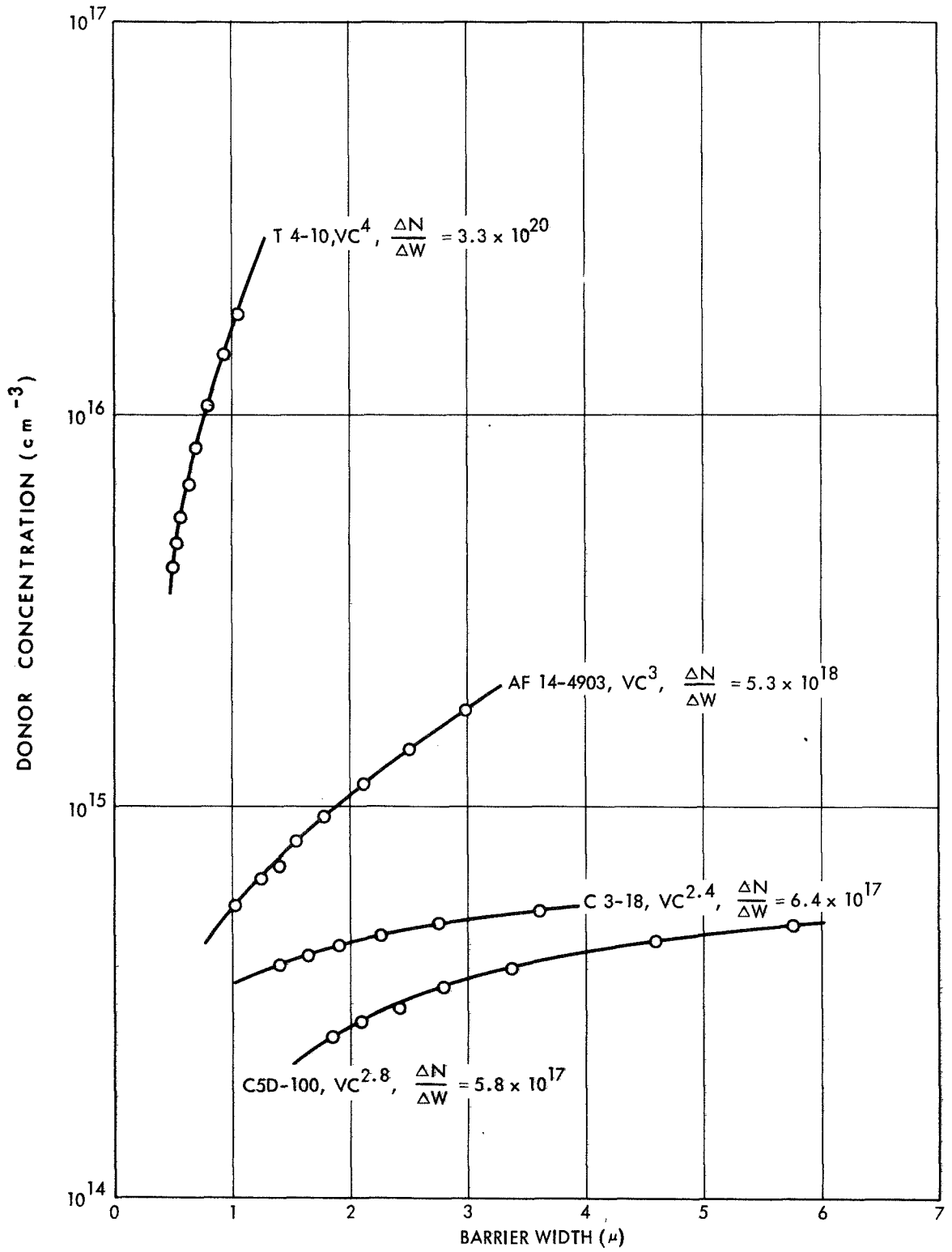


FIG. 26 DONOR CONCENTRATION VS. BARRIER WIDTH, VARIOUS FLOAT ZONE UNIRRADIATED CELLS

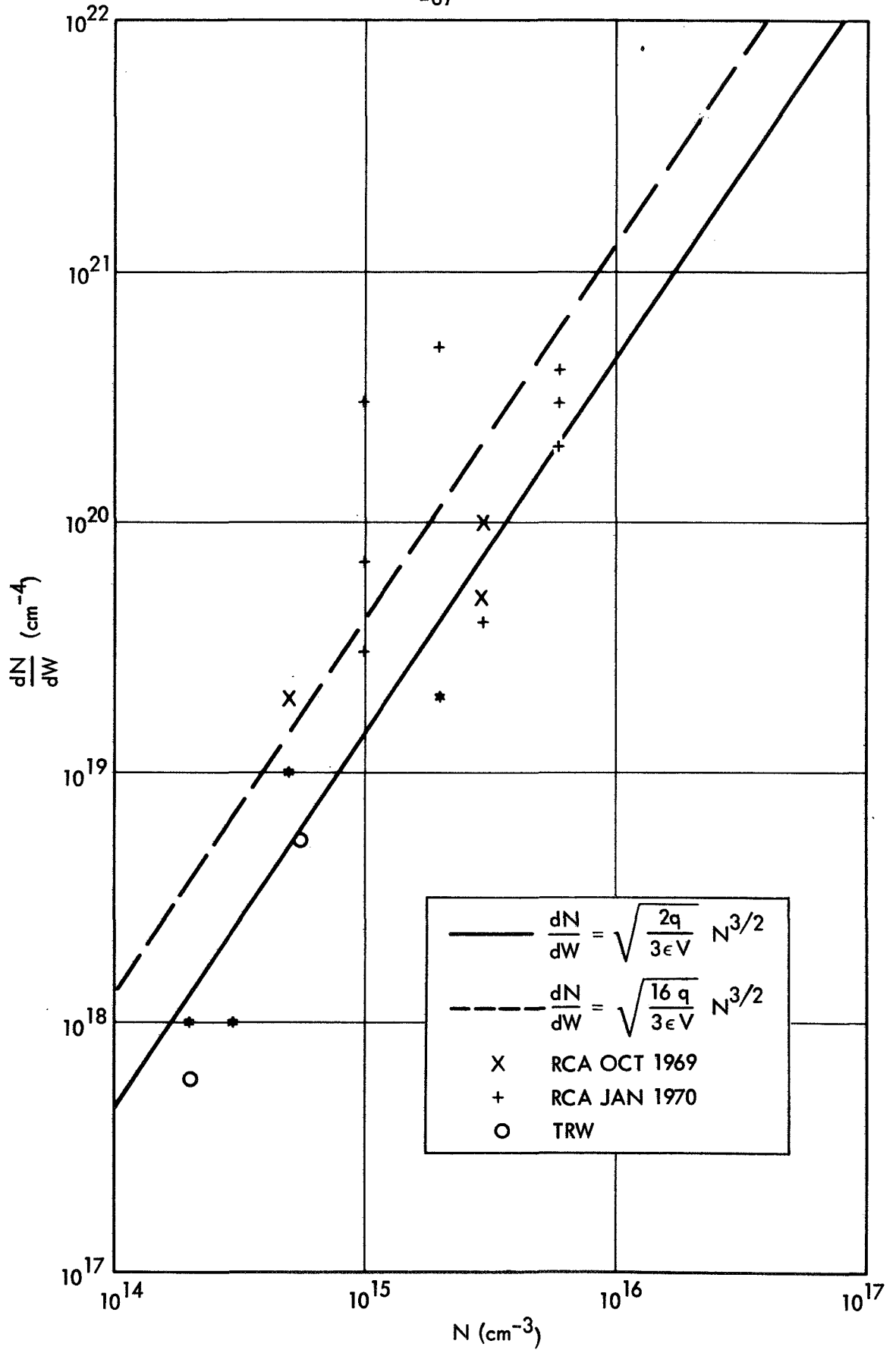


FIG. 27 LITHIUM CONCENTRATION GRADIENT VS. CONCENTRATION AT JUNCTION EDGE, LINEAR GRADIENT CELLS

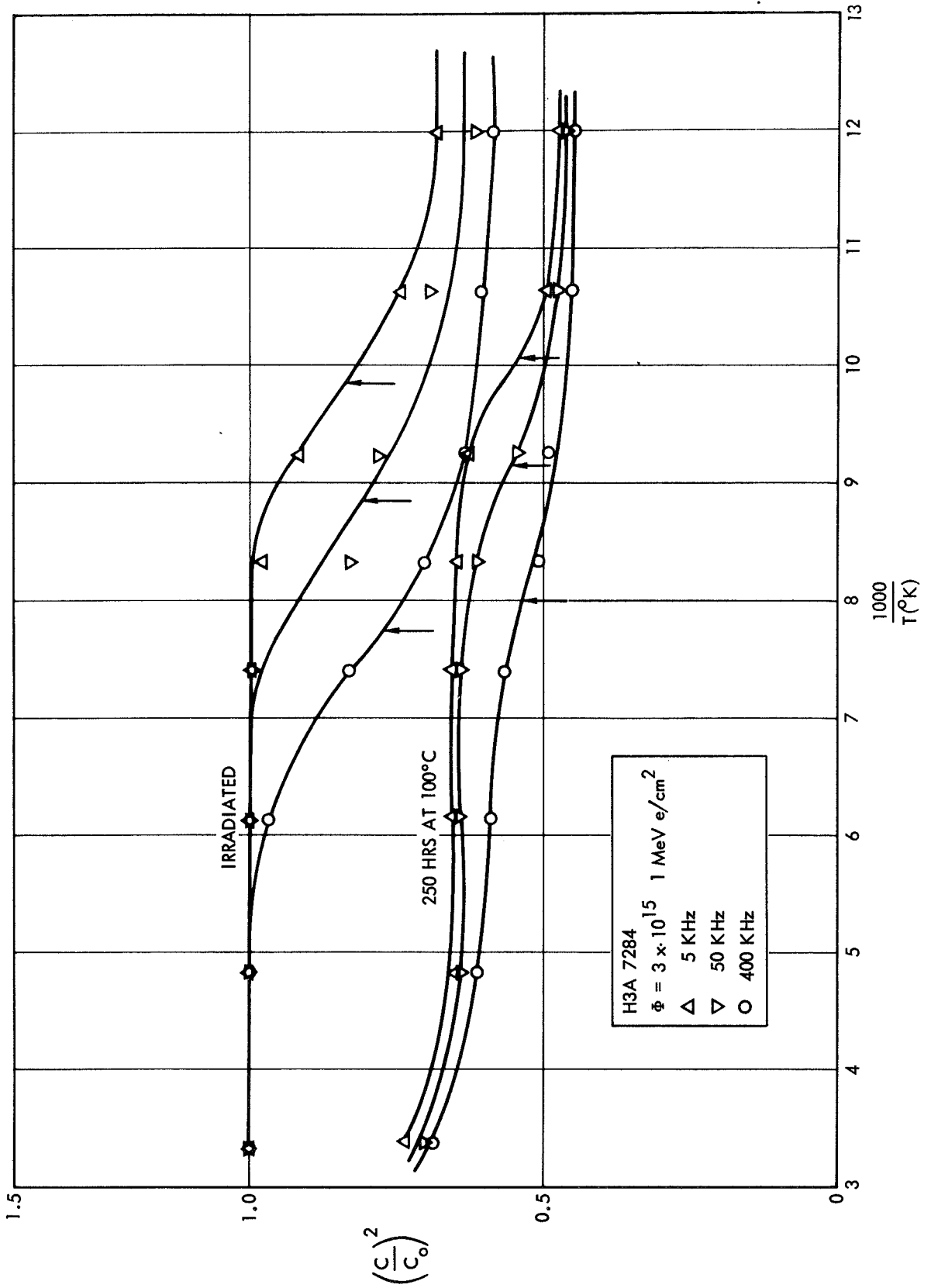


FIG. 28 CAPACITANCE VS. TEMPERATURE, VARIOUS FREQUENCIES

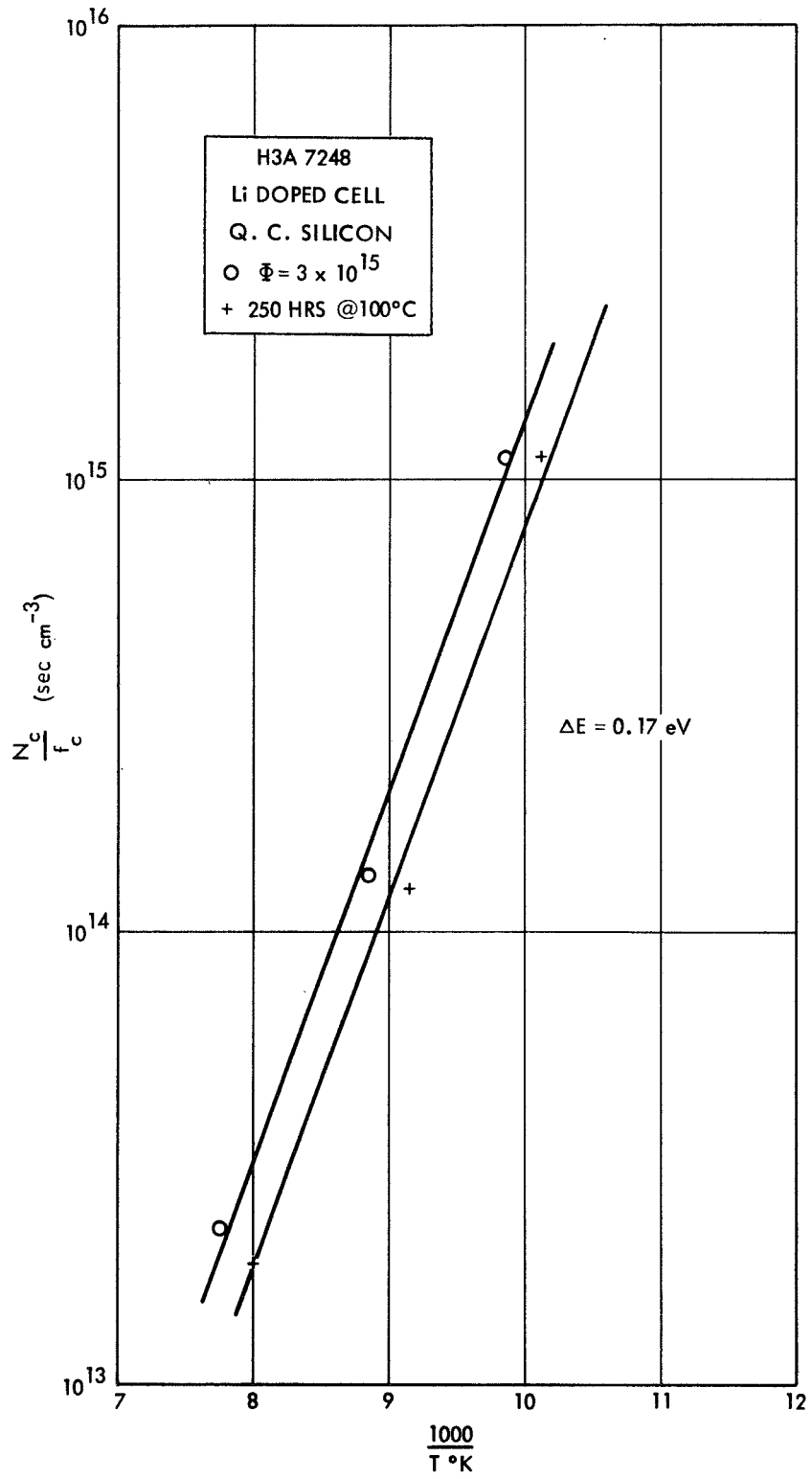


FIG. 29 ACTIVATION ENERGY PLOT, CELL H3A 7284

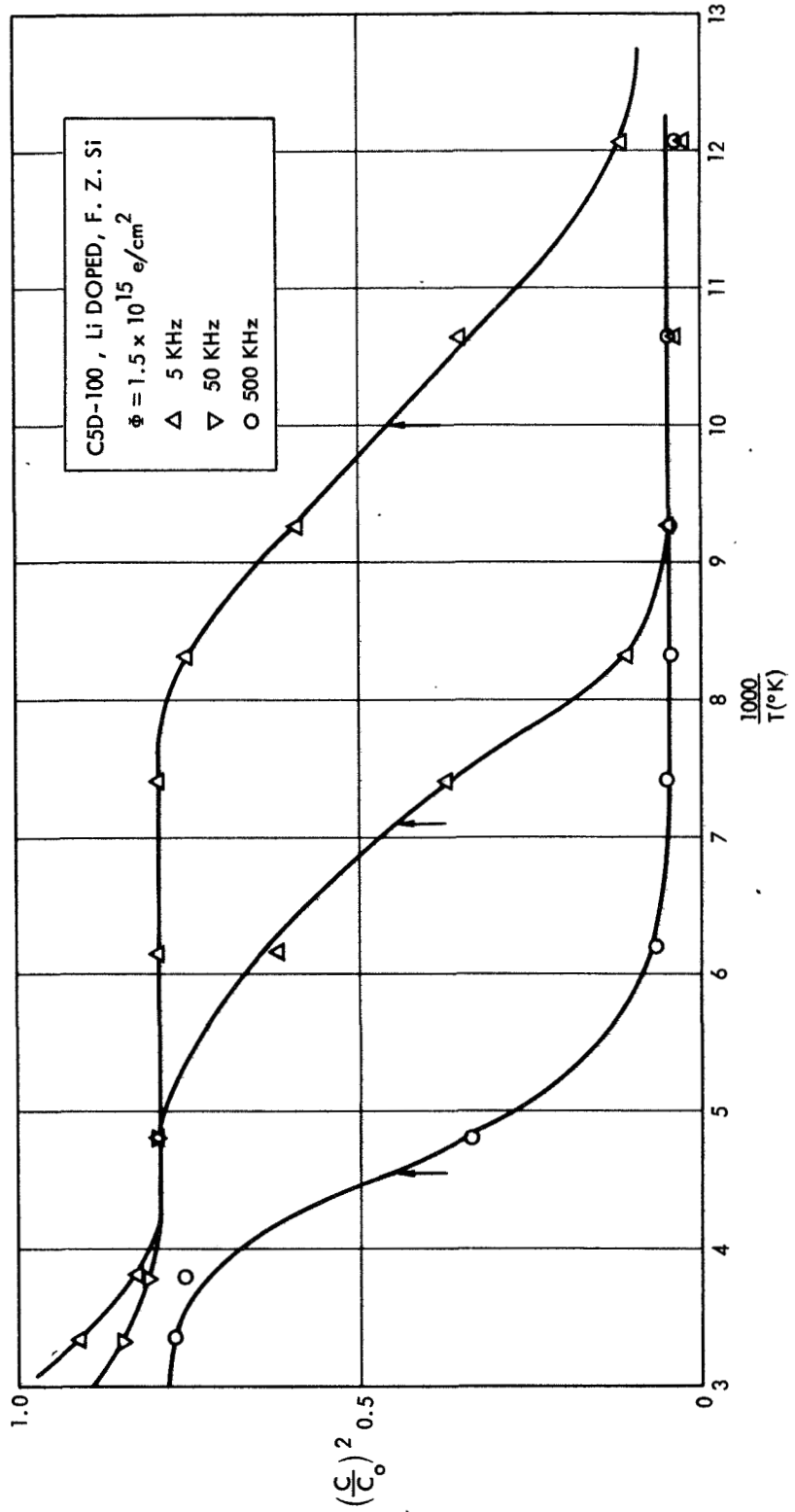


FIG. 30 CAPACITANCE VS. TEMPERATURE, VARIOUS FREQUENCIES, FLOAT ZONE CELL

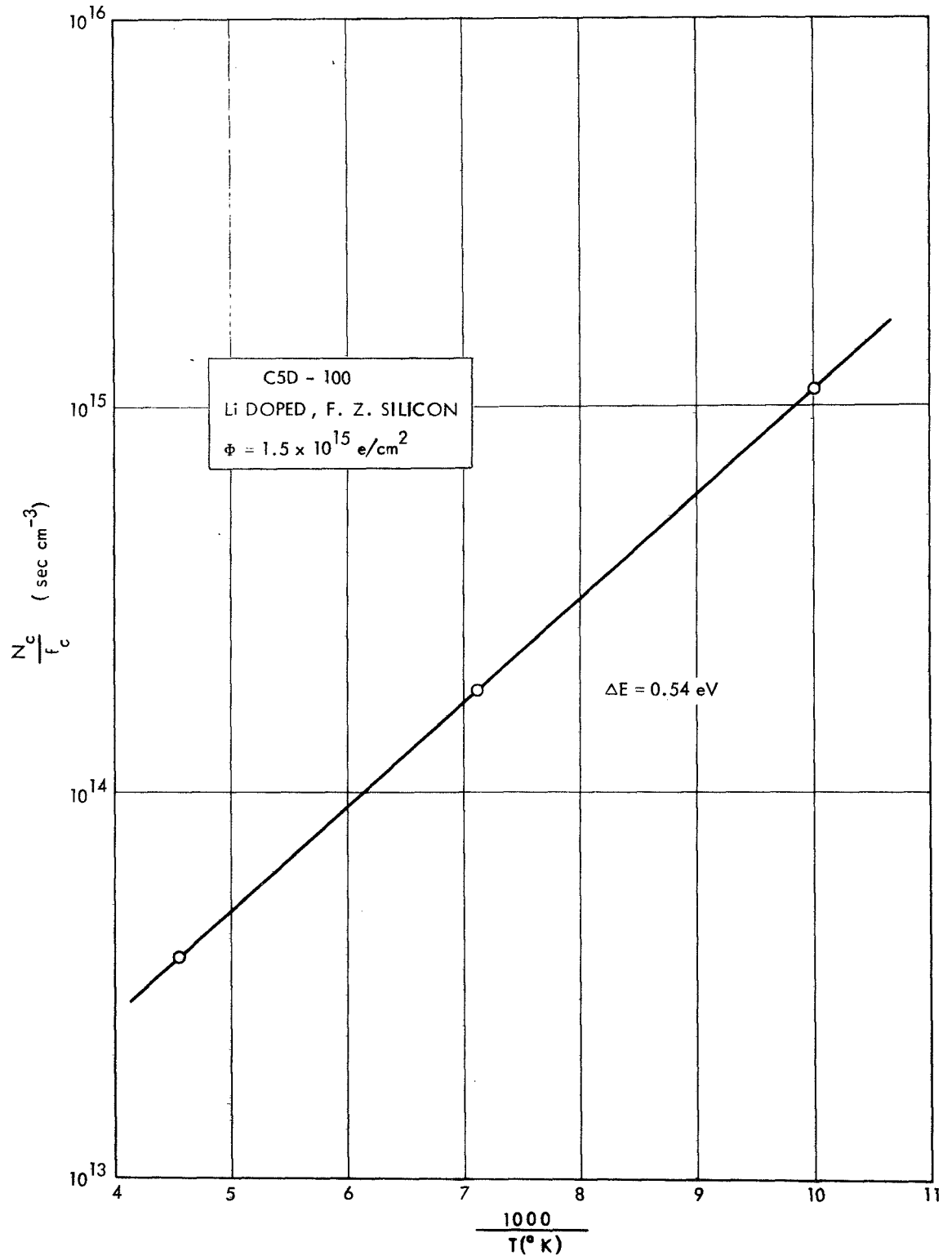


FIG. 31 ACTIVATION ENERGY PLOT, CELL C5D100

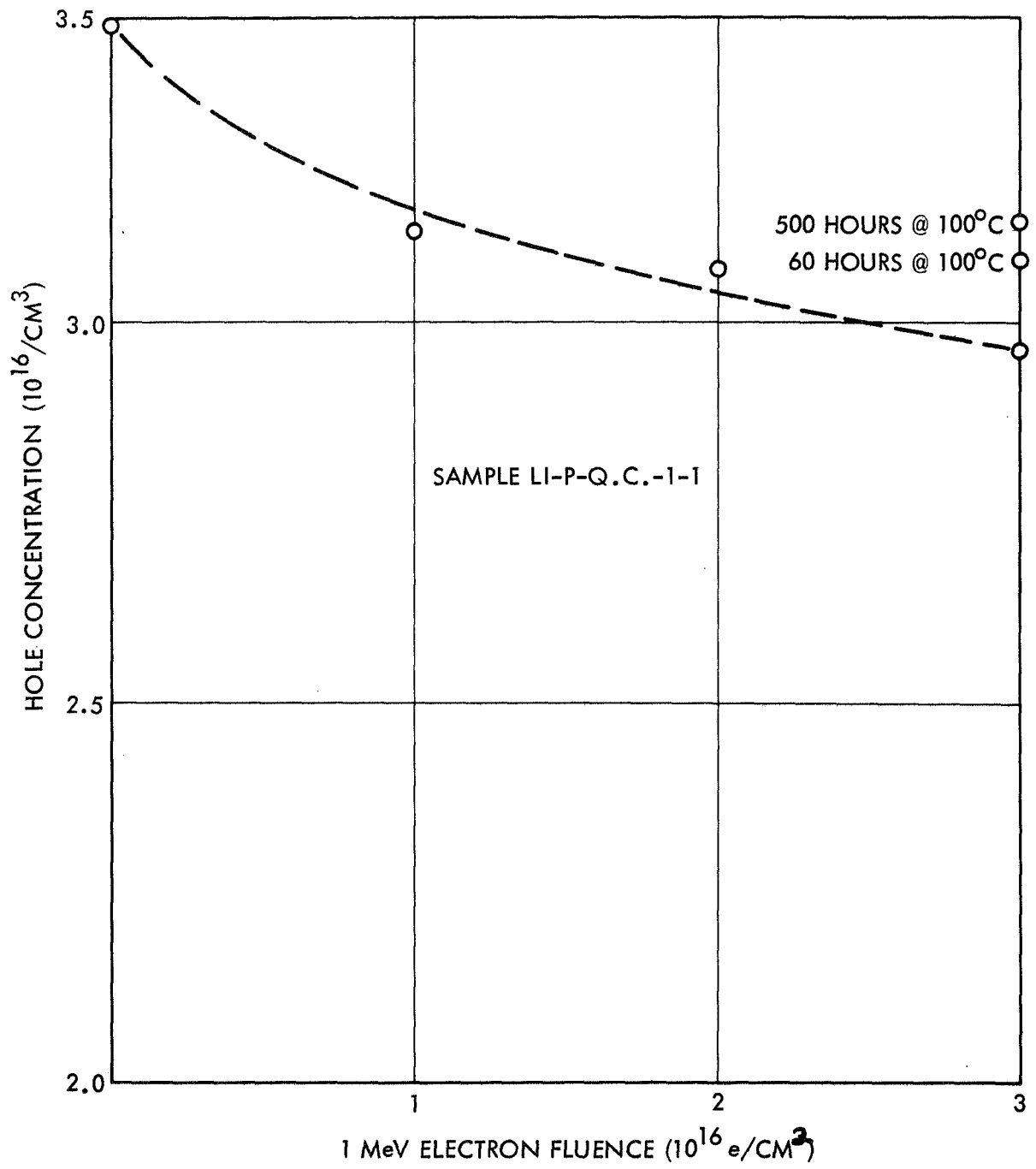
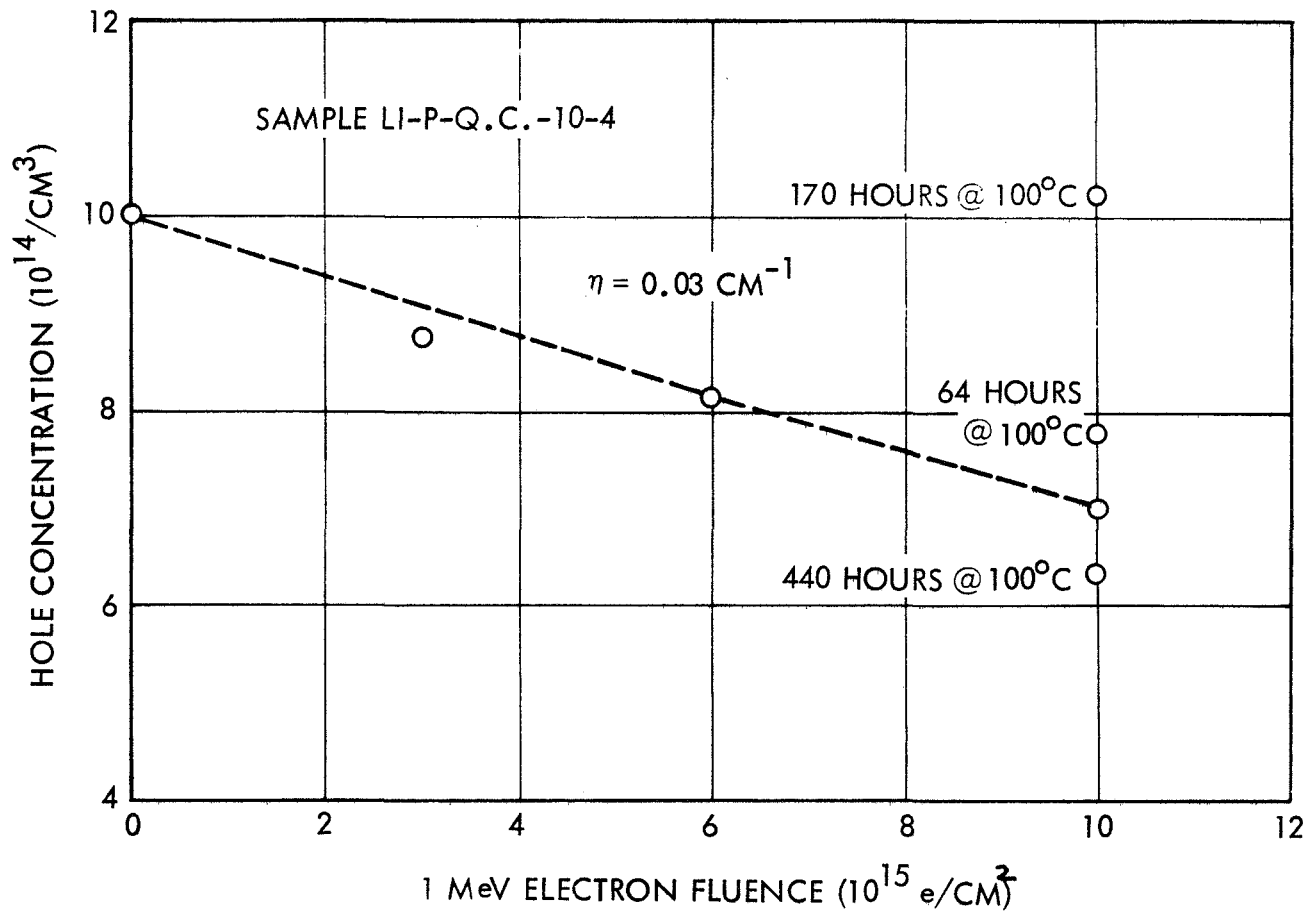


FIG. 32 LITHIUM COMPENSATED P-TYPE SILICON, Q.C.

FIG. 33 LITHIUM COMPENSATED P-TYPE SILICON, Q.C.





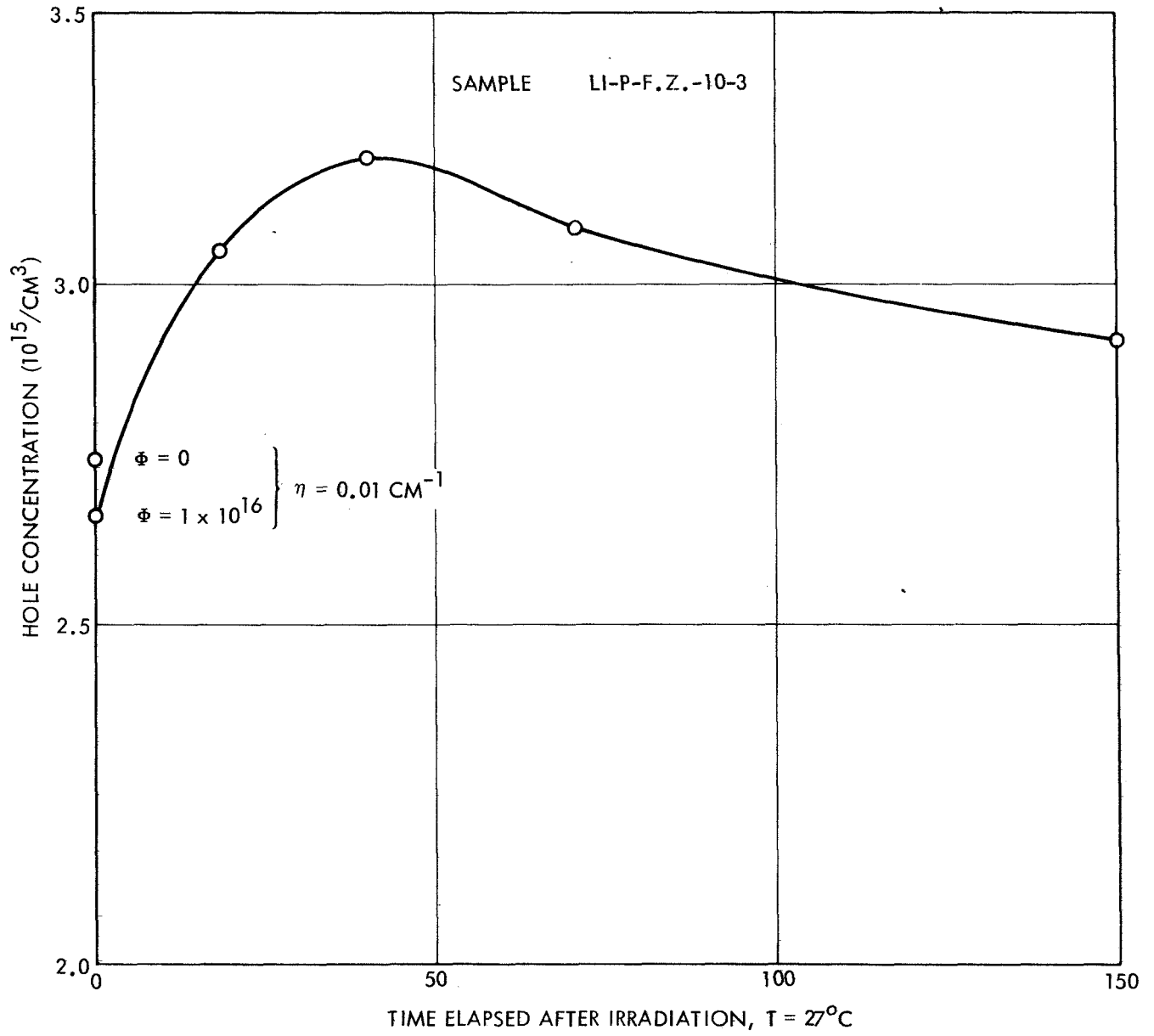


FIG. 34 LITHIUM COMPENSATED P-TYPE SILICON, F.Z.

FIG. 35 SOLAR CELLS WITH LARGE SUBSTITUTIONAL IMPURITY ATOMS

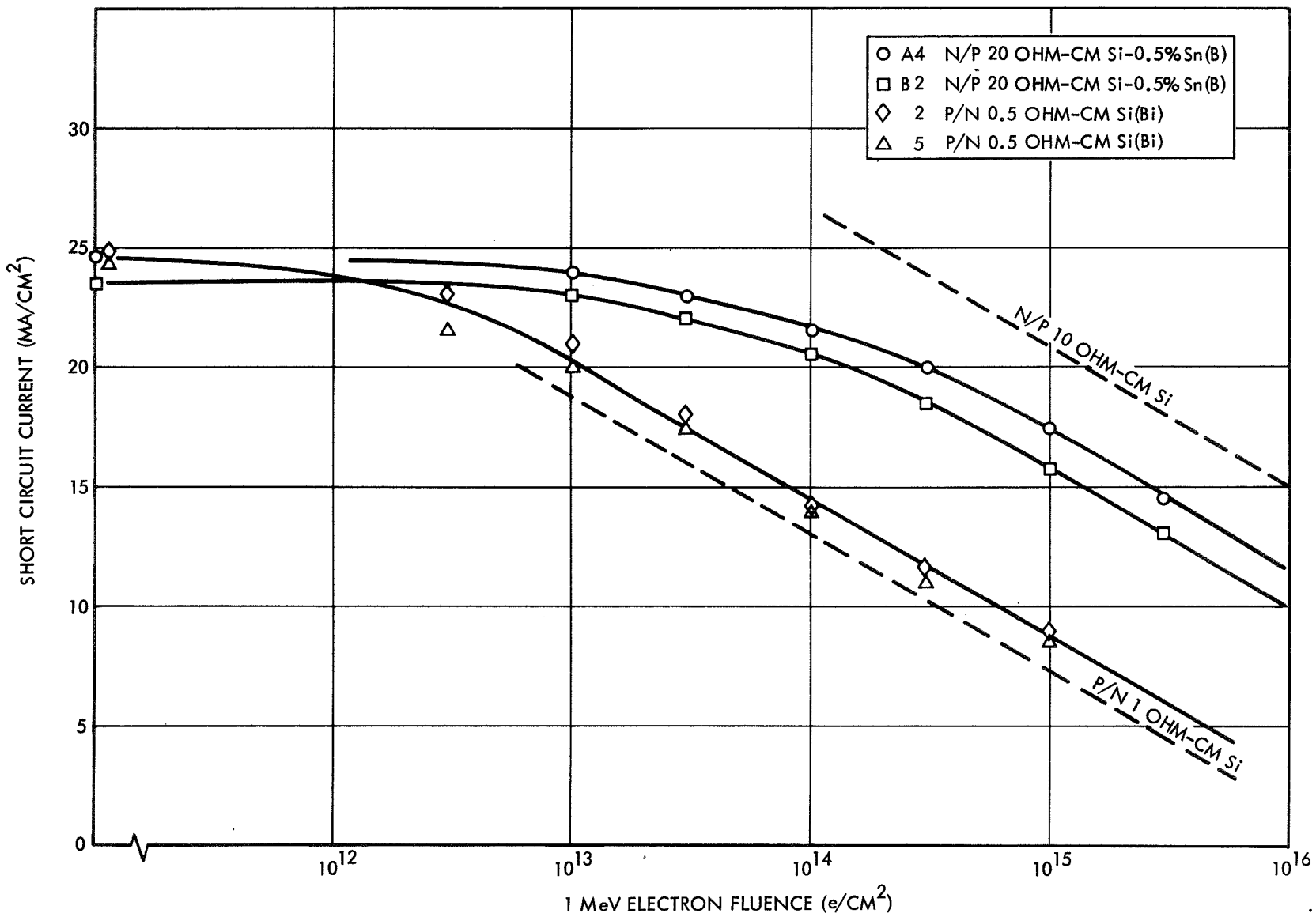


FIG. 35 SOLAR CELLS WITH LARGE SUBSTITUTIONAL IMPURITY ATOMS

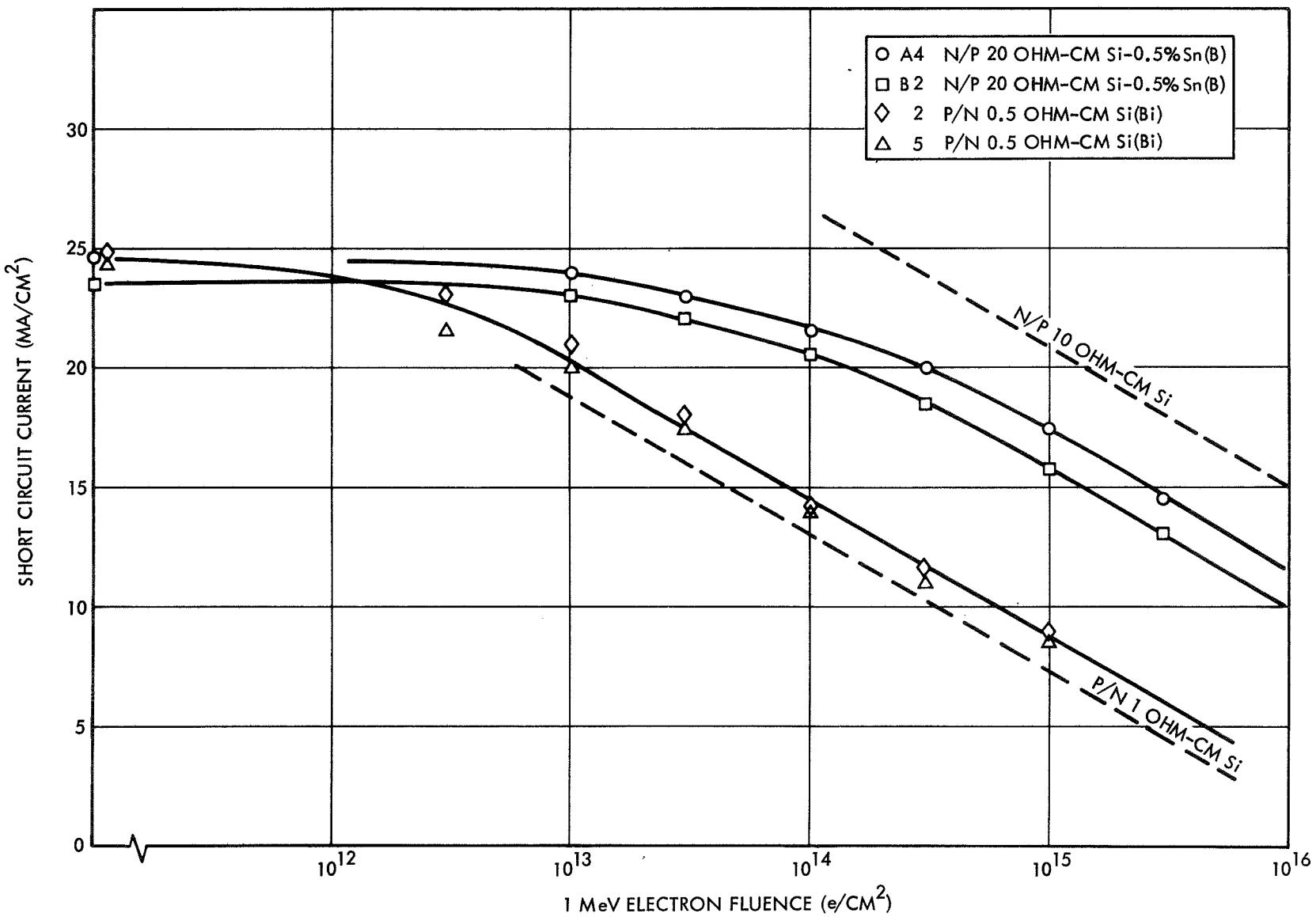
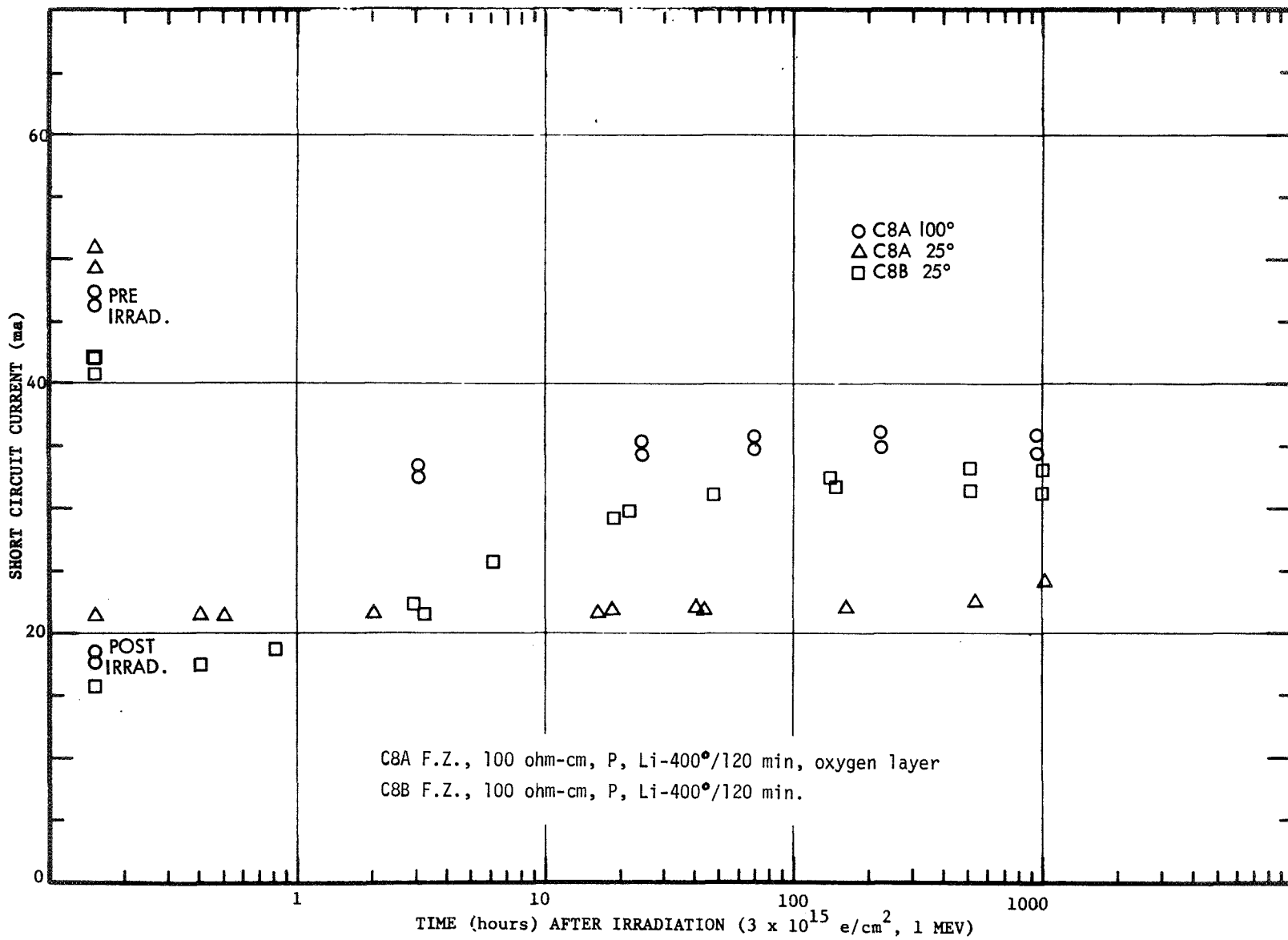


FIG. 36 RECOVERY OF GROUPS C8A and C8B LITHIUM SOLAR CELLS



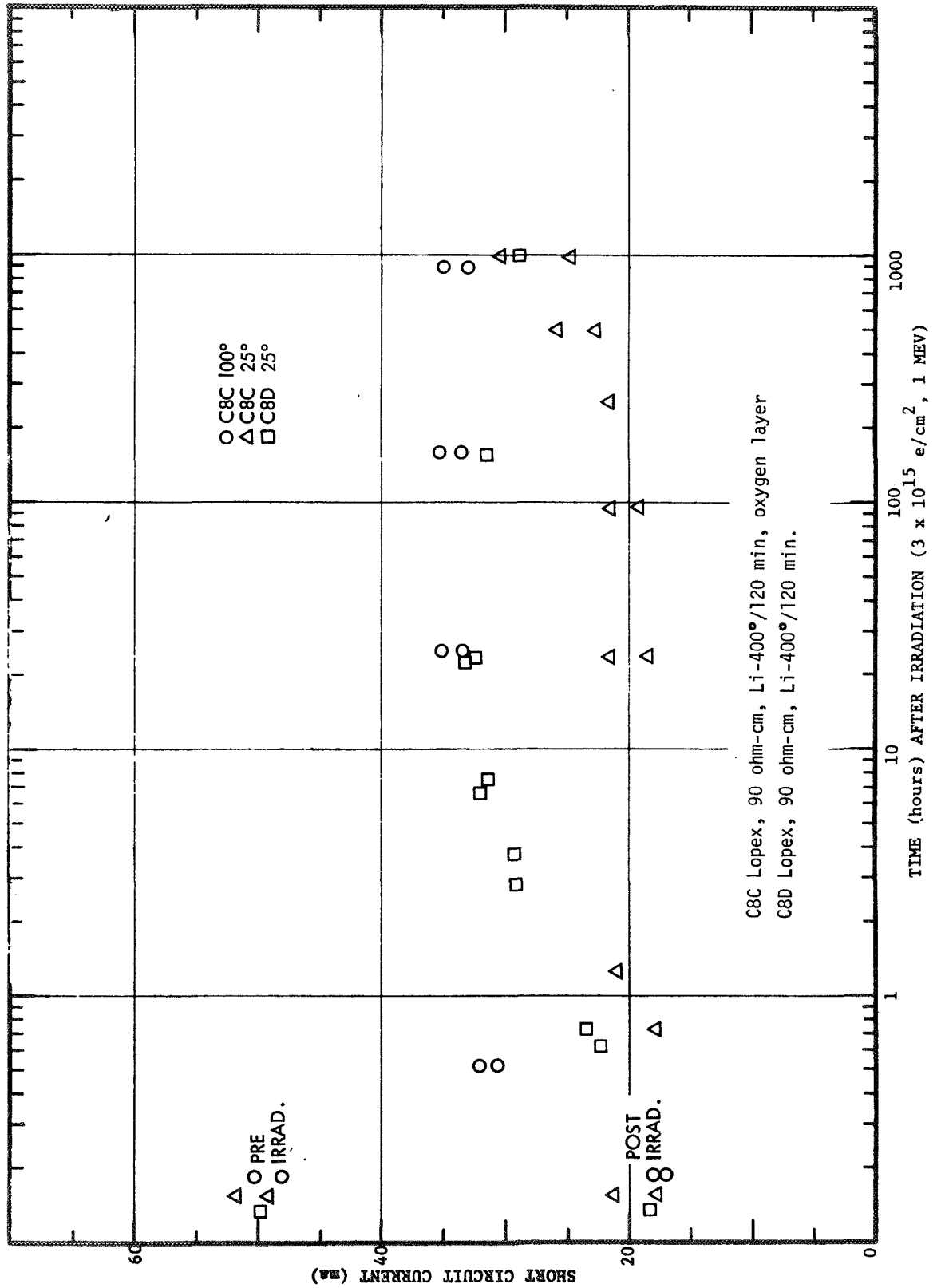


FIG. 37 RECOVERY OF GROUPS C8C AND C8D LITHIUM SOLAR CELLS

FIG. 38 RECOVERY OF GROUPS C8G and C8H LITHIUM SOLAR CELLS

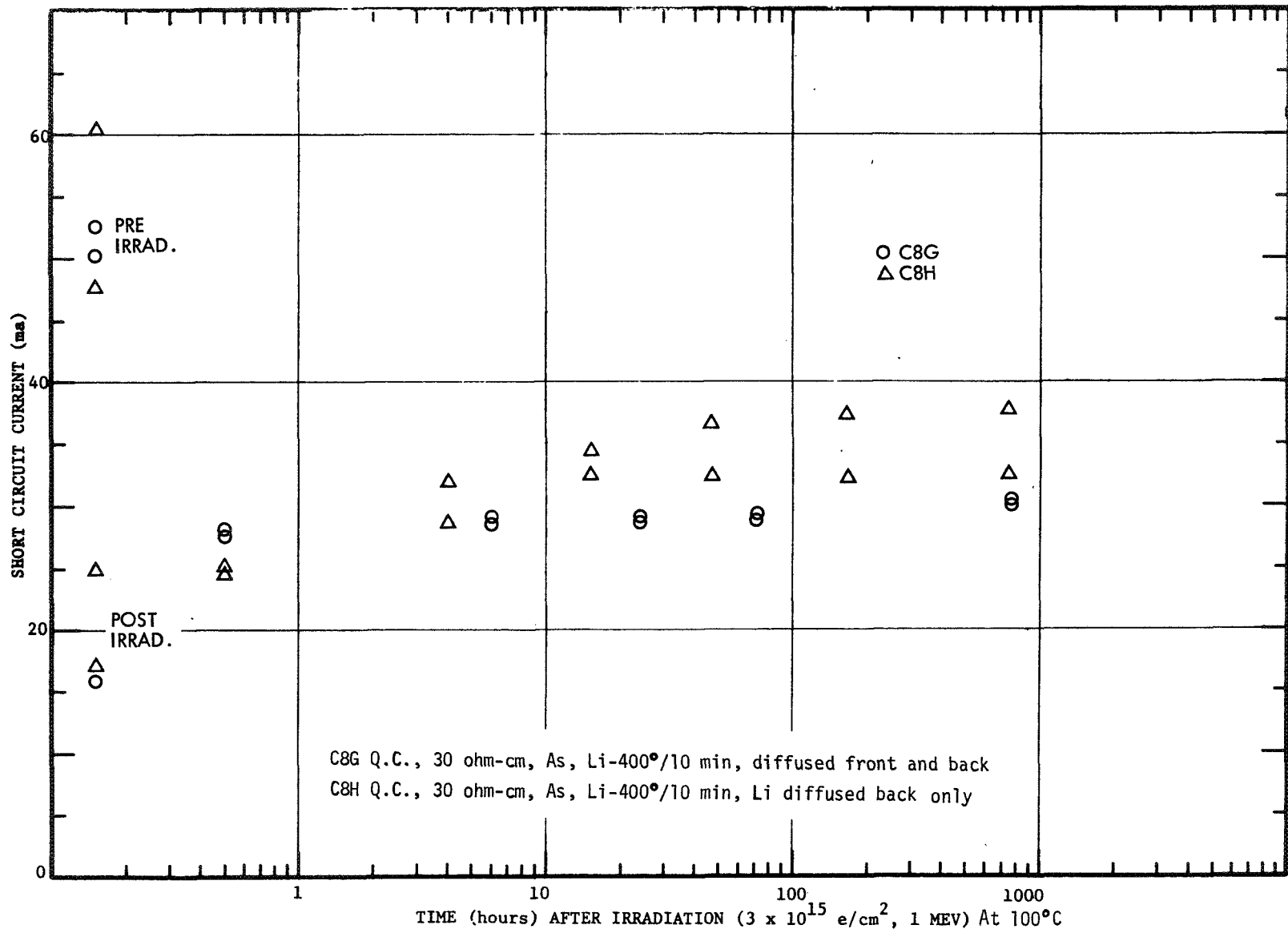


FIG. 39 RECOVERY OF GROUP T9 LITHIUM SOLAR CELLS

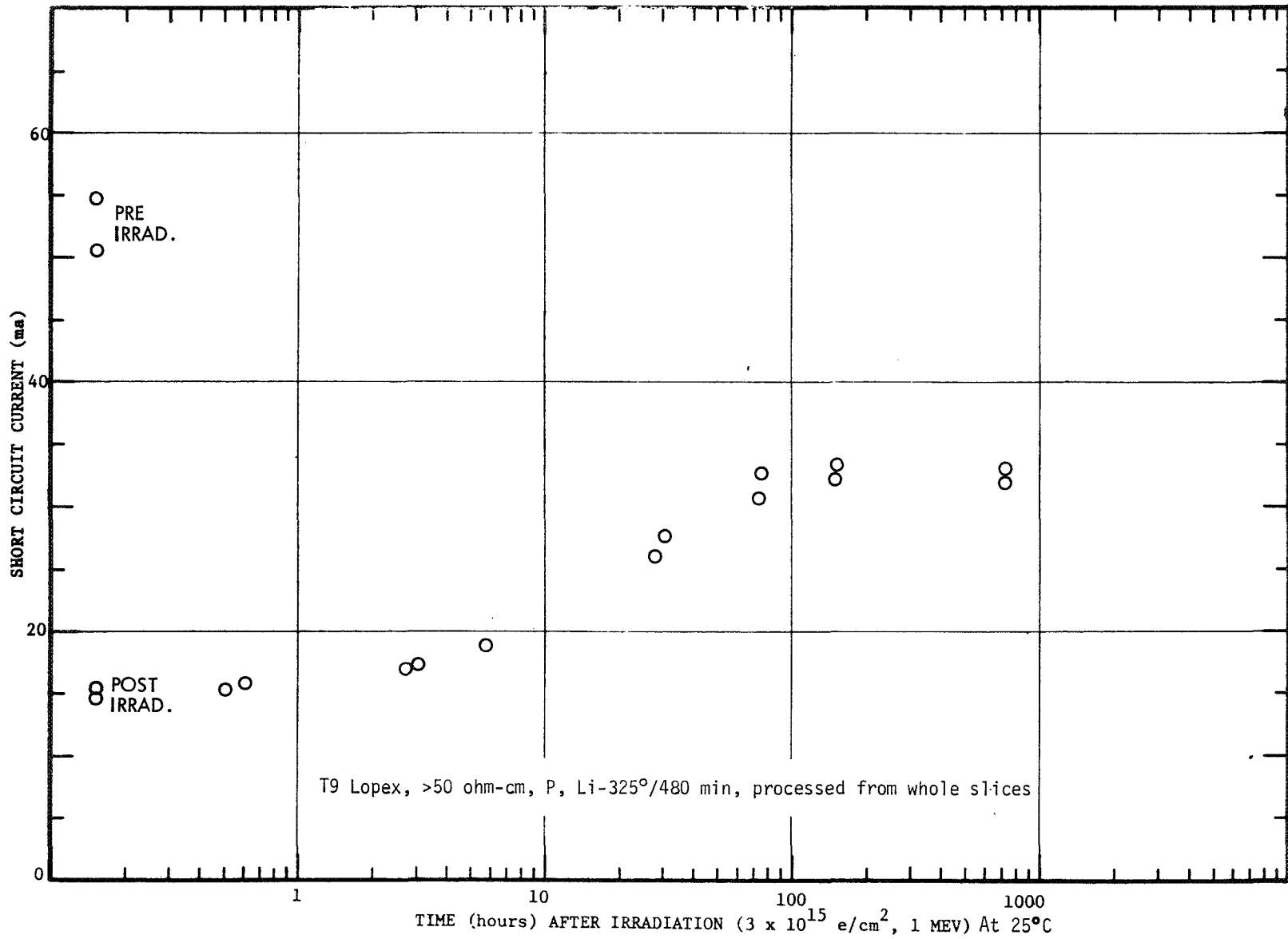


FIG. 40 RECOVERY OF GROUP T10 LITHIUM SOLAR CELLS

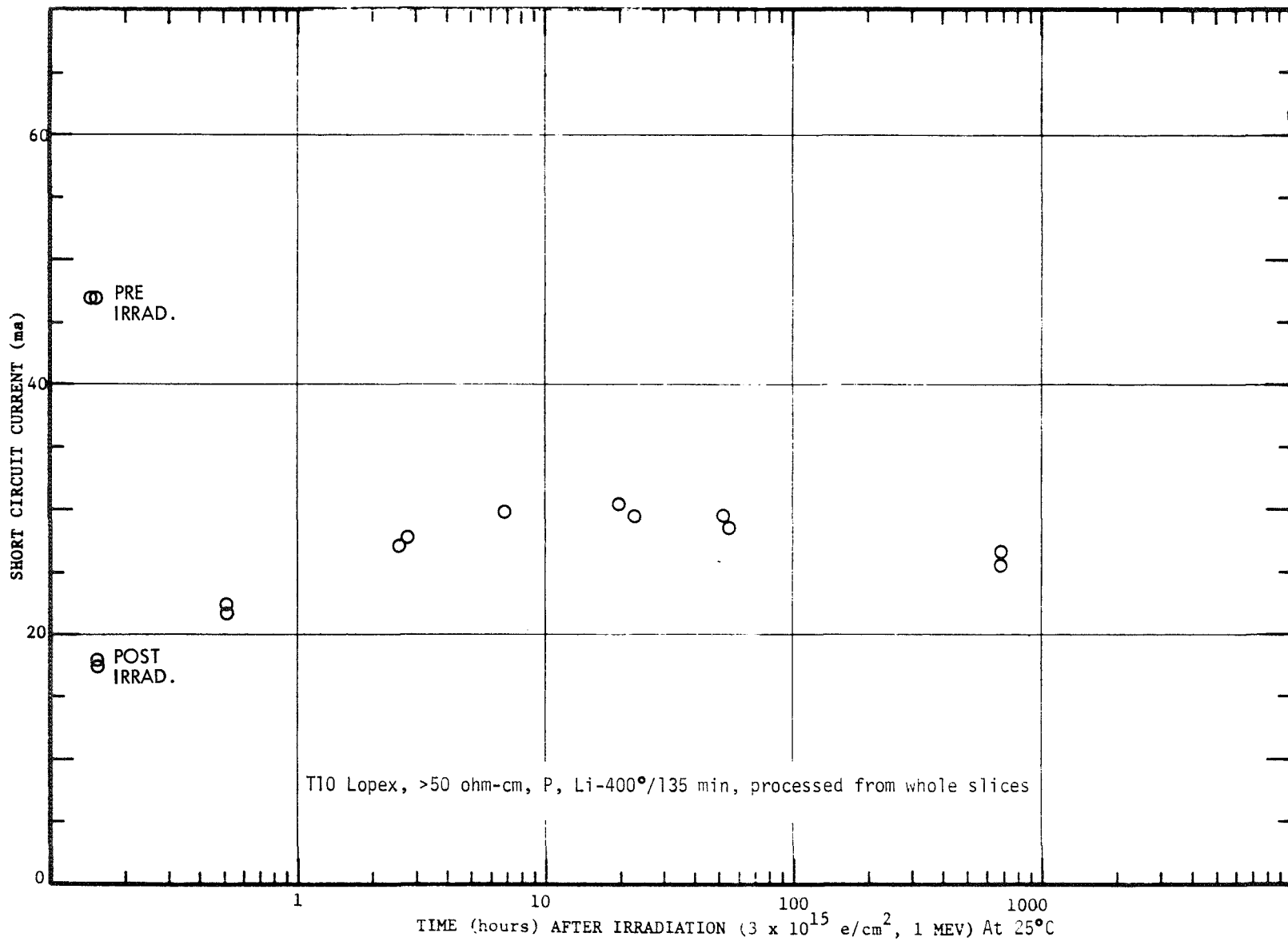




FIG. 41 RECOVERY OF GROUP H8 LITHIUM SOLAR CELLS

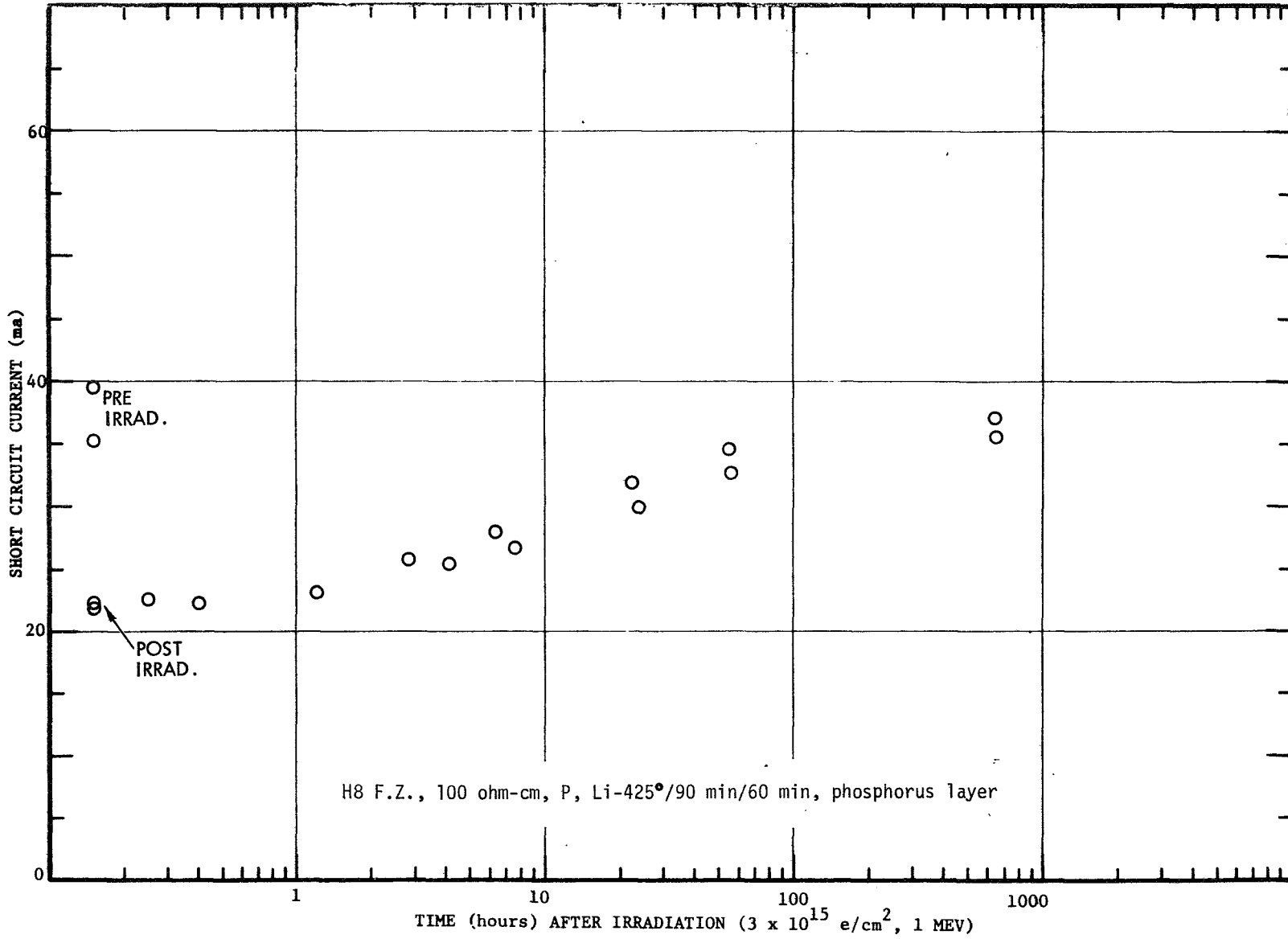


FIG. 42 RECOVERY OF GROUP H10 LITHIUM SOLAR CELLS AT 100°C

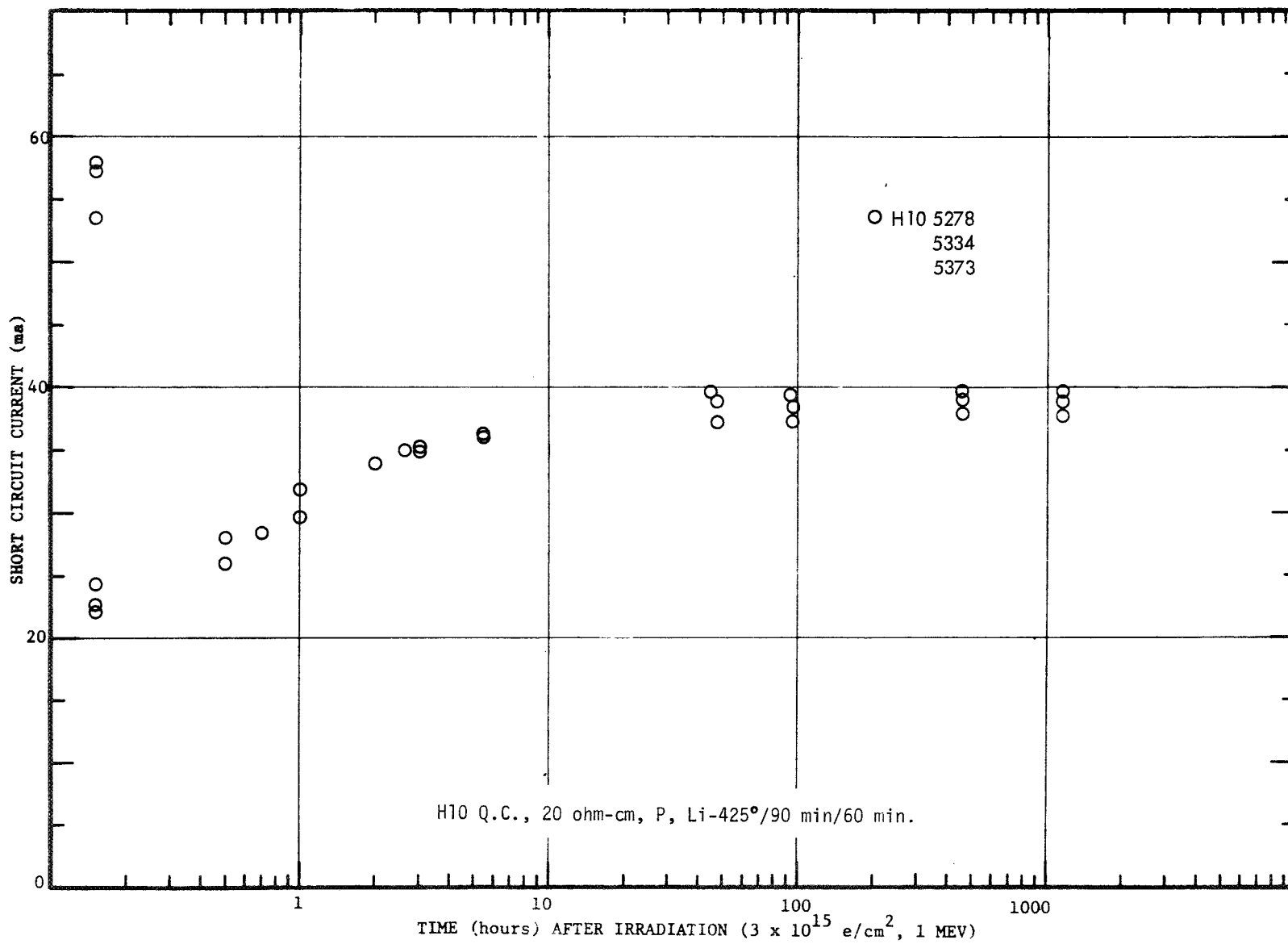


FIG. 43 RECOVERY OF GROUP H10 LITHIUM SOLAR CELLS AT 60°C

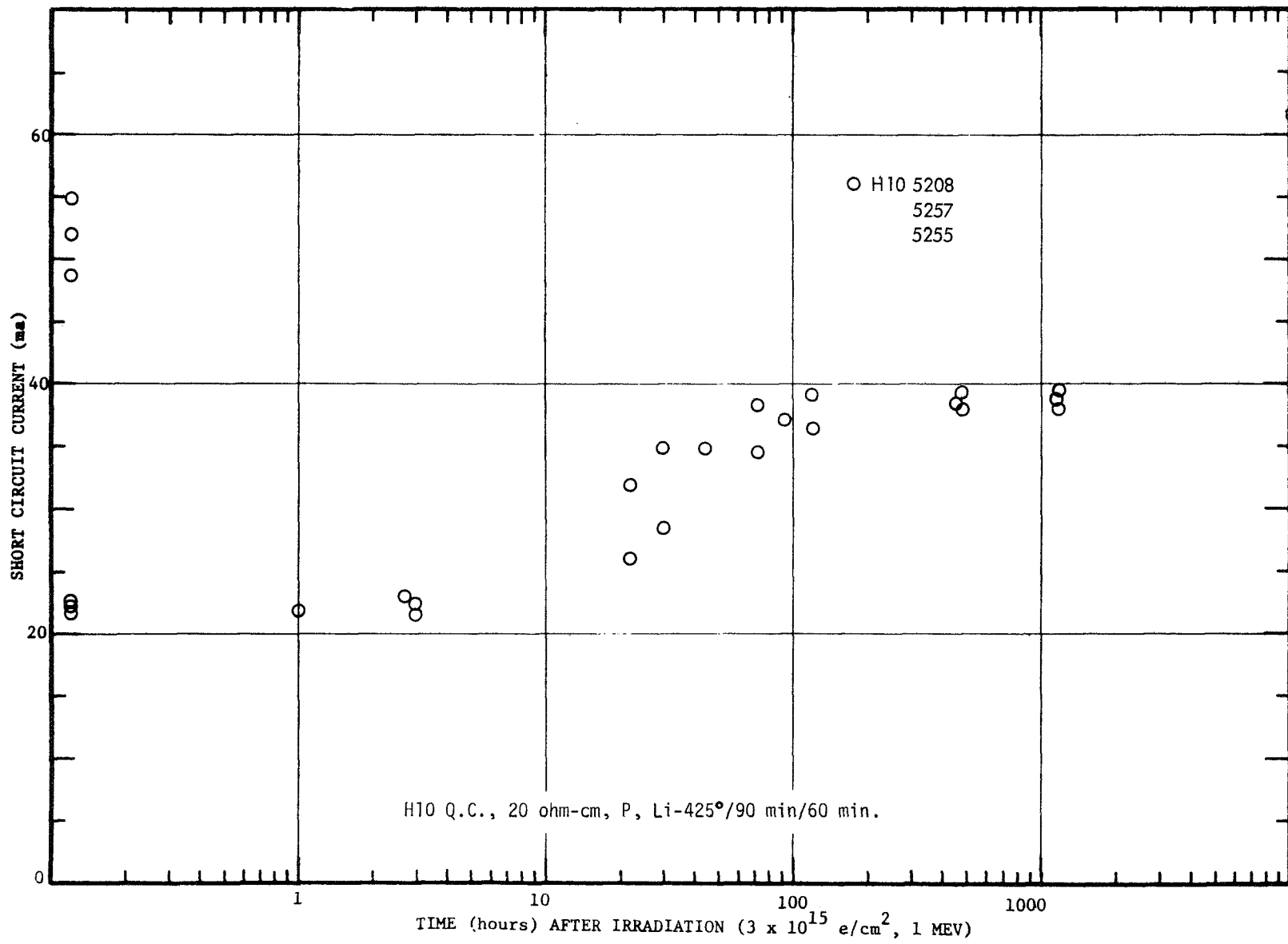


FIG. 44 RECOVERY OF GROUP H3A LITHIUM SOLAR CELLS AT 100°C

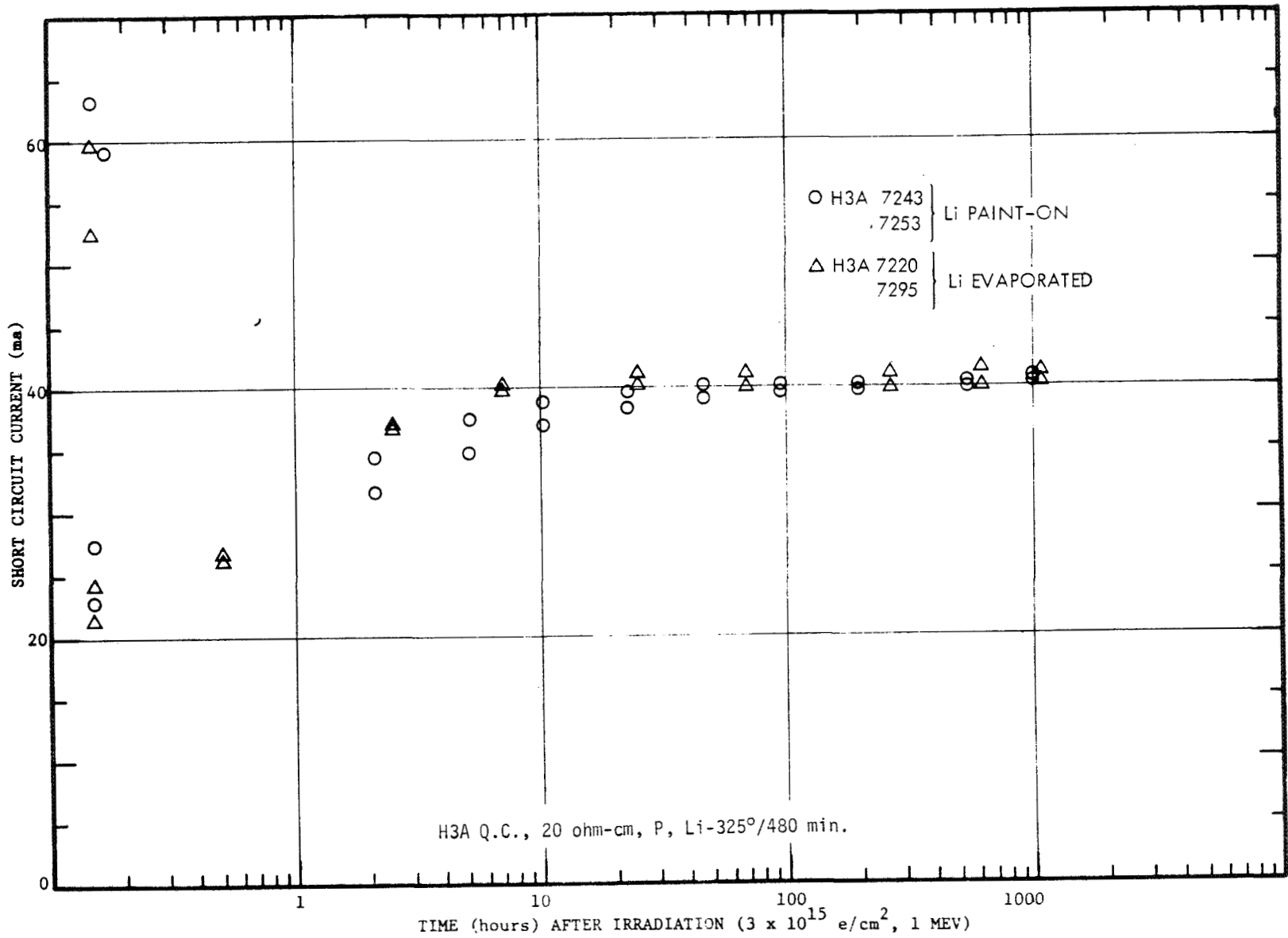


FIG. 45 RECOVERY OF GROUP H3A LITHIUM SOLAR CELLS AT 60°C

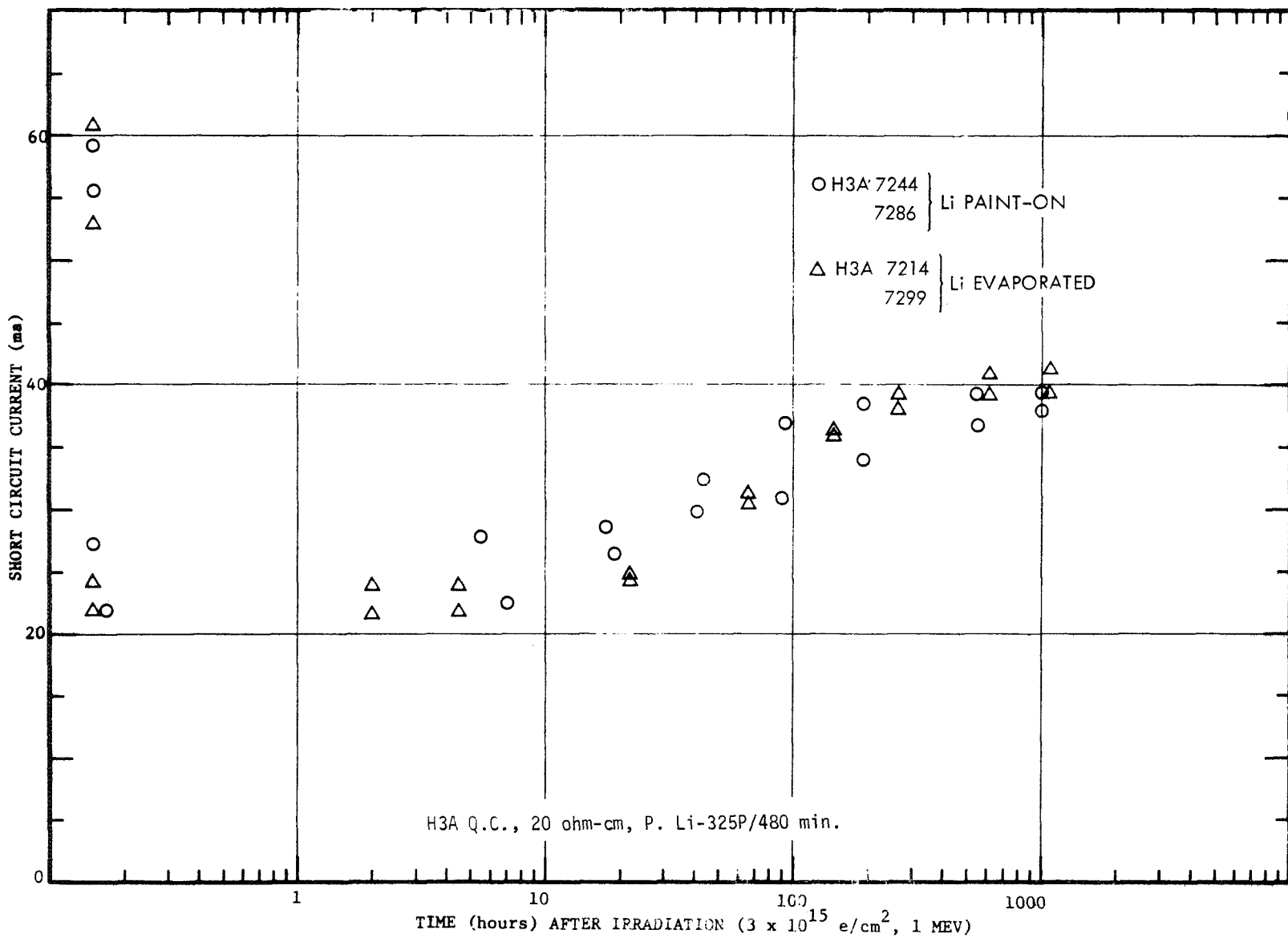


FIG. 46 RECOVERY OF GROUP H9 LITHIUM SOLAR CELLS AFTER  $3 \times 10^{14} \text{ e/cm}^2$

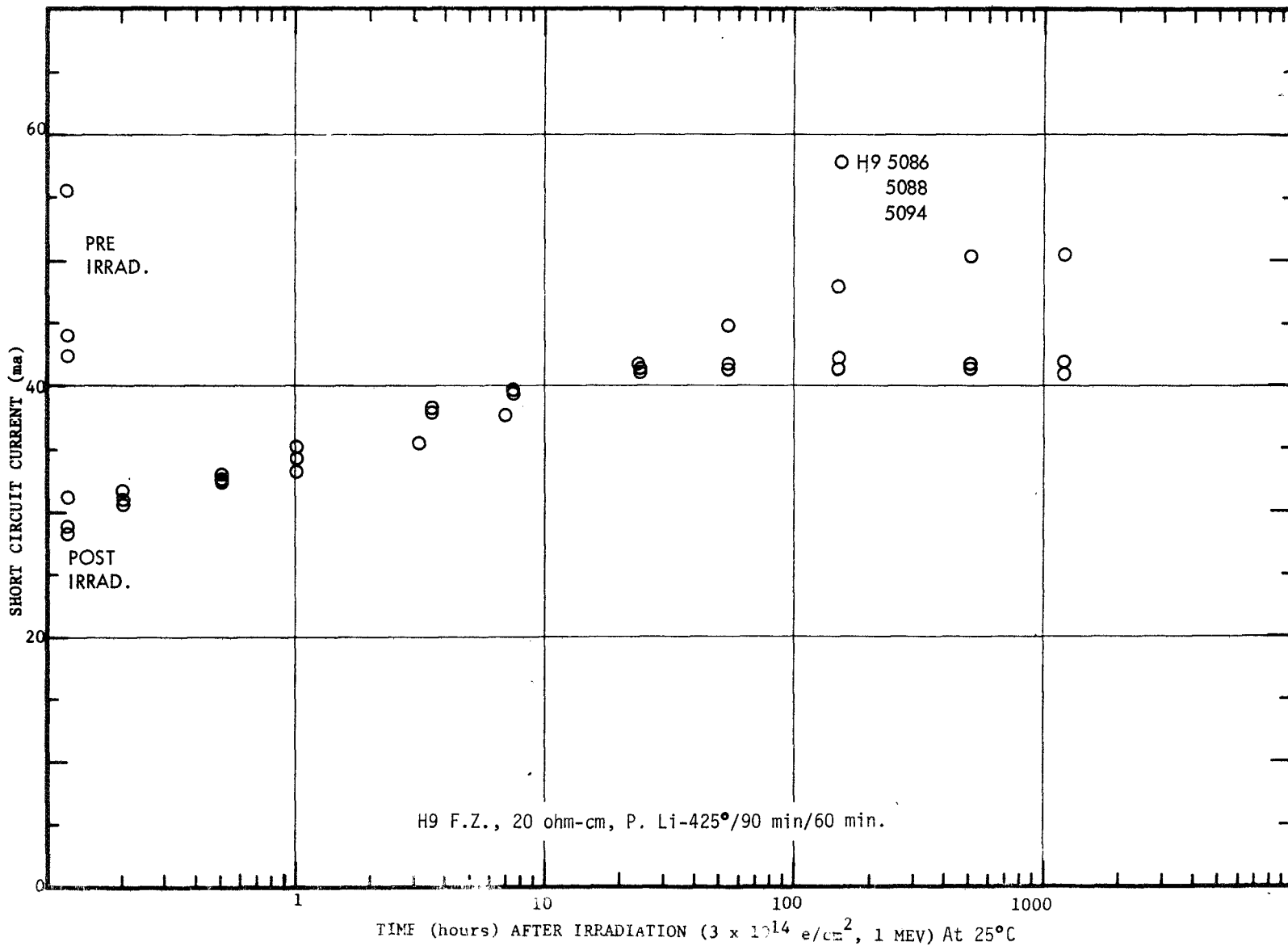
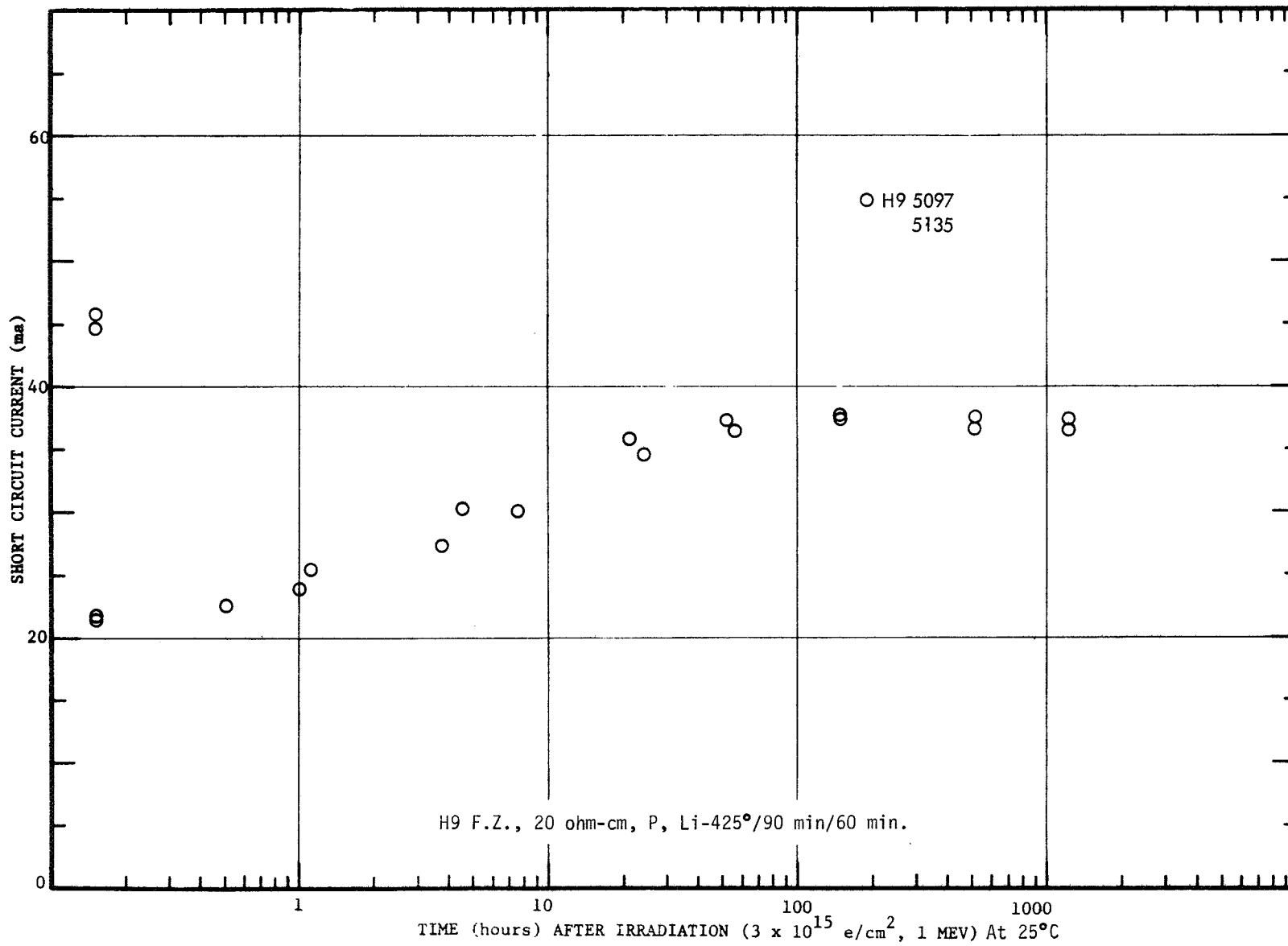


FIG. 47 RECOVERY OF GROUP H9 LITHIUM SOLAR CELLS AFTER  $3 \times 10^{15} \text{ e/cm}^2$



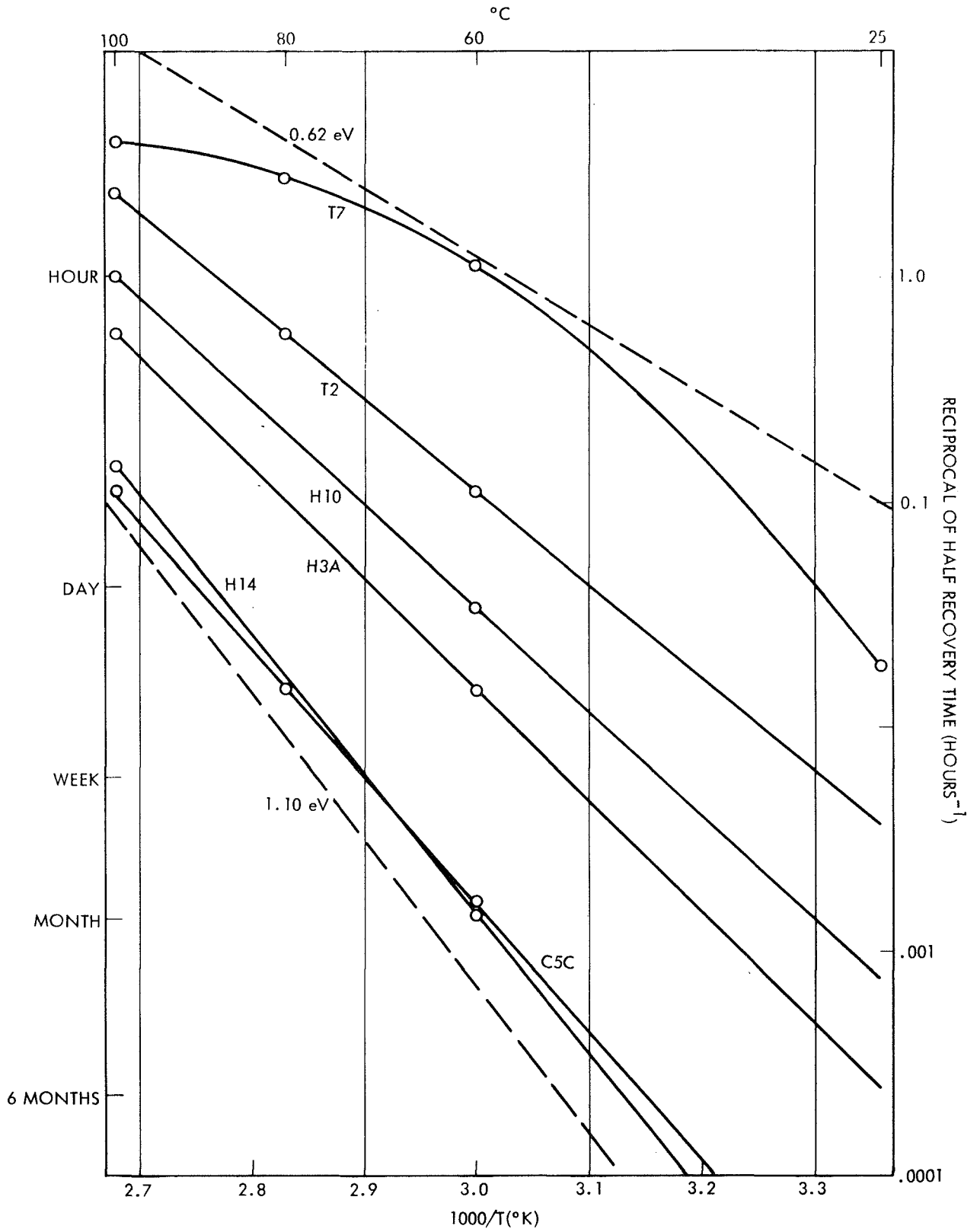


FIG. 48 ANNEALING TIME VS. STORAGE TEMPERATURE FOR CRUCIBLE LITHIUM SOLAR CELLS



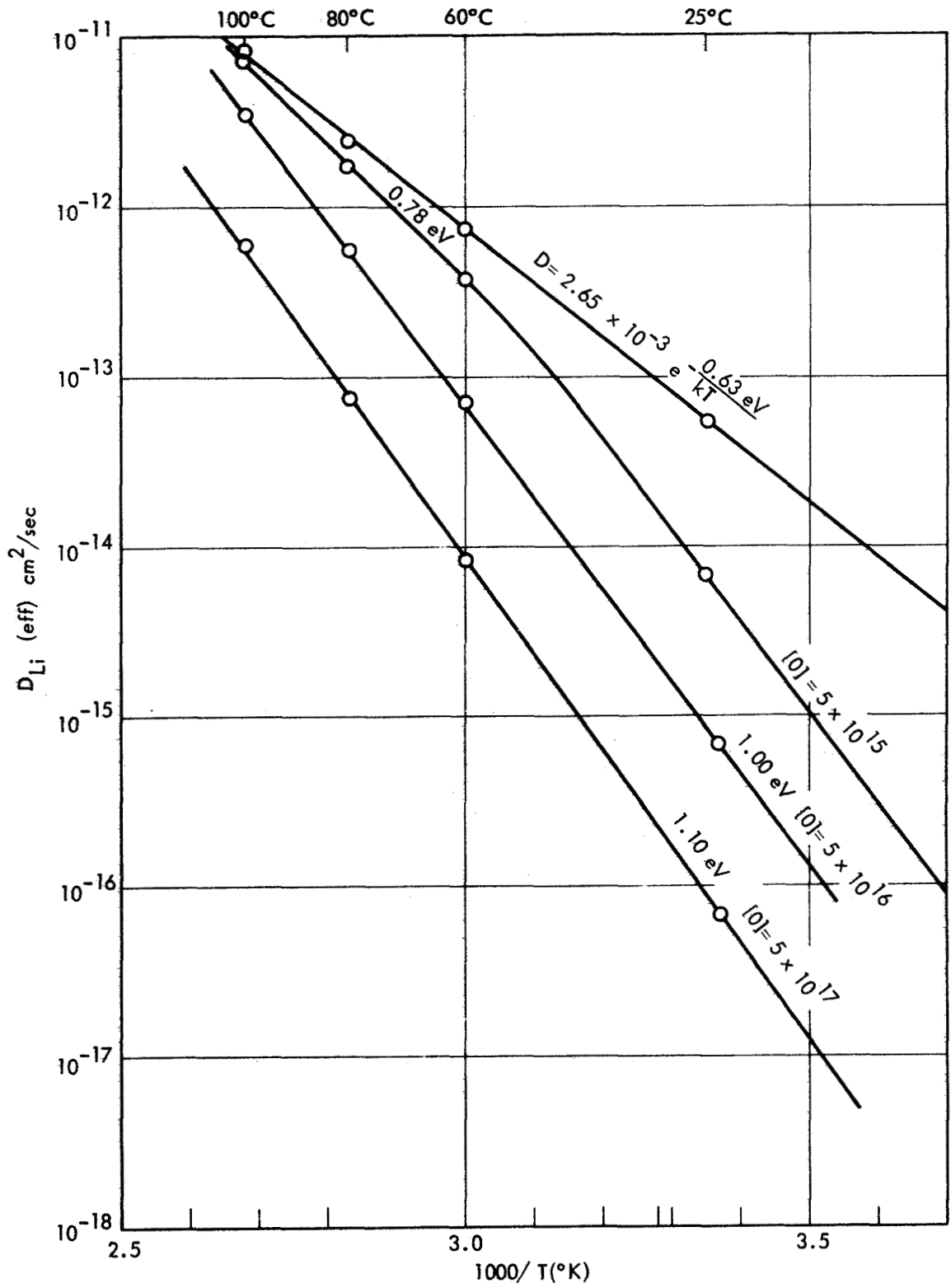


FIG. 49 EFFECT OF OXYGEN ON DIFFUSION COEFFICIENT OF LITHIUM IN SILICON

FIG. 50 RECOVERY OF MAXIMUM POWER POINT OF BEST CRUCIBLE CELLS AT 100°C USING SOLAR SIMULATOR ILLUMINATION

